LINEAR AND NONLINEAR FLEXURAL STIFFNESS MODELS FOR CONCRETE WALLS IN HIGH-RISE BUILDINGS

by

Ahmed M. M. Ibrahim

B.Sc., Cairo University, Cairo, 1990

M.A.Sc., Concordia University, Montreal, 1995

A THESIS SUBMITTED IN PARTIAL FULFILMENT OF

THE REQUIREMENTS FOR THE DEGREE OF

Doctor of Philosophy

in

The Faculty of Graduate Studies

Department of Civil Engineering

We accept this thesis as conforming to the required standard

THE UNIVERSITY OF BRITISH COLUMBIA

October 2000

In presenting this thesis in partial fulfilment of the requirements for an advanced degree at the University of British Columbia, I agree that the Library shall make it freely available for reference and study. I further agree that permission for extensive copying of this thesis for scholarly purposes may be granted by the head of my department or by his or her representatives. It is understood that copying or publication of this thesis for financial gain shall not be allowed without my written permission.

Department of Civil Engineering

The University of British Columbia
Vancouver, Canada

Date Oct/13/2000

DE-6 (2/88)

ABSTRACT

In the seismic design of high-rise wall buildings, the fundamental period of the building and the building drift are usually determined using linear elastic dynamic analysis. To carry out this analysis, designers need to assume a linear flexural stiffness of the wall sections that account for cracking. The commentary to the 1994 Canadian concrete code (CPCA 1995) suggests a stiffness value of 70% of the gross moment of inertia (I_g) of the wall section. The commentary to the 1995 New Zealand Standard (NZS 3101 1995) suggests much lower stiffness values. A wall subjected to axial compression of 10% of $f_c' A_g$ is suggested to have half what is recommended in the CPCA Handbook (i.e. 0.35 I_g). The NEHRP Guidelines for the Seismic Rehabilitation of Buildings (FEMA 273) suggests stiffness values of 0.8 I_g and 0.5 I_g for uncracked and cracked concrete walls, respectively. While it is not clear which of the recommended stiffness values should be used, it is certainly clear that the choice of stiffness value will have a significant influence on the predicted period and drift of the building.

The actual influence of cracking on the flexural stiffness of a concrete wall subjected to seismic loading is nonlinear. Nonlinear static analysis is increasingly used to capture this influence provided that an appropriate nonlinear model is used for the material.

In this thesis, a simple nonlinear flexural (bending moment-curvature) model for concrete walls in high-rise buildings is proposed. To validate the model, a 40 ft high slender concrete wall was constructed and tested under simulated earthquake loading. Results from the test were compared with the proposed model and showed good agreement. Based on the proposed piece-wise linear model, a general method to determine the linear "effective" flexural stiffness of concrete walls was developed. Results from the general method for the effective flexural stiffness showed that the large variation in effective stiffness that is recommended by various design guidelines does actually exist for different wall configurations under certain conditions. The general method presented in this thesis gives the appropriate stiffness for a particular wall considering all important parameters that influence the stiffness. A study was conducted to examine the influence of a variety of parameters on the stiffness of concrete walls and a set of simplified expressions are proposed for the effective flexural stiffness of concrete walls.

The piece-wise flexural model is implemented into a nonlinear static (pushover) analysis computer program to demonstrate the use of the model in predicting the nonlinear static response of concrete walls. Two example applications are presented, including the analysis of a 450 ft high coupled wall structure currently being constructed. The results from the analysis showed the importance of accurately modeling the nonlinear flexural stiffness of concrete walls.

Table of Contents

LIST OF TABLES

LIST OF FIGURES

ACKNOWLEDGMENTS

The author is indebted to Dr. Perry Adebar for his supervision, guidance, encouragement and constructive criticism throughout all stages of the research program. His willingness to help in every possible way is greatly appreciated.

Thanks are due to Mr. M. Bryson for his part in the experimental investigation carried out in this thesis.

Thanks are also due to the technical staff at the Structures Laboratory of The University of British Columbia.

Financial assistance provided by "BC GREAT Scholarship" in collaboration with Mr. Jim Mutrie, principal of Jones, Kwong, Kishi, and Dr. Ron DeVall, principal of Read, Jones, Christofferesen Ltd., is greatly appreciated.

To

Mokhtar, Fayza, Rania,

Omar and Salma

Chapter 1

Introduction

1.1 Concrete Structural Walls

Reinforced concrete structural walls, or shear walls, are the most commonly used system to resist lateral motions due to earthquakes in high-rise buildings on the west coast of Canada. Concrete walls have also been gaining in popularity in other parts of North America, particularly after steel moment resisting frames were found to have suffered serious weld failures during the 1994 Northridge Earthquake.

Meigs et al. (1993) surveyed numerous structural engineering consultants in the United States and Canada and cited the preference of structural wall systems when designing for earthquake resistance due to the "excellent performance in past earthquakes, ability to minimize lateral drift, and simplicity of design". Observations of buildings during earthquakes showed the superior performance of those with walls as the primary lateral load resisting system compared to those with other types of systems, particularly with regard to damage control, overall safety and integrity of the structure (Fintel 1991, Wallace and Moehle 1992, Saatcioglu and Bruneau, 1993).

In recent years, seismic design methodologies have put greater attention on limiting the maximum drift experienced by a structure during earthquake motions. Also, it is essential to protect the non-seismic structural systems, i.e. other structural components in the building that resist gravity forces, and the nonstructural elements such as windows, pipes, etc. Structural walls possess very large in-plane stiffness and provide excellent drift control. From the point of view of economy and drift control, structural walls may become imperative for tall buildings (Paulay and Priestley 1992).

Concrete walls are sometimes categorized into two different types: isolated cantilever walls and coupled walls. As the name suggests, isolated cantilever walls are relatively independent of other walls as the concrete slabs that connect the walls together are not capable of transmitting

significant bending moments. Coupled walls involve two or more walls that are interconnected by coupling beams. A common arrangement of coupled walls is in a central core of a building around the stairway and elevator shafts.

Structural walls in high-rise buildings are usually slender with a height-to-length ratio as high as 10 or 12. The behavior of slender walls is dominated by flexure, and the effect of shear deformations on the overall drift of a slender wall is negligible.

Concrete walls are constructed in a variety of different shapes and sizes. Isolated walls are often rectangular in cross-section, while coupled walls usually have flanges from the intersecting transverse walls. Thus coupled walls often have "I", "C" or "T" shaped cross-sections.

High-rise concrete walls are subjected to significant axial compression due to the self-weight of the wall as well as from the tributary floor area, and can usually sustain considerable lateral forces with only a minimum amount of vertical reinforcement. In Canada, concrete walls are typically reinforced with concentrated vertical reinforcement at the boundary zones and distributed vertical and horizontal reinforcement throughout the wall. The concentrated boundary zones are provided with lateral ties to avoid buckling of the concentrated vertical reinforcement.

1.2 Seismic Analysis of Buildings

In the seismic design of high-rise wall buildings, designers perform one or more of the following analysis procedures to determine the design actions (e.g., bending moments and shears forces) and/or design deformations (e.g., maximum drift).

- Linear static analysis
- Linear dynamic analysis
- Nonlinear static analysis
- Nonlinear dynamic analysis

The linear static analysis method is sometimes used to determine the design forces in low-rise buildings, while the linear dynamic analysis method is commonly used to determine design forces and design deformations in high-rise buildings.

To perform a linear dynamic analysis, designers need to assume an effective flexural stiffness of the concrete wall elements. The flexural stiffness of an uncracked wall is equal to $E_c I_g$ where E_c is the modulus of elasticity of concrete, and I_g is the moment of inertia of the gross (uncracked) concrete section. Once concrete cracks, the flexural stiffness reduces depending on the extent of cracking and the amount of vertical reinforcement. An average (effective) stiffness $E_c\ I_e$ less than the uncracked stiffness is normally used in linear dynamic analysis to account for the effects of cracking.

The commentary to the 1994 Canadian concrete code (CPCA, 1995) suggests using an effective moment of inertia I_e equal to 70% of the gross moment of inertia I_g of the wall section. The commentary to the 1995 New Zealand concrete code (NZS 3101, 1995) suggests a much lower stiffness value. A wall with no axial compression is suggested to have an effective moment of inertia equal to 25% of I_g, while a wall subjected to an axial compression of 10% of $f_c^{'}\ A_g$ (where $f_c^{'}$ is the concrete compressive strength and A_g is the gross area of the concrete section) is suggested to have an effective moment of inertia equal to 35% of I_g. Note that this value is half what is recommended in the CPCA Handbook. The Council on Tall Buildings and Urban Habitat (Council, 1992) recommends a stiffness value that is a linear function of the axial compression. For a wall subjected to an axial compression of 10% of $f_c^{'}\ A_g$, the effective moment of inertial is equal to 70% of I_g. The NEHRP Guidelines for the Seismic Rehabilitation of Buildings (FEMA 273) suggests stiffness values of 80% of I_g and 50% of I_g for uncracked and cracked concrete walls, respectively. Figure 1.1 summarizes the different stiffness recommendations that vary by about a factor of three from the highest to the lowest recommendation.

While it is not clear which of the recommended stiffness values should be used, it is certainly clear that the choice of stiffness value will have a very profound influence on the estimated drift of the building. Also, as most designers determine the fundamental period of vibration (and hence the lateral seismic design forces) using linear dynamic analysis, the choice of flexural stiffness may have a significant influence on the lateral seismic design forces.

In recent years, nonlinear analysis methods have become more common, and are now used relatively routinely in making retrofit decisions on existing structures or in the design of unusual structures. The method can provide valuable information about inelastic demands on the

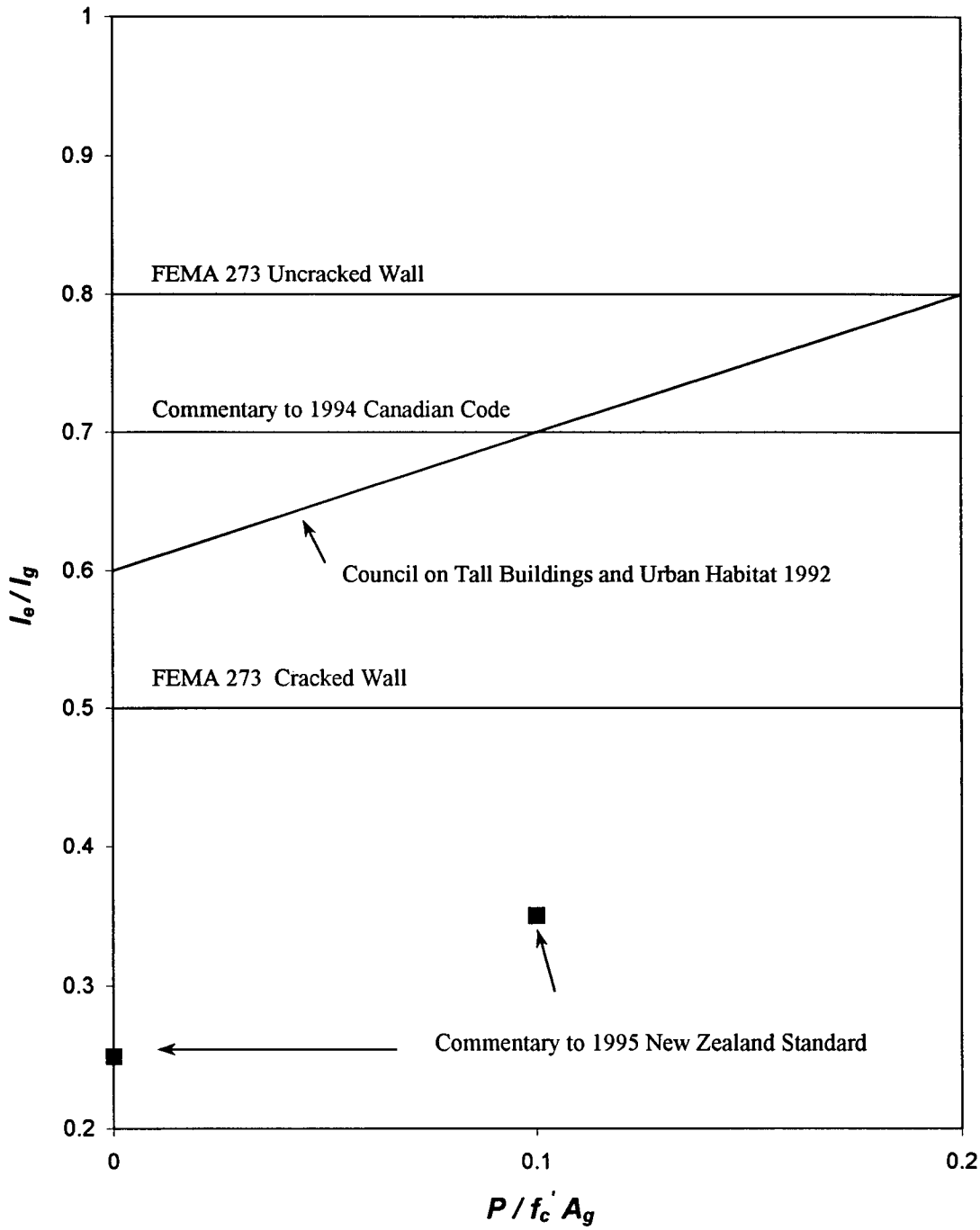

Figure 1.1 Comparison of different recommendations for the effective flexural stiffness of concrete walls.

elements of a structure provided that appropriate nonlinear models are used for the materials. A simple bilinear (elastic-plastic) model is often used for the non-linear static analysis of concrete walls, where the elastic stiffness is equal to the effective stiffness discussed above. Such an approach accounts for cracking in a very approximate way. Nonlinear static analysis provides the opportunity to account for cracking in a much more rigorous way. Unfortunately, the only alternative that currently exists to a simple bilinear model is a fully nonlinear model which greatly increases the complexity of the push-over analysis procedure.

1.3 Objectives of Thesis

The inconsistency in the recommended effective flexural stiffness values for the linear seismic analysis of concrete walls, and the need for a simple nonlinear model for the nonlinear seismic analysis of concrete walls is what led to the current study.

The approach taken in this study is as follows:

- Develop a simple (piece-wise linear) model for the bending moment – curvature response of concrete walls. While maintaining simplicity and transparency, the model should properly account for the influence of cracking on the flexural stiffness of a concrete wall subjected to cyclic loading.
- Conduct a large-scale slender wall test to observe first-hand the behaviour of such elements, and obtain the information needed to validate the proposed model.
- Validate the proposed bending moment – curvature model by comparing predictions of the model with the measured bending moment – curvature relationship.
- Based on the proposed bending moment – curvature model, develop a general method to determine the effective (linear) flexural stiffness of concrete walls.
- Based on the results from the general method for the effective flexural stiffness of concrete walls, study the influence of a variety of parameters on the stiffness of concrete walls, and propose a set of simplified expressions for the effective flexural stiffness of concrete walls.
- Implement the proposed bending moment – curvature model into a nonlinear static analysis program.
- Further validate the proposed concrete wall model by comparing the predicted load-deformation relationship with the measured response of the wall.

- Demonstrate the use of the proposed concrete wall model by predicting the nonlinear static response of a high-rise coupled wall system currently being constructed near the city of Seattle. The nonlinear static analysis was used to assess the ductility of the coupled wall system.

1.4 Organization of Thesis

This thesis is divided into six chapters. Chapter Two presents the theoretical piece-wise linear bending moment – curvature model for concrete walls. Chapter Three presents the results of a large-scale slender wall test conducted to validate the theoretical model. Chapter Four presents the use of the nonlinear model in determining the effective linear flexural stiffness of concrete wall sections. A general, as well as a simplified, method to determine the flexural stiffness of concrete walls is presented. Chapter Five illustrates the use of the proposed concrete wall model in the push-over analysis of wall structures. Numerical techniques required to implement the flexural model into a nonlinear analysis program are shown. Both isolated (cantilever) and coupled wall system examples are provided to illustrate the model. Chapter Six summarizes the work and the conclusions drawn from this study and provides recommendations for further work.

Chapter 2

Nonlinear Flexural Stiffness Model for Concrete Walls

2.1 Introduction

One of the primary objectives of this work is to study in depth the nonlinear flexural response of concrete walls and develop a simple model to account for the influence of cracking on the flexural stiffness.

The flexural response is expressed as the relationship between the applied bending moment and the gradient of the strain distribution along the wall cross section (i.e., curvature). The slope of this nonlinear relationship gives the actual stiffness properties of the concrete section characterizing the effect of cracking on the element stiffness. Also, flexural deformations of a concrete member can be estimated from the same relationship. The rotation and deflection between two points on a concrete element are determined from the integration of the curvature distribution along the member length.

The nonlinear bending moment-curvature relationship for a section is determined using an analysis procedure that satisfies the requirements of strain compatibility, equilibrium of forces, and the stress-strain relationships. The analysis procedure is based on the assumption that plane sections remain plane after bending (i.e., linear longitudinal strain distribution) and that the stress strain relationships for concrete and steel are known. The analysis involves determining the depth of the neutral axis that satisfies axial equilibrium (resultant of concrete and reinforcement stresses equals the applied axial load) at each curvature value and then calculating the corresponding bending moment.

Details of this well known analysis procedure and the stress-strain relationships used in this thesis for concrete and steel are summarized in Appendix A. Note that the stress-strain relationship for concrete in tension is discussed in detail later in this chapter.

The plane sections analysis procedure was implemented in a computer program "*Wall-Tools*" (See Appendix G) and the program was used to generate the bending moment-curvature relationships shown in the subsequent figures.

Simple piece-wise linear (bilinear or trilinear) bending moment - curvature relationships have been used in the literature to idealize the actual nonlinear relationship for various concrete elements: beams; columns; walls; etc. (among them: Park and Paulay 1975, Charney 1991, Paulay 1997, Heidebrecht et al. 1999). See Figure 2.1-a. Recently, Priestley and Kowalsky 1998 and Priestley 2000, suggested a bilinear bending moment-curvature relationship in which the linear elastic response is connected to the yield curvature (assumed constant for each concrete element) and the post elastic response (i.e., the ultimate moment capacity) is flat. Recommendations for the yield curvatures were introduced for different concrete elements: beams; circular columns; rectangular columns; and rectangular walls as illustrated in Fig. 2.1-b.

In the following, a typical response of a wall section in a high rise building is illustrated. The effect of the tensile stresses in cracked concrete is examined and the influence of several parameters on the elastic segment of the response is studied. A piece-wise linear bending moment-curvature relationship (model) is introduced and the necessary information to compute the relationship for any wall section is presented. The flexural model was originally developed for high-rise walls, but is general enough to provide a better representation of the flexural response of any concrete wall section.

2.2 Typical Bending Moment-Curvature Relationship of a Wall Section

Wall sections are subjected to axial compression due to gravity load from the tributary floor area in addition to its own self-weight. Unlike columns in high rise buildings which are subjected to high axial compressive forces, walls are subjected to compression forces that are well below the balanced point on the axial force-bending moment interaction curve. The axial compression acting on a wall ranges up to 20% of the product of concrete compressive strength, f_c', and gross area of the cross section, A_g.

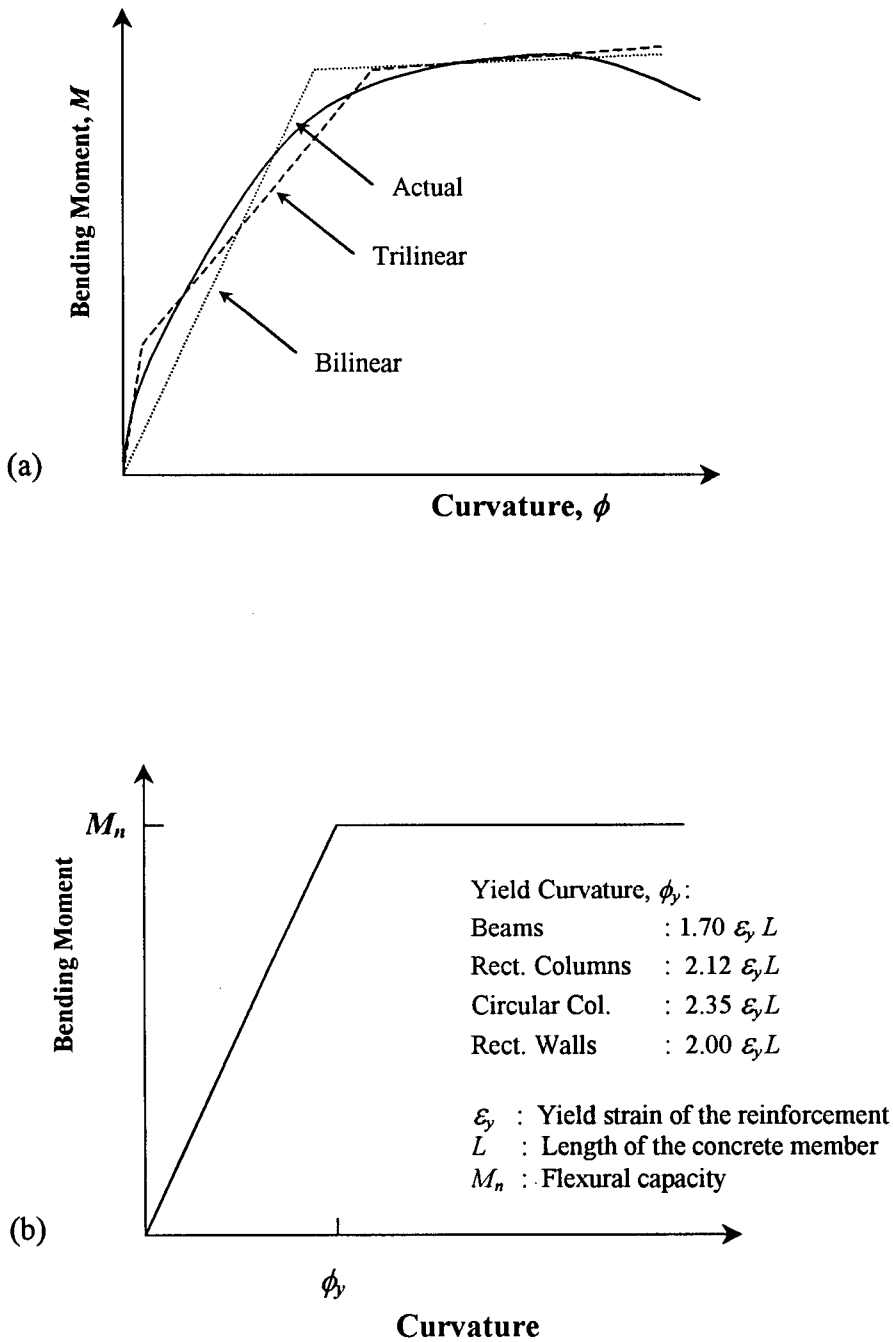

Figure 2.1 Bending moment – curvature relationships for reinforced concrete members: (a) some simple piece-wise linear models compared to the actual nonlinear curve, (b) bilinear model suggested by Priestley and Kowalsky 1998, and Priestley 2000.

Figure 2.2 depicts a typical bending moment-curvature relationship for a wall section in a high-rise building subjected to monotonic loading. When the bending moment is applied to the concrete wall section, the initial response is the linear elastic with the flexural stiffness (rigidity) equal to the well known gross section property of E_cI_g. As the bending moment increases beyond the initial elastic range, first cracking occurs and the flexural stiffness reduces by further growth of the first crack and initiation of additional cracks. The slope of this phase of the response was found to be approximately parallel to the well known flexural stiffness of the cracked transformed section E_cI_{cr} (where I_{cr} is the cracked transformed section moment of inertia) for typical wall sections. Low axial compression in the wall section and therefore linear concrete stresses along the wall section at this stage of loading is the reason (i.e., concrete compressive stresses are predominantly linear in the cracked-elastic phase of loading). Further increase of the applied moment results in yielding of the reinforcement and hence reaching the ultimate capacity of the under-reinforced concrete section.

The bilinear bending moment curvature model suggested by Priestley and Kowalsky 1998, and Priestley 2000, is compared with the predicted relationship for the rectangular wall section in Figure 2.3-a and for a bridge column (pier) section in Figure 2.3-b. While the suggested bilinear model is reasonable for the bridge column section, the model does not provide a good representation of the elastic deformation of the wall section.

A combination of high initial stiffness of the wall response and light amount of the vertical reinforcement (often in high-rise buildings) makes the predicted bending moment-curvature response fairly trilinear and therefore, it is inappropriate to use a bilinear model connecting to the yield curvature for wall sections in high-rise buildings. In other words, the elastic linear stiffness of the wall response is not properly captured if estimated as the capacity of the wall section divided by the yield curvature.

2.3 - Tensile Stresses of Cracked Concrete

When concrete cracks, all the tension stresses are carried by the steel reinforcement at the cracked sections. Between cracks and due to bond between the concrete and steel, some tensile stresses are transferred from steel to the surrounding concrete. As a result, reinforcement stresses are less between cracks than its maximum values at the crack, and clearly the concrete

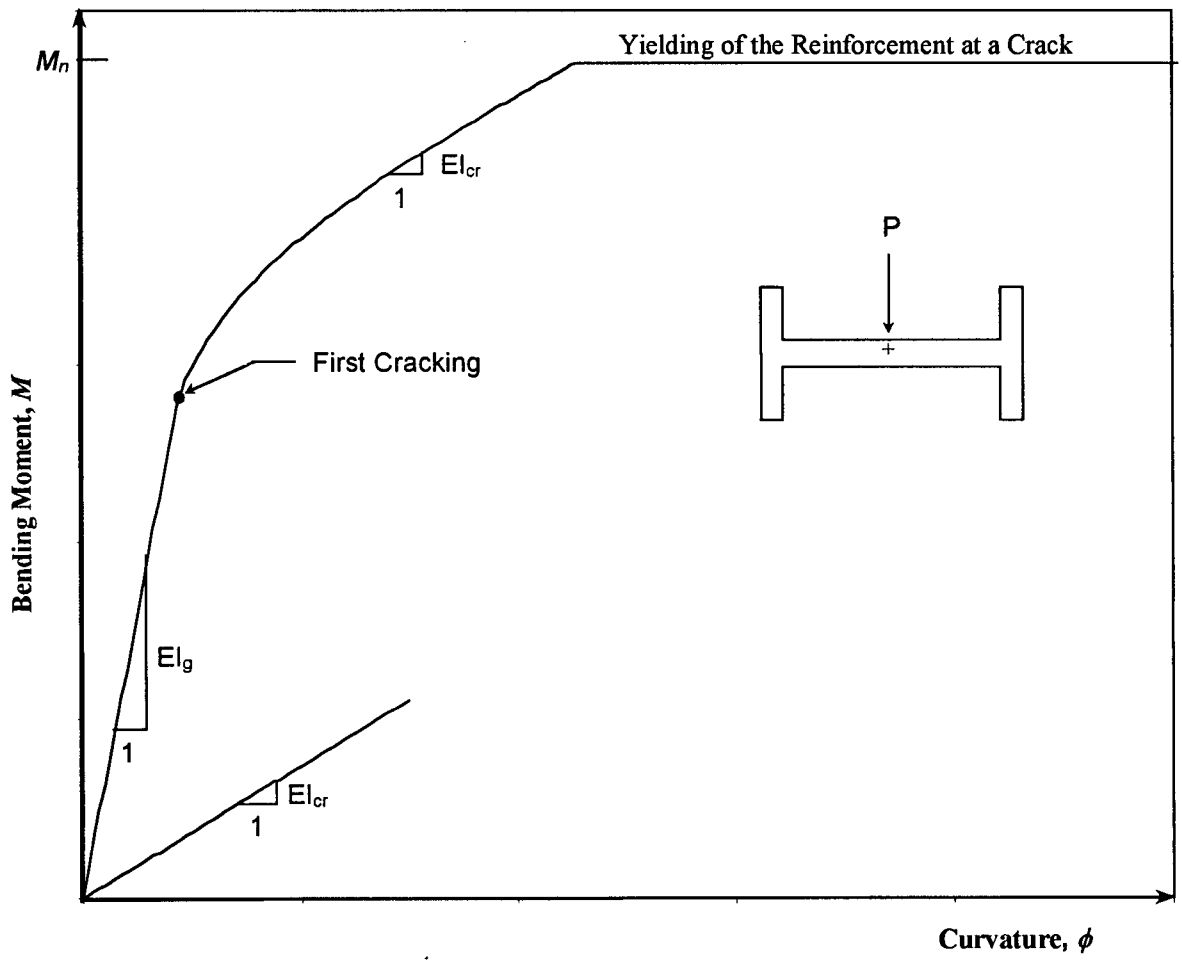

Figure 2.2 Typical bending moment - curvature relationship for a wall section in a high-rise building.

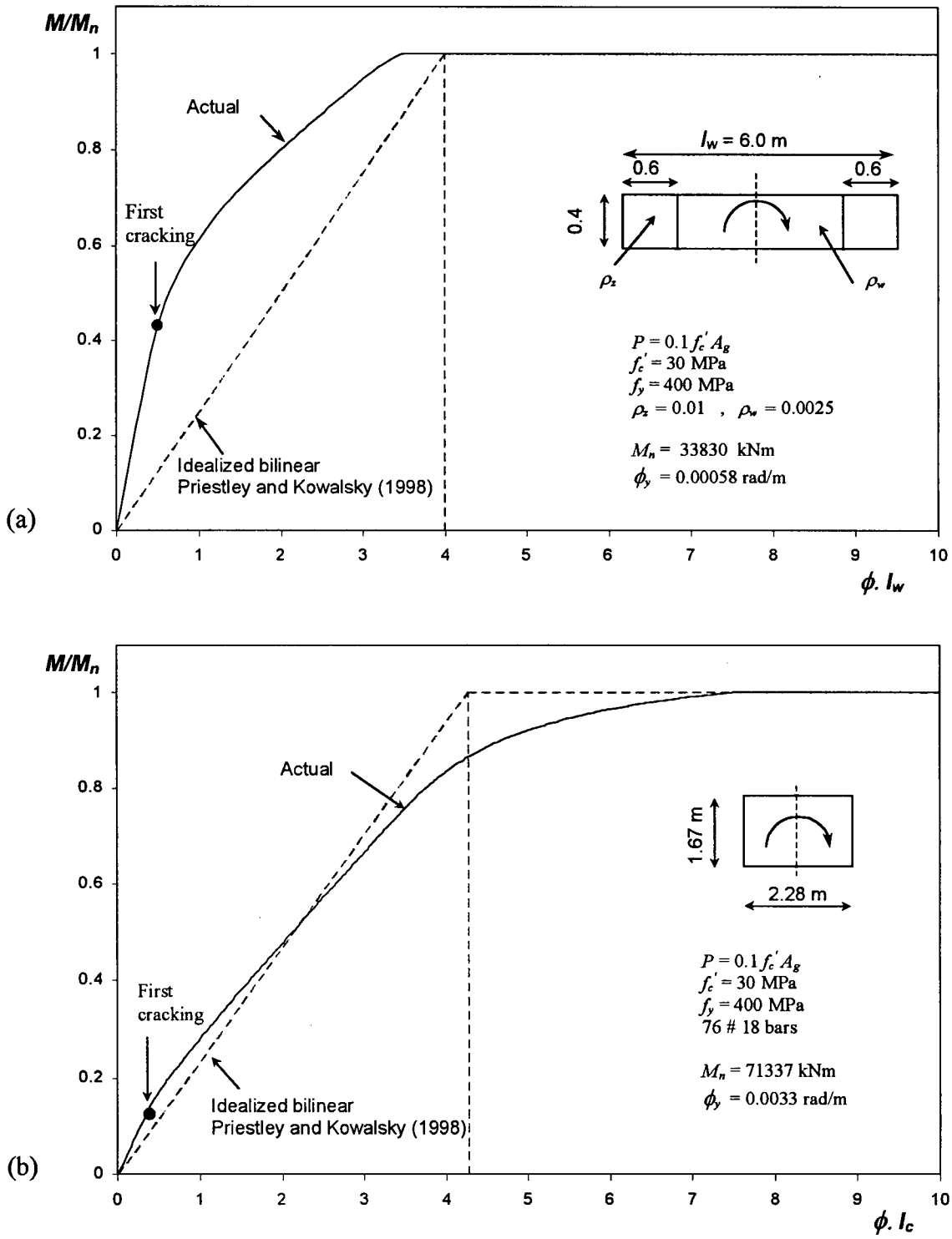

Figure 2.3 Bending moment - curvature relationships for: (a) a typical rectangular wall in a high-rise building, (b) a typical bridge pier.

stiffness (rigidity) is greater between cracks than at the crack itself (Figure 2.4), a phenomenon known as tension-stiffening.

A fundamental approach to account for the tension stiffening effect is to use the average stress-average strain relationship for concrete in tension (Vecchio and Collins, 1986). The average strain is less than the maximum strain at a crack, and since the capacity of reinforced concrete member is limited by the capacity of reinforcement at a crack where there are no tensile stresses, a separate crack check calculation is necessary to determine the capacity of reinforced concrete member whenever an average stress-average strain formulation is used.

An experimental investigation conducted at The University of British Columbia (Fronteddu and Adebar 1992) involved tests on a series of 1.50 m long elements with 8-20M reinforcing bars and varying cross-sectional dimensions to study the tension stiffening characteristics of concrete under monotonic and reverse cyclic axial load. The test specimens may be considered full-scale elements from a portion of a concrete wall. The elements were subjected to known values of axial tension, and the resulting average tensile strains were measured. The force resisted by the reinforcement was calculated from the measured strain and the bare bar stress-strain relationship. This force was subtracted from the total force to determine the force resisted by the concrete in tension. The average concrete stress at a particular strain level was determined by dividing the calculated concrete force by the concrete cross-sectional area. Comprehensive study and analysis of the test results can be found in Fronteddu, 1993.

Figure 2.5-a shows an example average stress-average strain relationship for concrete in tension determined by the above-described procedure for an element subjected to monotonic tension. When the crack first formed during the test, there was only a small reduction in the average concrete tensile stress over the entire length of the element. As additional cracks developed, the average concrete tensile stresses reduced further, however, even after the concrete was severely cracked, the average concrete tension stress (the tension stiffening effect) did not completely disappear.

Fig. 2.5-b shows an average stress-average strain relationship for concrete in tension determined from an element subjected to cyclic loading. The envelope of the cyclic average stress-average strain relationship is very similar to the monotonic relationship. Unloading and reloading of the

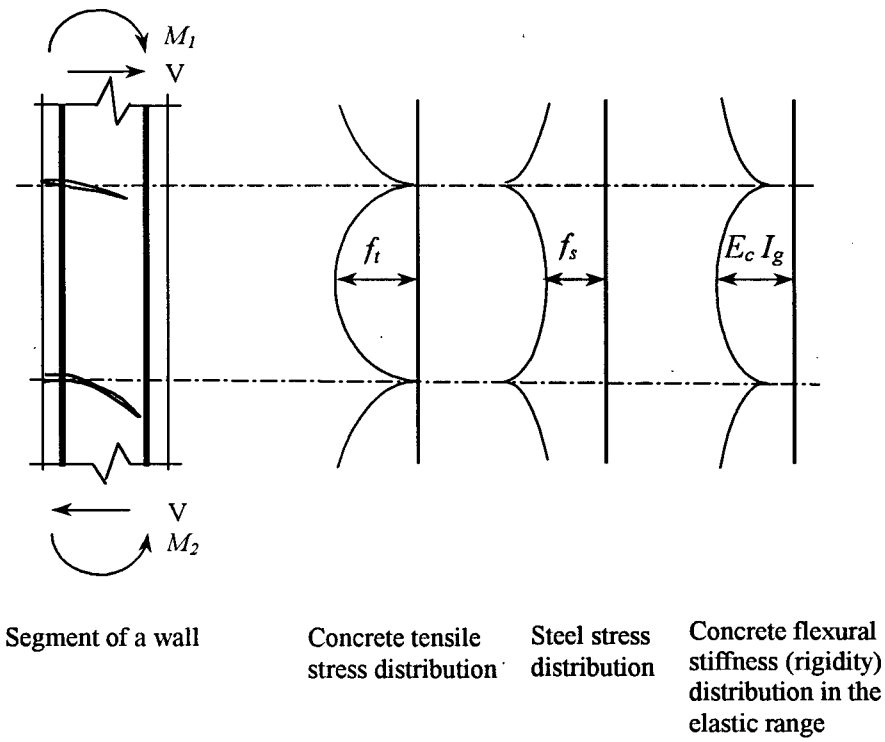

Figure 2.4 Tension stiffening effect of a cracked reinforced concrete wall element.

concrete specimen followed a reduced slope (i.e., softer path) than the initial slope (concrete modulus of elasticity in this case). The unloading and reloading slope continues to reduce further as the concrete is subjected to higher strain. Fig. 2.5-c shows a simplified model for the average stress-average strain relationship for concrete under cyclic tension, where the small residual strains under zero stress are ignored for simplicity. Prior to cracking, concrete is an elastic material. After cracking, the unloading and reloading path, i.e., the slope of the average stress-average strain relationship, depends on the maximum tensile strain previously reached. A similar model for the average stress-average strain relationship has been suggested by Vecchio 1999.

2.4 Bending Moment-Curvature Response Under Monotonic Loading

The monotonic average stress-average strain relationship for concrete in tension (Figure 2.5-a) is combined with the stress-strain relationship for concrete in compression and the stress-strain relationship for reinforcement (illustrated in Appendix A) to develop the relationship between the applied bending moment and the curvature for a typical wall section subjected to a variety of applied axial compression and amount of vertical reinforcement (see Figure 2.6).

As mentioned earlier, the slope of the initial portion of the relationship depends only on the concrete geometry and is equal to E_cI_g.. The extent of the initial linear response depends on the concrete tensile strength and the axial compression acting on the wall. Increasing the applied axial compression increases the wall flexural capacity and extends the initial linear elastic response of the wall section (Fig. 2.6-a). The secondary slope of the bending moment-curvature relationship depends on the concrete geometry and the amount of the vertical reinforcement and is approximately equal to the flexural stiffness of the cracked transformed section, E_cI_{cr}.

Increasing the amount of the vertical reinforcement in the tension side of the wall section increases the secondary slope of the bending moment-curvature relationship as well as the flexural capacity of the section (see Fig. 2.6-b). The point at which the bending moment-curvature relationship becomes nonlinear does not change significantly with increasing the reinforcement amount.

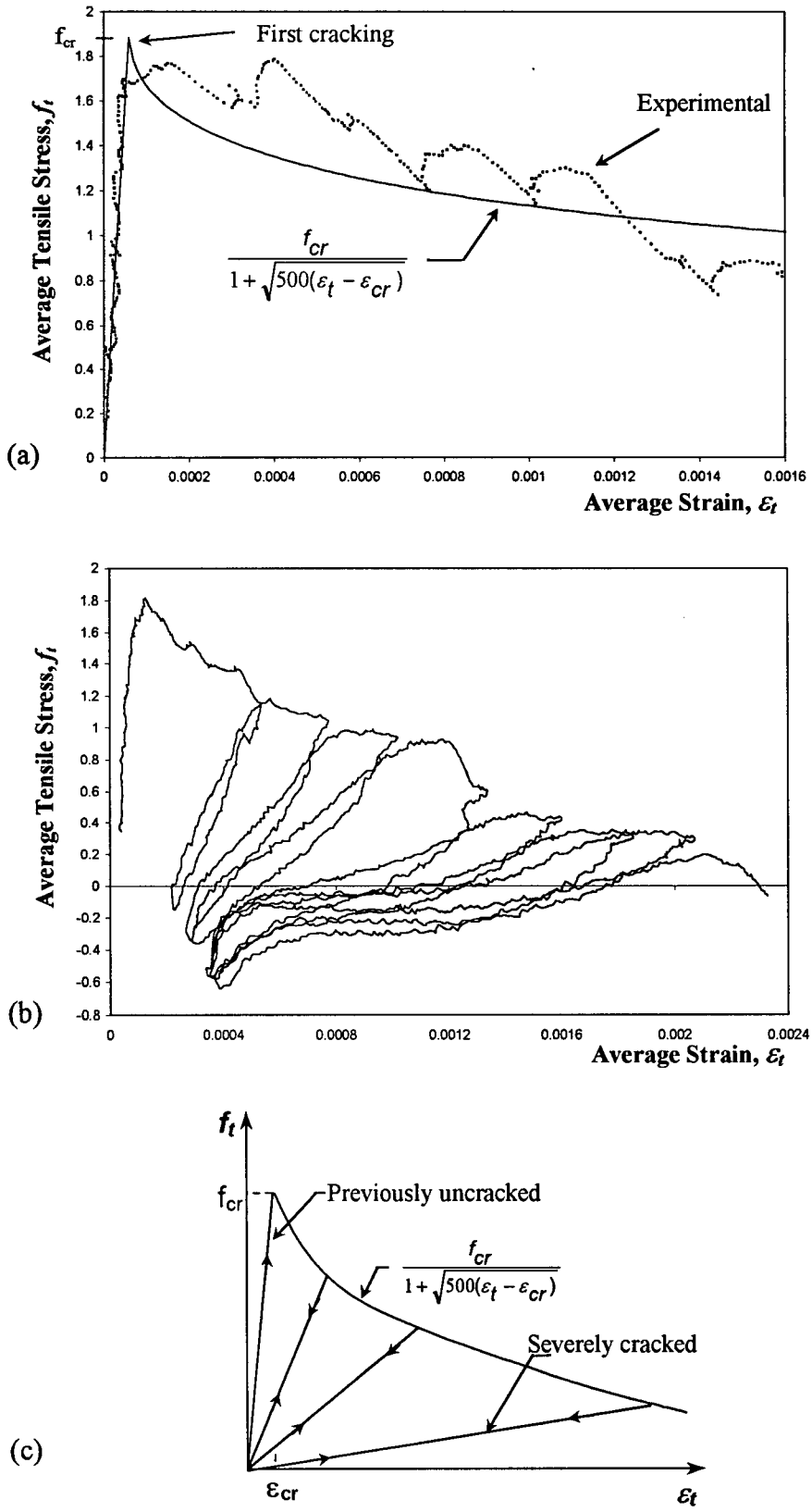

Figure 2.5 Response of concrete in tension (experimental results from Fronteddu, 1993): (a) monotonic loading (predicted and observed), (b) cyclic loading, (c) proposed model for cyclic loading.

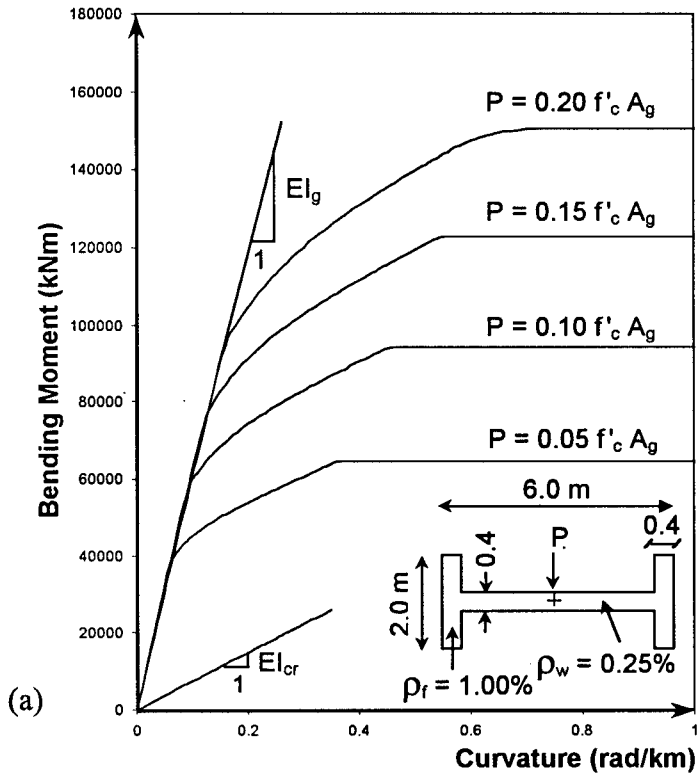

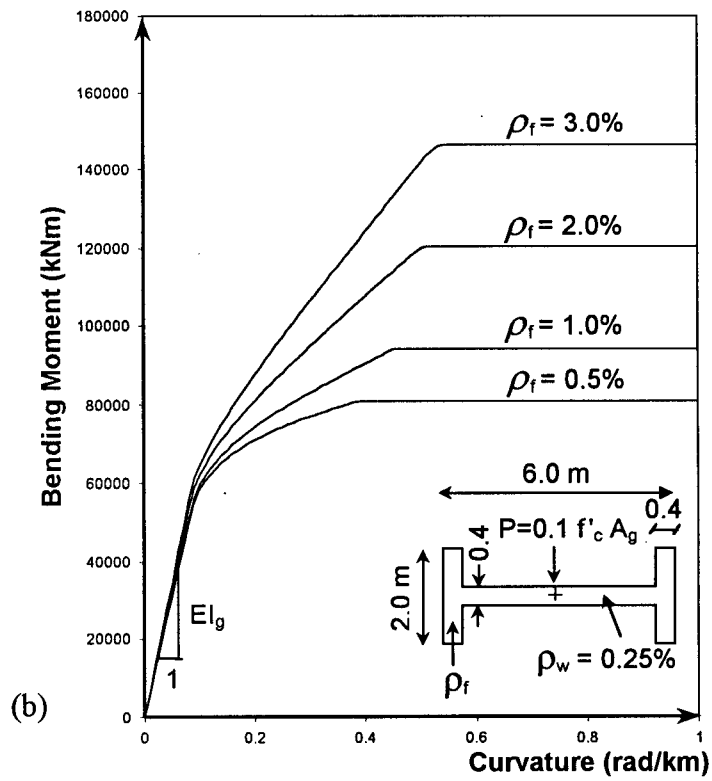

Figure 2.6 Bending moment-curvature relationships for typical concrete walls subjected to monotonic loading: (a) influence of axial compression, (b) influence of reinforcement.

2.5 Bending Moment-Curvature Response under Cyclic Loading

Figure 2.7-a shows the bending moment-curvature response of a typical wall section subjected to increasing cycles of bending. The wall response during any one cycle of loading depends on how far the wall was loaded in the previous cycle. Therefore, the tensile strain at each layer along the wall was recorded for each load cycle. As the tensile strain for a particular load cycle varies at each concrete layer, the average stress-average strain relationship varies at each layer according to the relationship shown in Fig. 2.5-c.

The different average tensile stress-average tensile strain relationships recorded in each load cycle and used in the prediction of the consecutive cycle are shown in Fig. 2.7-b. These relationships are shown and labeled only for the outer layer of the wall section. Interior wall layers (next to the outer fiber) have experienced less tensile strain in the previous cycle and therefore have more tensile stress. This is depicted by the dotted lines on the average stress-average strain relationship for each load cycle.

Figure 2.7 indicates that during an earthquake motion, a wall section would experience a response that is bounded by two extremes, a "previously uncracked" section response in which there are significant concrete tensile stresses, and a "severely cracked" section response in which there are very little residual concrete tensile stresses. The severely cracked response is different than the response predicted by completely ignoring the concrete tensile stresses (Fig. 2.7-b, label D and E).

The change of section response due to extensive cracking during the earthquake motion degrades the flexural stiffness of a wall building and as a result, lengthens the building period, a well known effect long recognized in the literature (e.g., Paulay and Priestley, 1992). More elaborate discussion follows in Chapter 4.

Note that in making the prediction of the bending moment-curvature relationships shown in Figure 2.7-a, only the influence of cyclic loading on degrading the tensile stresses of concrete was considered. Cyclic response of concrete in compression and of the reinforcement are known to result in residual strains at zero load upon reloading to an increased deformations. An investigation carried out (in Appendix B) on a typical wall section showed that the residual strains are small and the resulting relationships are only slightly offset from the origin and

therefore these can be ignored without significantly affecting the results. This assumption is discussed further in Chapter 3, Section 3.8.

2.6 Trilinear Bending Moment-Curvature Relationship for Concrete Walls

It is proposed that the bending moment-curvature response of a wall section including the effect of axial compression acting on the wall, the amount of vertical reinforcement and the state of cracking (i.e., tension stiffening effect) can be represented by a simple trilinear relationship.

The trilinear relationship that represents the stiffest response that the wall would experience if loaded monotonically to failure without having been previously cracked (i.e., previously uncracked response) is termed *upper-bound* response. The trilinear relationship that represents what is observed when the wall is reloaded after being severely damaged from a previous load cycle (i.e., severely cracked response) is termed *lower-bound* response (See Figure 2.8).

Both the upper-bound and lower-bound trilinear relationships are defined by four parameters: the slope of the elastic linear response (first linear segment) E_cI_g , the slope of the second linear segment (secondary slope), E_cI_{cr} , the bending moment defining the intersection of the first and second linear segments, M_l, and the flexural capacity M_n. In the following, each of the four parameters is described further and a method to determine each parameter is presented.

2.6.1 Slope of the Linear Elastic Response, E_cI_g

The gross moment of inertia, I_g, is easily determined by hand calculations for typical wall sections. The gross concrete geometry is normally used as the effect of typical reinforcement amount is negligible.

The modulus of elasticity of concrete, E_c, has several definitions and several formulae in the literature. The secant modulus of elasticity at a stress of $0.4f_c'$ is adopted in this thesis and the expression used is the one adopted by CSA Standard A23.3-94.

$$E_c = (3300\sqrt{f_c'} + 6900)(\gamma_c / 2300)^{1.5} \qquad [2.1]$$

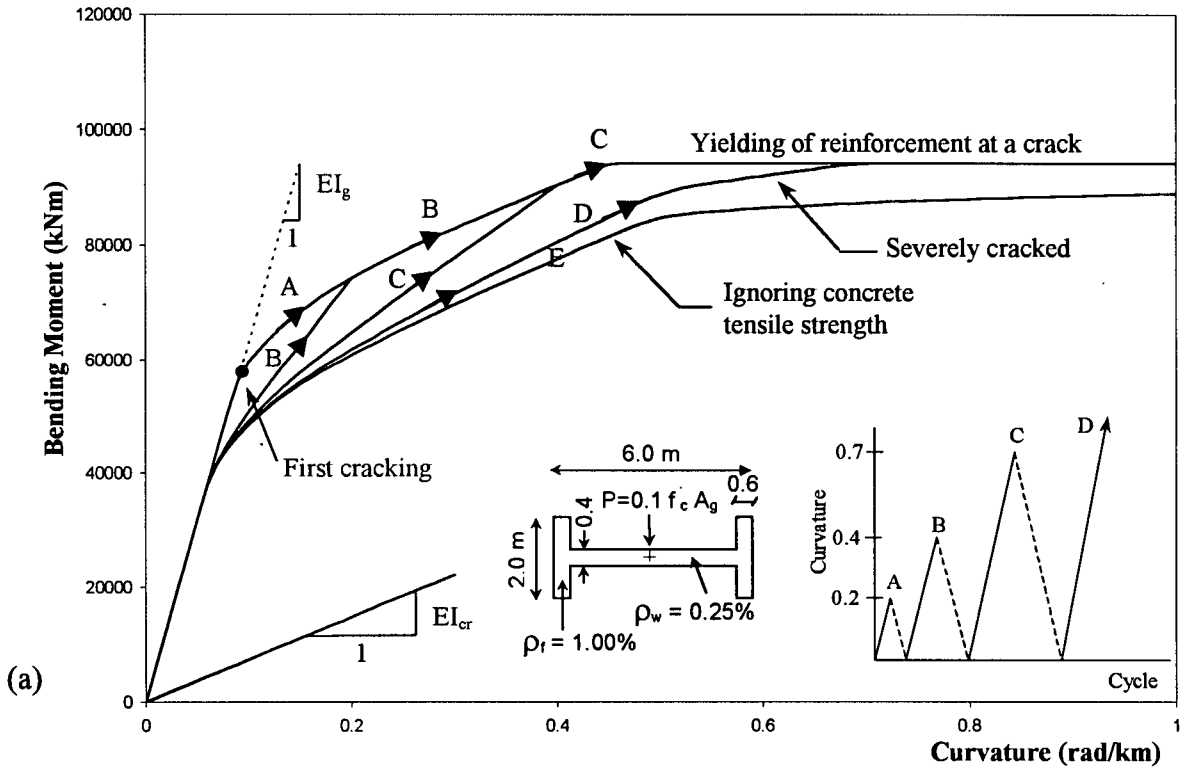

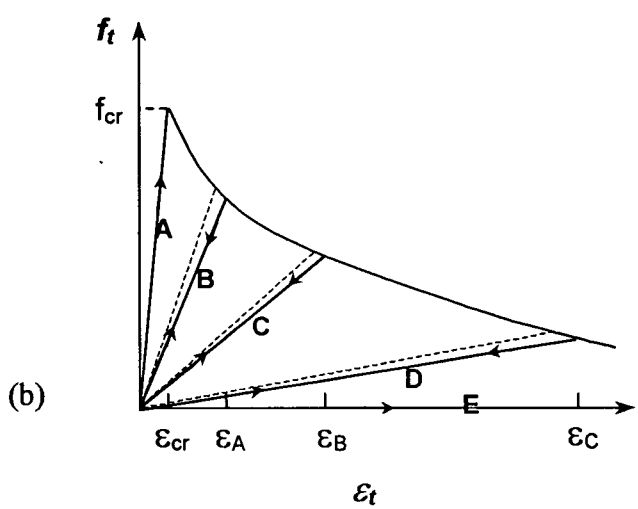

Curvature (rad/km)	Max. tensile strain previously reached:
$\phi_A = 0.2$	$\varepsilon_A = 0.00059$
$\phi_B = 0.4$	$\varepsilon_B = 0.0016$
$\phi_C = 0.7$	$\varepsilon_C = 0.0037$

Figure 2.7 Predicted influence of cyclic loading on: (a) bending moment - curvature relationship of a typical concrete wall, (b) the tension stress-strain relationship for the most highly strained concrete in the wall.

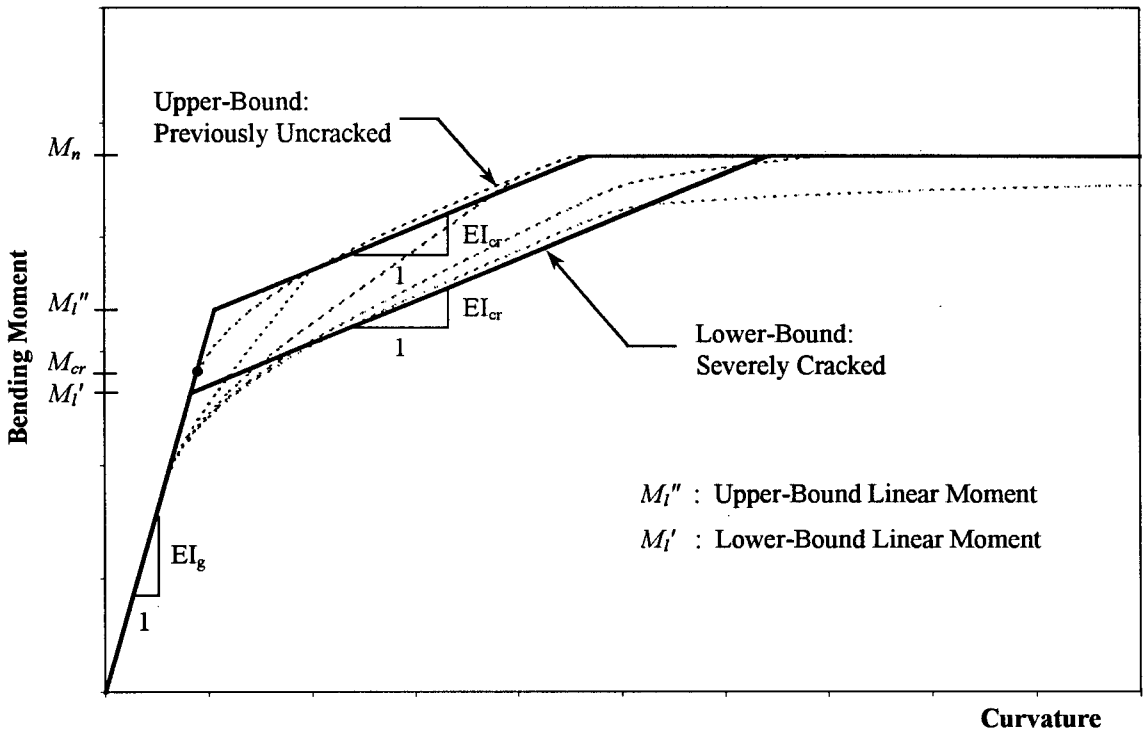

Figure 2.8 Upper-bound and lower-bound trilinear approximations to the bending moment-curvature relationships for a typical concrete wall subjected to cyclic loading.

Where E_c is the modulus of elasticity in MPa, γ_c is the mass density of concrete in kg/m^3, and f_c' is the specified compressive strength in MPa. For normal density concrete (γ_c = 2400 kg/ m^3), having a compressive strength less than 40 MPa, the following expression can be also used.

$$E_c = 4500\sqrt{f_c'} \qquad [2.2]$$

2.6.2 Slope of the Second Linear Segment, E_cI_{cr}

The secondary slope of the trilinear bending moment-curvature relationship depends primarily on the concrete geometry and the amount of reinforcement. This slope is assumed to be equal to the flexural stiffness of the cracked transformed section, E_cI_{cr}. The value of E_cI_{cr} for a wall section of arbitrary shape and reinforcement arrangement can be computed using a plane section analysis program and is equal to the initial slope of the bending moment-curvature relationship for zero axial load and no tensile stresses in the concrete.

The cracked section moment of inertia, I_{cr}, can easily be calculated for a rectangular section with concentrated tension reinforcement. Complex wall geometry with distributed vertical reinforcement makes the calculation of I_{cr} difficult. Appendix C illustrates the detailed calculation of I_{cr} for a general flanged wall section.

Figure 2.9 is a design chart that can be used to determine I_{cr} for rectangular and flanged wall sections. Program "*Wall-Tools*" was used to generate the data for the chart.

For rectangular walls (Fig. 2.9-a), the reinforcement area in the boundary zone and in the web, and the length of the concentrated boundary zone are required to determine the value of I_{cr}. Figure 2.9-a may also be used for a T-shaped wall in which the flange is on the tension side. The reinforcement in the tension flange is considered as the area of reinforcement in the boundary zone, A_{sz}..

For flanged walls (Fig 2.9-b), the geometry of the compression flange (width, b_f, and thickness, l_f), the reinforcement in the tension flange expressed as a ratio of the concrete area, ρ_f, and the web geometry (length, l_w, and width b_w) are needed to determine the value of I_{cr}. Although the data for I_{cr} plotted in Fig. 2.9-b was obtained for symmetrical flanged wall sections, the value of

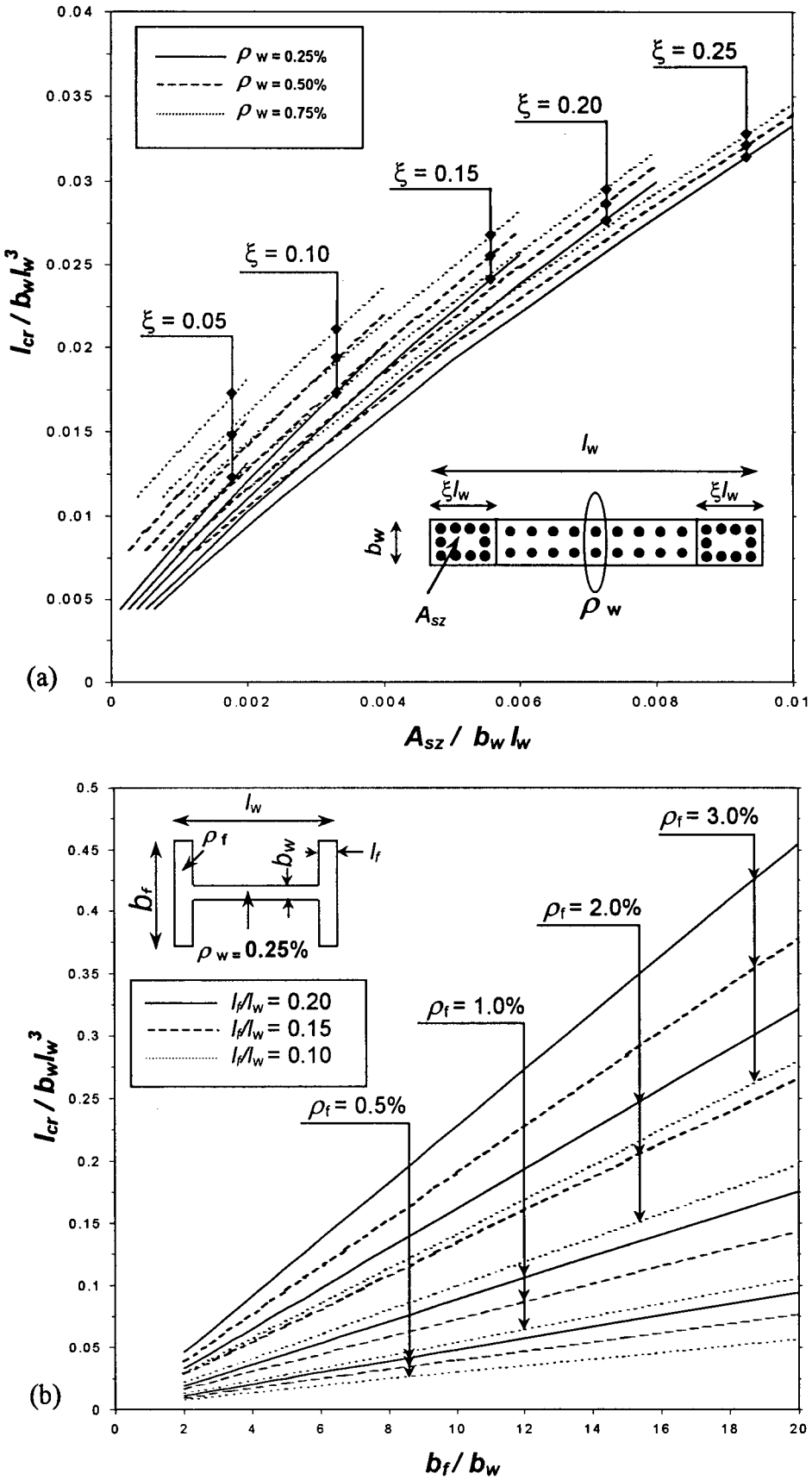

Figure 2.9 Cracked section moment of inertia, I_{cr}, for: (a) rectangular wall sections, and (b) flanged wall sections.

I_{cr} may be approximated for unsymmetrical flanged wall sections by using the geometry of the compression flange to determine b_f / b_w and l_f / l_w and calculate ρ_f from the area of reinforcement in the tension flange divided by the area of the compression flange.

2.6.3 Flexural Capacity, M_n

As mentioned, the flexural capacity of an under-reinforced wall section is limited by yielding of the reinforcement at a crack where no tensile stresses exist in the concrete. The flexural capacity can be determined as the maximum bending moment in the bending moment-curvature response. Alternatively, the ultimate compression strain ε_{cu}, and the stress block factors α_1 and β_1 can be used to determine the strain distribution and the stress resultant along the wall section. This well known procedure is summarized in Fig. 2.10 for completeness. Since an accurate estimate of the flexural capacity is required to determine the corresponding maximum seismic shear, the longitudinal web reinforcement should be accounted for when computing the flexural capacity of a wall section as illustrated in Fig. 2.10.

2.6.4 Linear Bending Moment, M_l

The linear bending moment, M_l, is the bending moment that defines the transition from the primary slope E_cI_g (first linear segment) to the secondary slope E_cI_{cr} (second linear segment) of the trilinear bending moment-curvature relationship. This bending moment is influenced by the amount of axial compression acting on the wall and the tension stiffening effect of concrete. A rigorous approach to determine the M_l value is to define a trilinear bending moment-curvature relationship (with the other three parameters previously defined) that has the same area under the curve as the actual nonlinear bending moment-curvature relationship. This approach requires the determination of the actual nonlinear bending moment-curvature relationship using plane sections analysis. Integrating the area under the actual nonlinear relationship and making it equal to the area under the trilinear relationship gives a quadratic equation for M_l. Solution of this equation is shown in Appendix D.

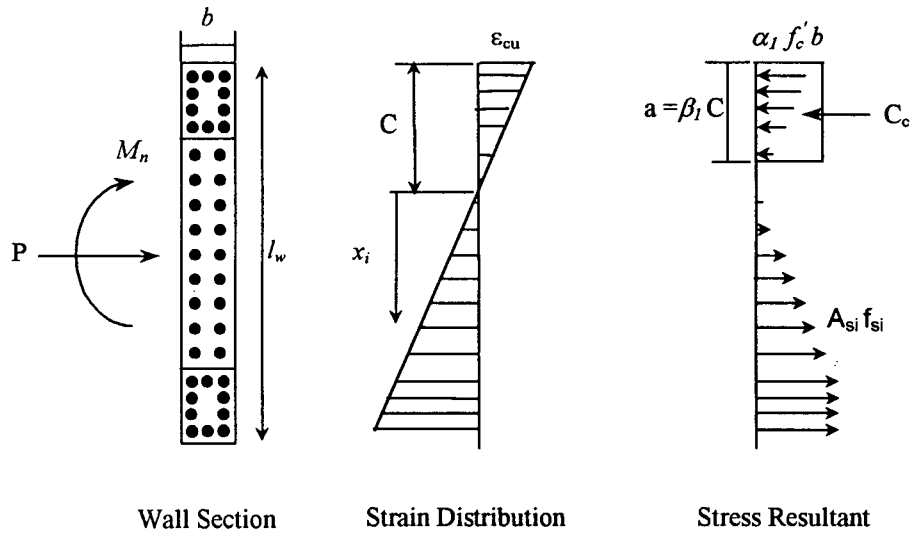

(I) Assume depth of neutral axis, C, & $a = \beta_1 . C$

(II) $\varepsilon_{si} = \varepsilon_{cu} . \frac{C - x_i}{C}$

$f_y \geq f_{si} = E_s . \varepsilon_{si} \geq -f_y$

(III) $C_c = \alpha_1 f_c' \; a \; b$

(IV) If : $C_c + \sum A_{sc} f_{si} = P$

Then : $M_n = C_c [C - a/2] + P (l_w/2 - C) + \sum A_{sc} f_{si} (C - x_i)$

Else : Repeat from Step (I)

Where: (from CSA-A23.3-94)

$\varepsilon_{cu} = 0.0035$; $\alpha_1 = 0.85 - 0.0015 \; f_c' \geq 0.67$; $\beta_1 = 0.97 - 0.0025 \, f_c' \geq 0.67$

Figure 2.10 Procedure to determine the flexural capacity, M_n, of a typical wall section.

A trilinear bending moment-curvature relationship that has the same area under the curve as the actual nonlinear relationship makes the rotation of a wall segment along the height of the building being similar whether computed by the actual nonlinear relationship or the trilinear relationship. Further discussion and use of this concept is illustrated in Chapter 5.

The approach of equal area under both the nonlinear and trilinear curves can be used to determine the value of M_l for both the upper-bound and lower-bound responses. The linear bending moment for upper-bound response, designated as M_l'', is obtained when integrating the area under the actual nonlinear upper-bound response (i.e., previously uncracked section with monotonic tensile stresses in concrete; envelope of Fig. 2.7-a). The linear bending moment for lower-bound response, designated as M_l', is obtained when integrating the area under the actual nonlinear lower-bound response (i.e., severely cracked section with little tensile stresses; Fig 2.7-a case D). Since the maximum tensile strains reached in the previous load history are not known, the average tensile stress-average tensile strain relationship is not uniquely defined. Therefore, the actual nonlinear bending moment-curvature relationship that is calculated by completely ignoring the concrete tensile stresses (Fig. 2.7-a case E) is modified to account for some residual tensile stresses in the concrete and used for the integration procedure. The actual nonlinear bending moment-curvature relationship with zero tensile stress is modified so that the fairly rounded part of the curve is ignored and the somewhat linear secondary slope is extended to intersect the ultimate flexural capacity M_n (see Fig. 2.8). It is interesting to note that the linear bending moments (M_l'' and M_l') are different from the first cracking moment, M_{cr}, as shown in Fig. 2.8.

The rigorous method just described for determining M_l was incorporated in program "*Wall-Tools*" and the program was used to generate the data for different wall sections as shown in Fig. 2.11. For each wall section with certain material properties and given axial compression, "*Wall-Tools*" computes E_cI_g, E_cI_{cr} and M_n; determines the actual nonlinear moment-curvature relationship; integrates the area under the nonlinear relationship; and finally determines the best-fit value of M_l (that gives the same area under both relationships). Each wall section was run for a variety of axial compression values and the results of the linear bending moment (both upper-bound and lower-bound) are plotted in Fig 2.11.

The results in Figure 2.11 show that M_l is approximately a linear function of the axial compression (similar to the well-known axial compression-bending moment interaction relationship for under-reinforced sections) and that both upper and lower-bound linear bending moment have nearly the same slope. The influence of tension stiffening on the predicted linear bending moment is transparent in the difference between the upper and lower-bound responses, and can be approximated as a linear relationship as well. Hence, to develop a simple relationship to determine the linear bending moment, M_l, the following expression was used:

$$M_l = C_1.P + C_2.f_{cr} \qquad [2.3]$$

Where, P is the compression force acting on the wall, f_{cr}, the cracking strength of concrete defined conservatively as 0.33 $(f_c')^{1/2}$, and C_1 and C_2 are linear coefficients.

The previous expression resembles the cracking moment, M_{cr}, linear equation:

$$M_{cr} = (\frac{S}{A_g}).P + (S).f_{cr} \qquad [2.4]$$

In which, A_g is the gross concrete area of the wall section, and S is the section modulus (I_g/y) to the tension side of the wall. Thus, the linear bending moment function can be simply expressed as the cracking moment equation with two additional parameters α, and β, to consider the difference in the M_l values from the cracking moment:

$$M_l = \alpha.(\frac{S}{A_g}).P + \beta.(S).f_{cr} \qquad [2.5]$$

As shown in Figure 2.11, the slope of the linear bending moment (as function of P) was nearly equal for both the upper and lower bound M_l and thus α, would be the same for both M_l'' and M_l'. The intercept of the lower-bound linear bending moment function, M_l', was equal to zero as the cracking strength, f_{cr}, was ignored. Therefore, the cracking strength, f_{cr}, may be taken equal to zero or alternatively, β = 0.0 and the second term in the above equation drops out when determining the lower-bound response, M_l'.

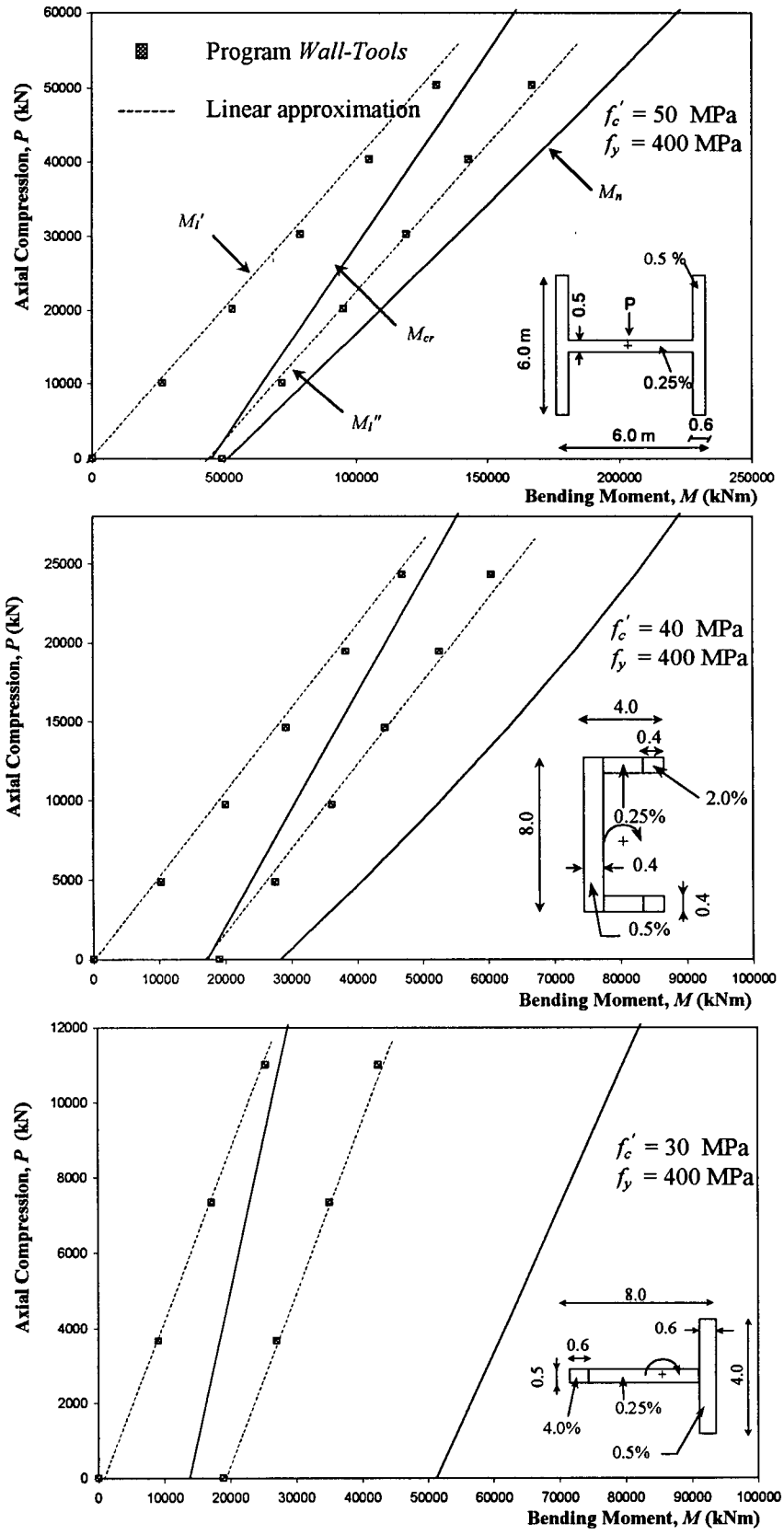

Figure 2.11 Linear approximations to the axial load - bending moment interaction diagrams for the upper-bound and lower-bound M_l values.

To estimate the parameters α, and β (for upper-bound only), program "*Wall-Tools*" was used to determine M_l, using the rigorous method, for numerous wall sections with various concrete geometry and reinforcement amount and arrangement (Fig. 2.12). Each wall section was run for different material properties (concrete compressive strength f_c' ranging from 30 to 60 MPa, and the corresponding E_c and f_{cr}). In each analysis, both the upper and lower bound M_l was determined for a range of axial compression on the wall.

Data points obtained for M_l for the different axial compression levels in each analysis were fitted to a straight line using the least squares method. The slope of the fitted M_l linear function divided by the slope of the cracking moment function (S/A_g) gives the parameter α, and the intercept of the fitted linear function divided by the cracking moment at zero axial compression ($S f_{cr}$) determines the parameter β.

Figures 2.13 and 2.14 show the variation of the parameters α, and β, plotted against the geometrical properties of the wall sections. Figure 2.13 indicates that the trend of the parameter α, can be approximated by the following expression:

$$\alpha = 1.0 + 0.08 \cdot \left(\frac{l_w . A_g}{S} \right) \qquad [2.6]$$

where l_w, is the length of the wall section.

Figure 2.14 shows the scatter of the data for the parameter β with respect to the geometry of the wall section (note that $\beta = 0.0$ for the lower-bound predictions and the data shown are only for the upper-bound linear bending moment). Despite the large scatter of β values (ranging from approximately 1.0 to 3.0), it has little effect on the predicted M_l value for the upper bound response, particularly if the wall is subjected to a relatively high axial compression. A β of 1.5 is suggested for the upper-bound M_l value (M_l'').

Incorporating Equations [2.5] and [2.6] and the suggested values of β, a simple relationship to determine M_l is as follows:

$$M_l = \left(\beta . f_{cr} + \frac{P}{A_g} \right) S + 0.08 P l_w \qquad [2.7]$$

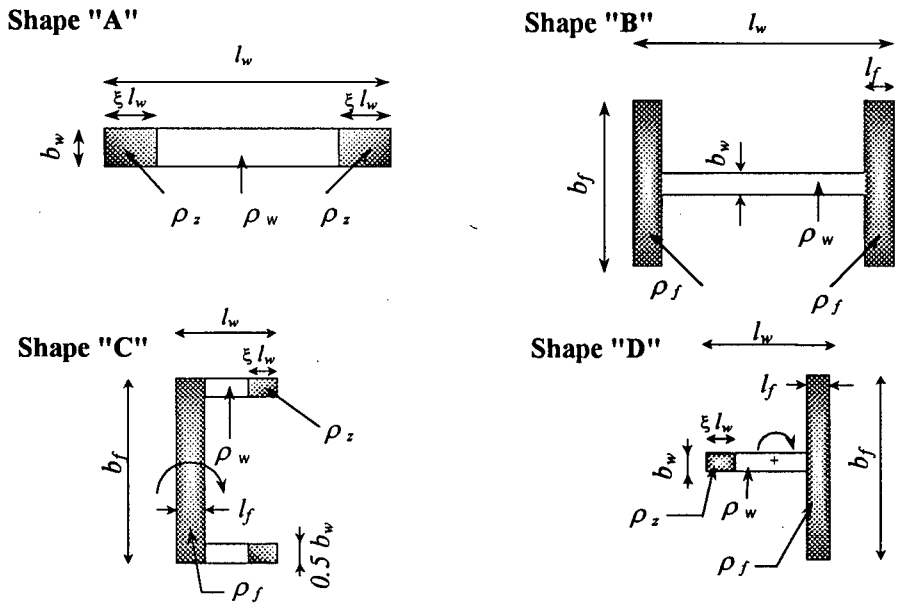

Shape	l_w (m)	l_f (m)	b_f (m)	b_w (m)	$\xi\, l_w$ (m)	ρ_f (%)	ρ_w (%)	ρ_z (%)
A	6.0	-	-	0.4	0.6	-	0.25	2.0
A	4.0	-	-	0.4	0.4	-	0.25	2.0
A	2.0	-	-	0.4	0.3	-	0.25	2.0
A	10.0	-	-	0.9	1.0	-	0.5	3.0
B	6.0	0.4	2.0	0.4	-	2.0	0.25	-
B	4.0	0.4	2.0	0.4	-	0.5	0.25	-
B	10.0	0.6	2.0	0.6	-	0.5	0.5	-
B	6.0	0.5	6.0	0.5	-	1.0	0.5	-
B	4.0	6.0	0.4	0.4	-	0.5	0.25	-
C	3.2	0.4	6.4	0.8	0.4	0.6	0.25	1.9
C	3.58	0.45	10.65	1.62	0.8	0.5	0.25	0.5
C	6.0	0.5	6.0	1.4	0.6	0.5	0.5	4.0
C	6.0	0.5	4.0	1.4	0.6	0.5	0.5	4.0
C	6.0	0.5	2.0	1.4	0.6	0.5	0.5	4.0
C	6.0	0.5	2.0	0.5	0.8	0.5	0.5	4.0
C	4.0	0.5	6.0	1.0	0.6	0.5	0.25	4.0
C	2.0	0.5	6.0	1.0	0.4	0.5	0.25	4.0
C	7.29	0.81	6.35	0.9	0.5	0.64	0.25	3.0
C	1.905	0.56	6.35	0.9	0.35	0.64	0.25	1.5
C	3.75	0.4	6.4	0.4	0.4	0.6	0.25	2.0
D	3.2	0.4	6.4	0.8	0.4	0.6	0.25	1.9
D	3.58	0.45	10.65	1.62	0.8	0.5	0.25	0.5
D	6.0	0.5	6.0	1.4	0.6	0.5	0.5	4.0
D	6.0	0.5	4.0	1.4	0.6	0.5	0.5	4.0
D	6.0	0.5	2.0	1.4	0.6	0.5	0.5	4.0
D	6.0	0.5	2.0	0.5	0.8	0.5	0.5	4.0
D	4.0	0.5	6.0	1.0	0.6	0.5	0.25	4.0
D	2.0	0.5	6.0	1.0	0.4	0.5	0.25	4.0
D	7.29	0.81	6.35	0.9	0.5	0.64	0.25	3.0
D	1.905	0.56	6.35	0.9	0.35	0.64	0.25	1.5
D	3.75	0.4	6.4	0.4	0.4	0.6	0.25	2.0

Figure 2.12 Various concrete wall shapes considered in the determination of a simple expression for M_l.

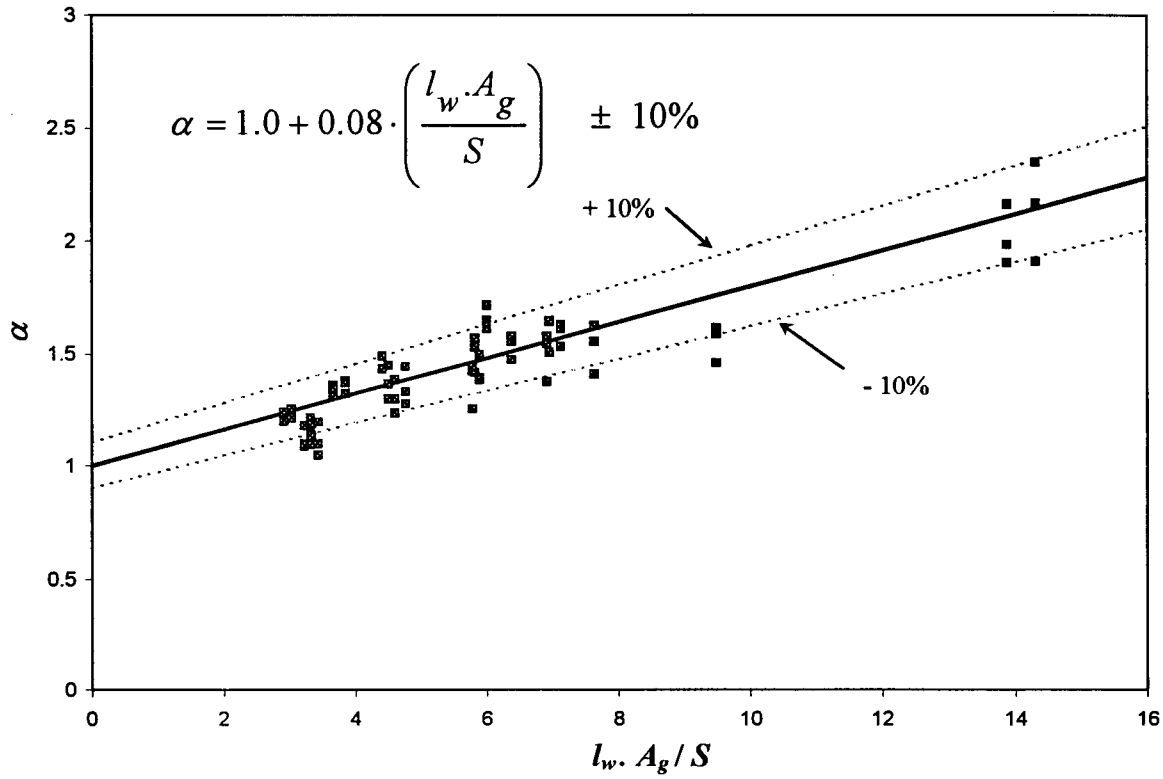

Figure 2.13 Determination of the slope, α, of the linear expression for M_l.

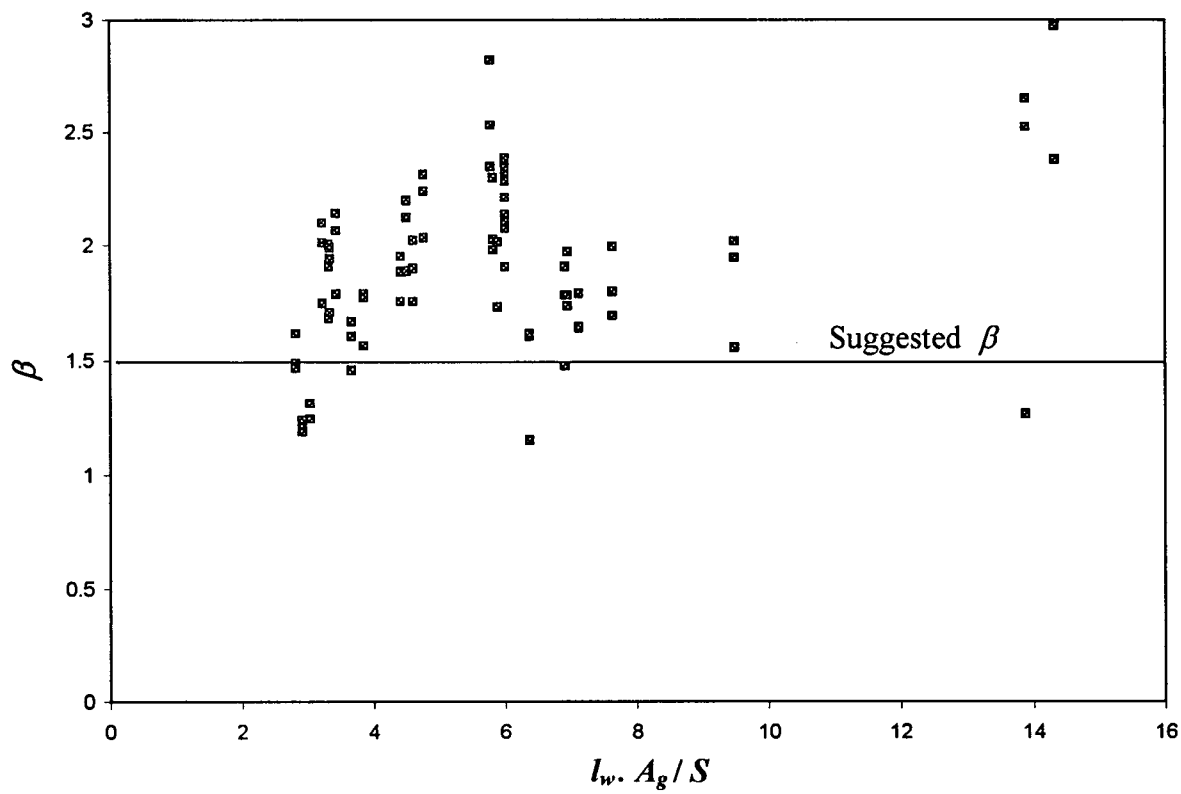

Figure 2.14 Determination of the intercept, β, of the linear expression for M_l.

where, $\beta = 1.5$ for the upper-bound response, and $\beta = 0$ for the lower-bound response. Equation [2.7] is used to determine M_l in an approximate way in lieu of the more rigorous method (equal area under the curve method) described earlier. Figure 2.15 compares the results from Equation [2.7] with the results of M_l determined using the rigorous method. A reasonable agreement is found.

Figure 2.16 shows the actual nonlinear upper-bound and lower-bound bending moment-curvature relationships for a selection of wall sections. Idealized trilinear models determined using both the rigorous method and Equation [2.7] for both the upper and lower-bound are also shown for comparison. A reasonable accuracy (within approximately ±10%) is found as previously shown in Figure 2.15.

2.7 Concluding Remarks

A study of the response of wall sections with high initial stiffness and light amounts of vertical reinforcement (typical in most high rise walls) indicated that the uncracked portion of the bending moment-curvature response is very significant and therefore, the elastic deformations of the response are not appropriately represented by other simpler models that tend to ignore the uncracked stiffness.

A trilinear bending moment-curvature relationship (nonlinear flexural stiffness), that captured the effect of cracking, was proposed for concrete walls in high rise buildings and the parameters needed to determine the model were presented. While the largest advantage of the proposed relationship over other simpler models occurs with high rise walls, the proposed model is applicable to all concrete walls.

Calibration of the proposed trilinear bending moment-curvature relationship against test results from a large-scale slender concrete wall is illustrated in the next chapter.

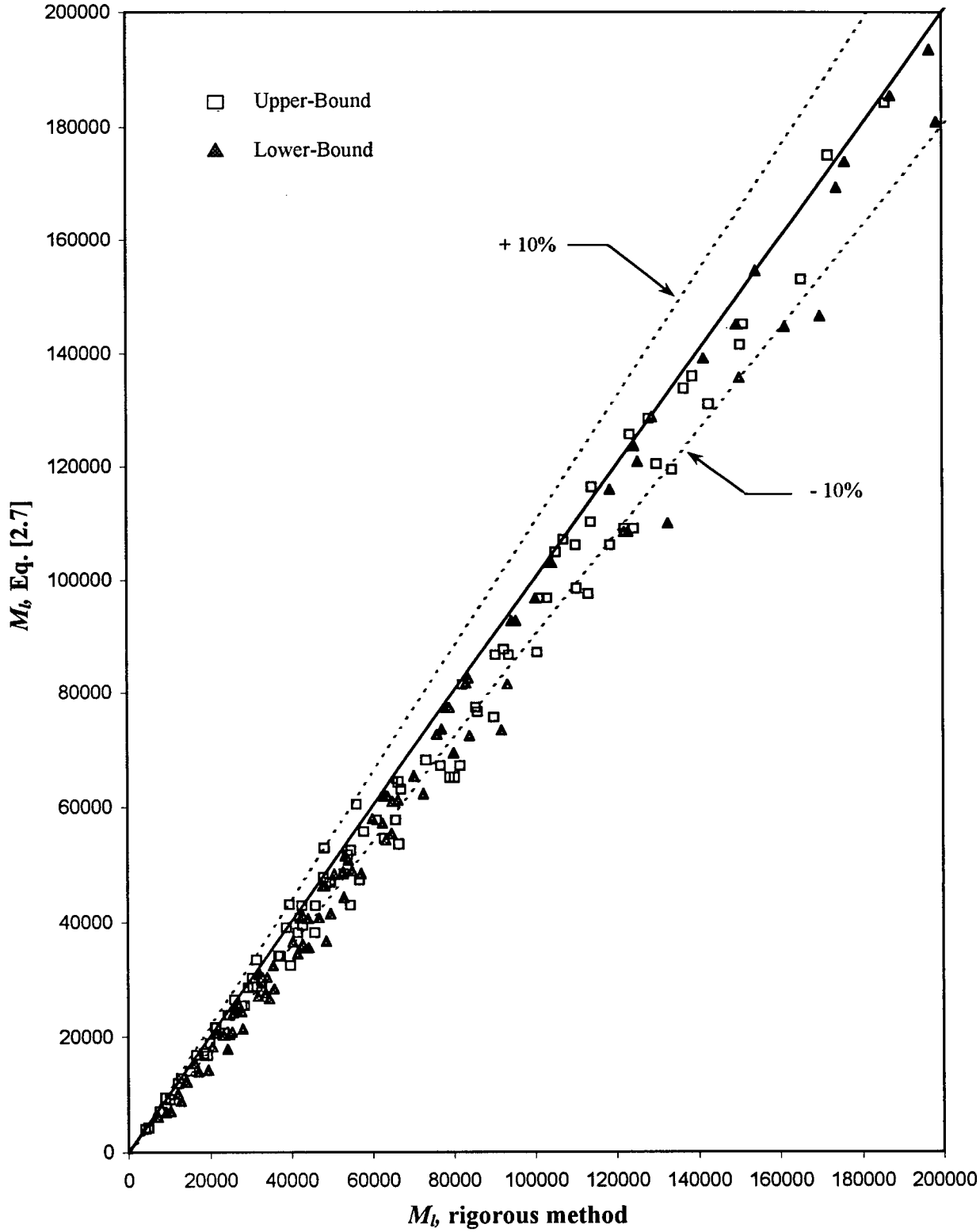

Figure 2.15 Comparison of M_l determined using the simple expression (Eq. [2.7]) with the value determined using the more rigorous method.

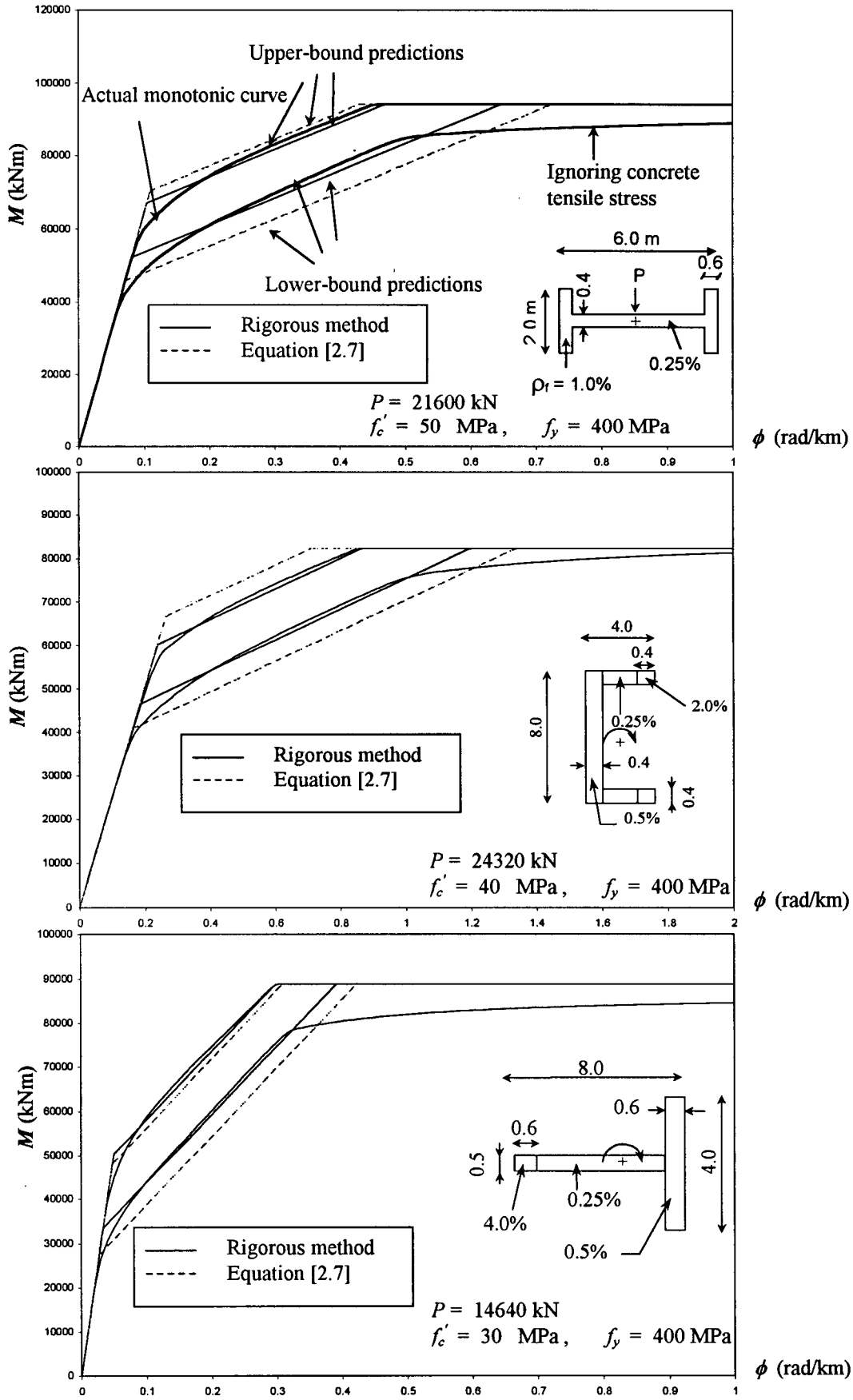

Figure 2.16 Comparison of the actual nonlinear bending moment – curvature relationships with the proposed trilinear model for typical wall sections.

Chapter 3

Experimental Study of a Large-Scale Slender Wall

3.1 General

In order to validate the trilinear bending moment-curvature model developed in Chapter 2, an experimental investigation was carried out on a tall slender wall where the response is dominated by flexural deformations. The experimental study was done jointly with Bryson (2000) who was responsible for the design and construction of the test specimen. The instrumentation and testing procedure was done jointly, while the analysis of the test results was done entirely as part of this thesis. In this chapter a brief overview of the experimental program is given and the results that are relevant to the analytical developments in this thesis are presented. A complete report on the test is given by Adebar, Ibrahim and Bryson (2000).

Several researchers and numerous studies have been conducted to measure different aspects of concrete wall response. Abrams (1991) listed 44 references for the measured response of concrete walls. Thomsen and Wallace (1995) summarized the work to date. To the author's knowledge, none of these studies involved a wall that was as slender as the wall tested in this study and none were conducted on such a large-scale specimen.

3.2 Description of Test Specimen

The prototype wall was assumed to be 240 ft high and to have a length of 22 ft. A 1/4 scale model of the prototype wall (i.e., a 60 ft high wall) was considered for testing under simulated seismic loading. A triangular load distribution along the wall height simulating seismic loading may be represented by the resultant lateral load at two-thirds of the height of the wall (i.e., 40 ft from the base). Accordingly, a 40 ft high wall specimen was constructed for testing under single lateral load at the top of the wall (see Figure 3.1).

The specimen was 40 ft high by 5 ft - 4 in. long with a flanged cross section. The web was 4 ft long by 5 in. thick and the flanges were 8 in. long and 15 in. thick. The vertical reinforcement in

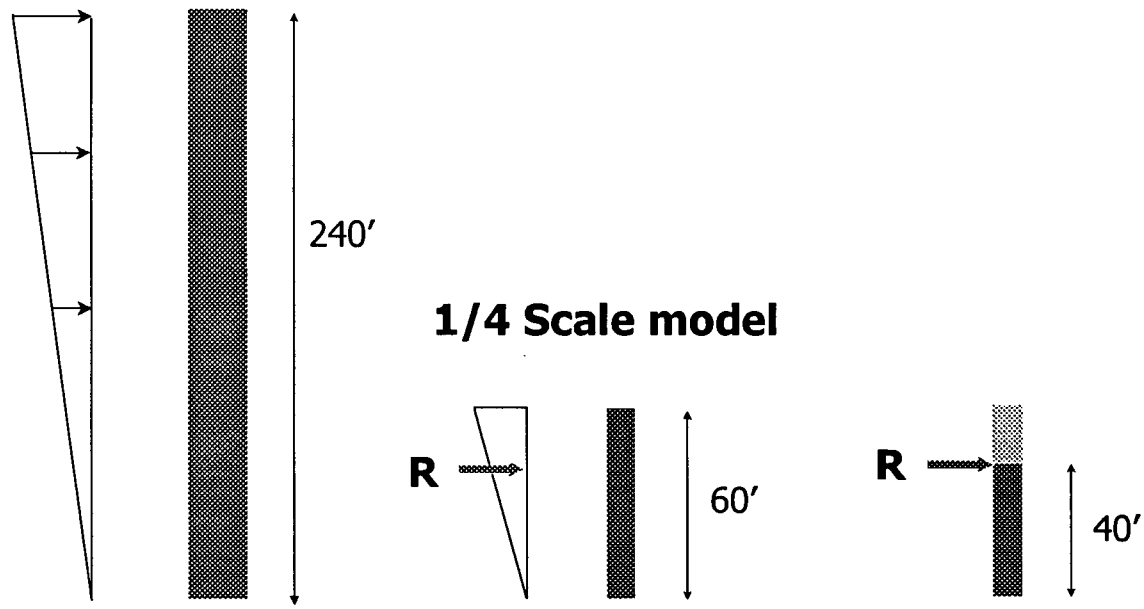

Figure 3.1 Prototype wall specimen considered for testing under cyclic loading (3.28 ft = 1 m).

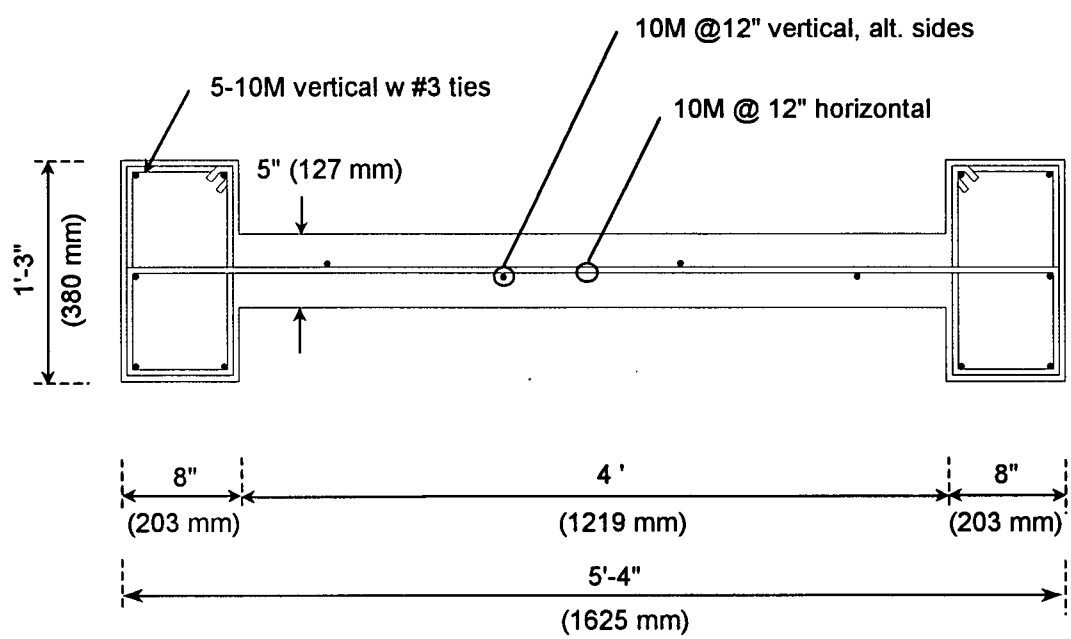

Figure 3.2 Cross sectional dimensions and reinforcement details of the 40' wall test specimen.

the flange consisted of 5-10M reinforcing bars enclosed by 10M ties spaced at 2.5 in. in the lower 10 ft of the wall and spaced at 6 in. in the remaining height of the wall. The web was reinforced with 10M bars spaced at 12 in. vertically and horizontally. Figure 3.2 shows the cross sectional dimensions and reinforcement details.

In most high-rise buildings there are numerous levels of parking below grade. The parking structure is normally considerably larger than the tower and has perimeter walls that are tied to the tower walls by the concrete slabs at each level. As a result, the critical section of the tower walls (i.e., the potential plastic hinge region) is normally at grade level, not immediately above the foundation as is normally the case in bridge columns. One consequence of this is that there is much less pull-out of the vertical reinforcement from wall foundations. To simulate this effect in the wall specimen, the critical section was located 16 in. up from the base of the wall. The wall and the base were cast separately, and the construction joint was located at the desired critical section. Additional vertical wall reinforcement was provided below the critical section.

Due to the limited height in the laboratory, the wall specimen was constructed and tested in the horizontal position (see Figures 3.3 and 3.4). The wall was cast horizontally in a wooden form. After the concrete had gained sufficient strength (approx. four weeks), the wall was removed from the wooden form and lifted into place on top of Teflon sliding bearings located at 9'-9" from the base of the wall and at 8'-5" from the top of the wall (see Figure 3.5). Prior to constructing the base of the wall, a test was conducted to determine the magnitude of the lateral force at the "top" of the wall that was required to overcome the friction in the Teflon bearings that supported the dead weight of the wall. The lateral load required to maintain movement of the wall was determined to be 3.65 kN which is approximately 2% of the maximum load applied during the test. The base of the wall was cast around shear pins and bolts inserted into the laboratory strong floor in order to minimize movement of the base during loading of the wall.

The specimen was tested after the concrete in the wall above the critical section had reached an age of 140 days (approx. 4.5 months). At that time the cylinder compressive strength of the wall concrete was measured to be 49 MPa.

All of the 10M reinforcing bars that were used to construct the wall came from a single heat of reinforcing steel. Samples of the reinforcing bars were tested. Based on an assumed cross-

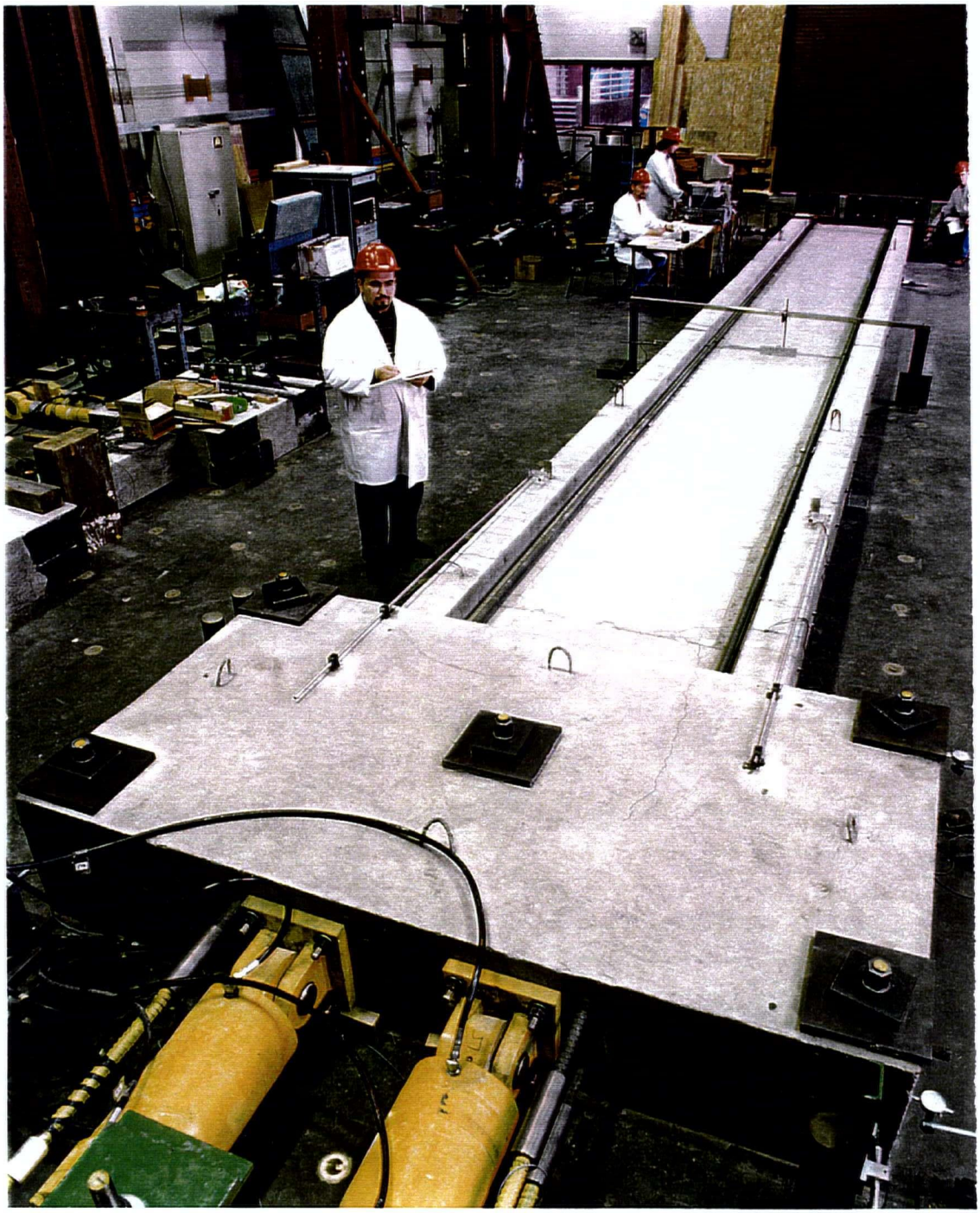

Figure 3.3 Large-scale slender wall test undertaken to validate the proposed trilinear model.

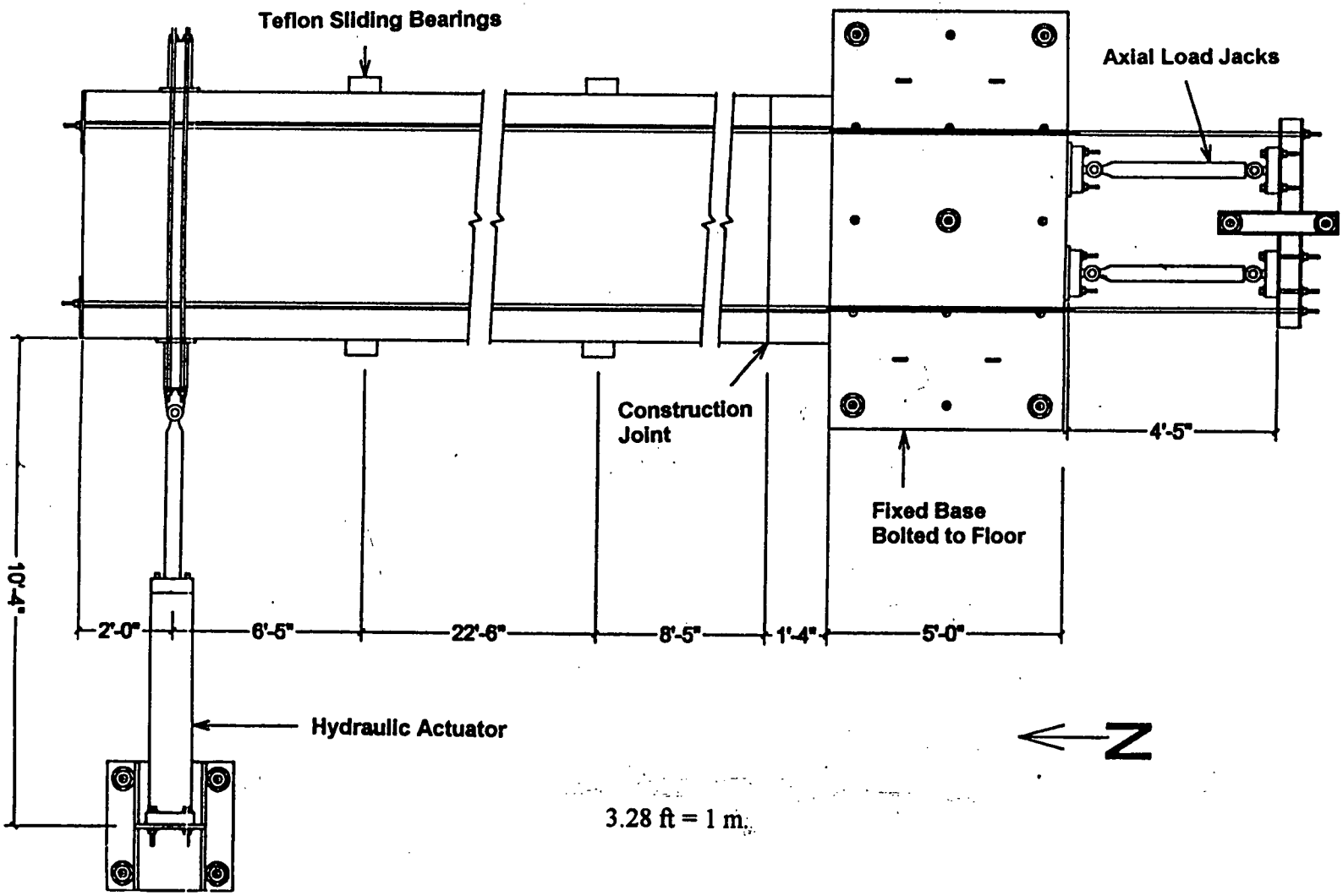

Figure 3.4 Schematic of the slender wall test set-up (from Bryson 2000).

sectional area of 100 mm^2, the yield strength was determined to be 455 MPa, while the ultimate strength was found to be 650 MPa.

3.3 Test Set-up

In addition to applying a lateral load at the "top" of the wall, an axial load of 1500 kN (10% of f_c' A_g) was applied to the wall during the test. Two hydraulic actuators located below the base of the wall applied the axial load. The actuators were used to pull down on four 1-1/4 in. diameter Dywidag bars attached to the top of the wall (see Figures 3.3 and 3.4). The hydraulic actuators, which were subjected to a constant pressure during the test, had sufficient stroke to allow the required movement of the Dywidag bars during the cycling of the lateral load. To reduce the shear force between the wall base and laboratory floor, the hydraulic actuators that applied the axial force were reacted directly against the base of the wall (see Figure 3.4).

The lateral load was applied using an MTS hydraulic actuator with a maximum stroke capability of +/- 12 in. The lateral load was applied at 38 ft – 7 in. from the base of the wall which corresponds to 37 ft – 3 in. from the critical section (construction joint). The actuator was mounted horizontally on a reaction steel column that was bolted to the lab floor and was controlled by a wave-form generator.

3.4 Instrumentation

Instrumentation was used to measure displacements at various points on the wall, the lateral and axial loads, and strains at various locations in the wall specimen. Figure 3.6 shows a summary of the instrumentation used during the test.

Two LVDT's (each with +/- 6 in. stroke) were mounted at the top of the wall to verify the lateral displacement measurements obtained from the LVDT within the hydraulic actuator. An additional LVDT was used to measure the lateral movement of the wall at 200 in. from the base. Axial displacement was measured at the middle of the cross section at 200 in. from the base of the wall using an LVDT mounted to a fixed steel frame supported on the floor. Two additional LVDT's were used to measure the longitudinal displacement over a 64 in. gage length in the

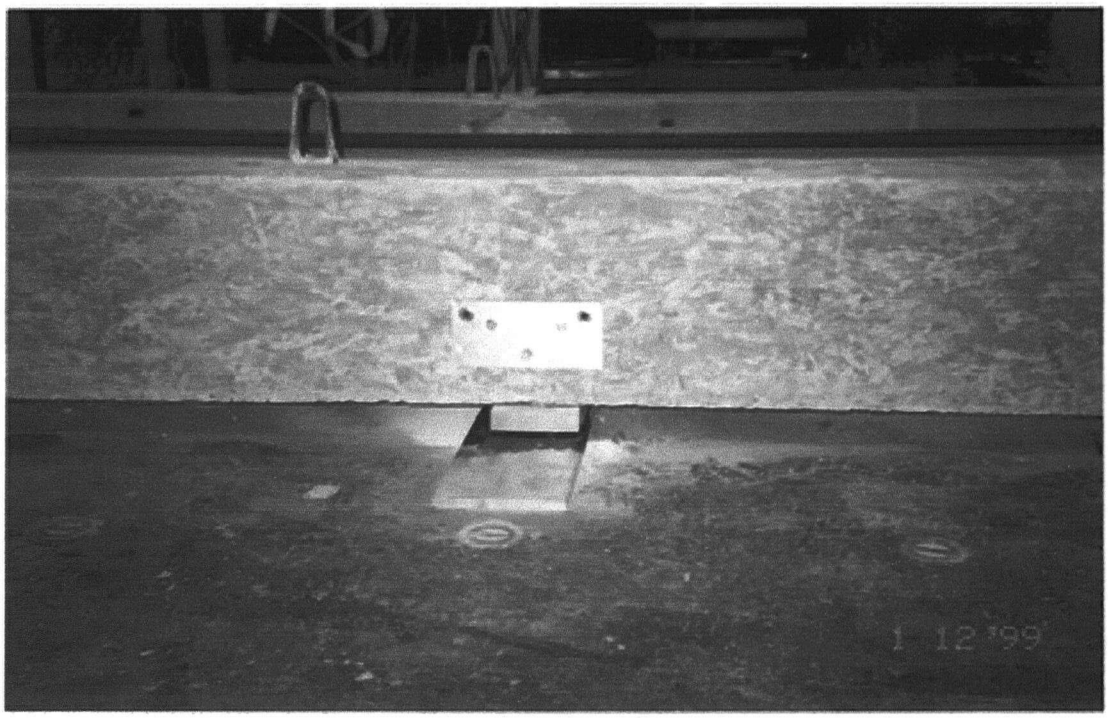

Figure 3.5 Teflon sliding bearings supporting the slender wall specimen tested in a horizontal position.

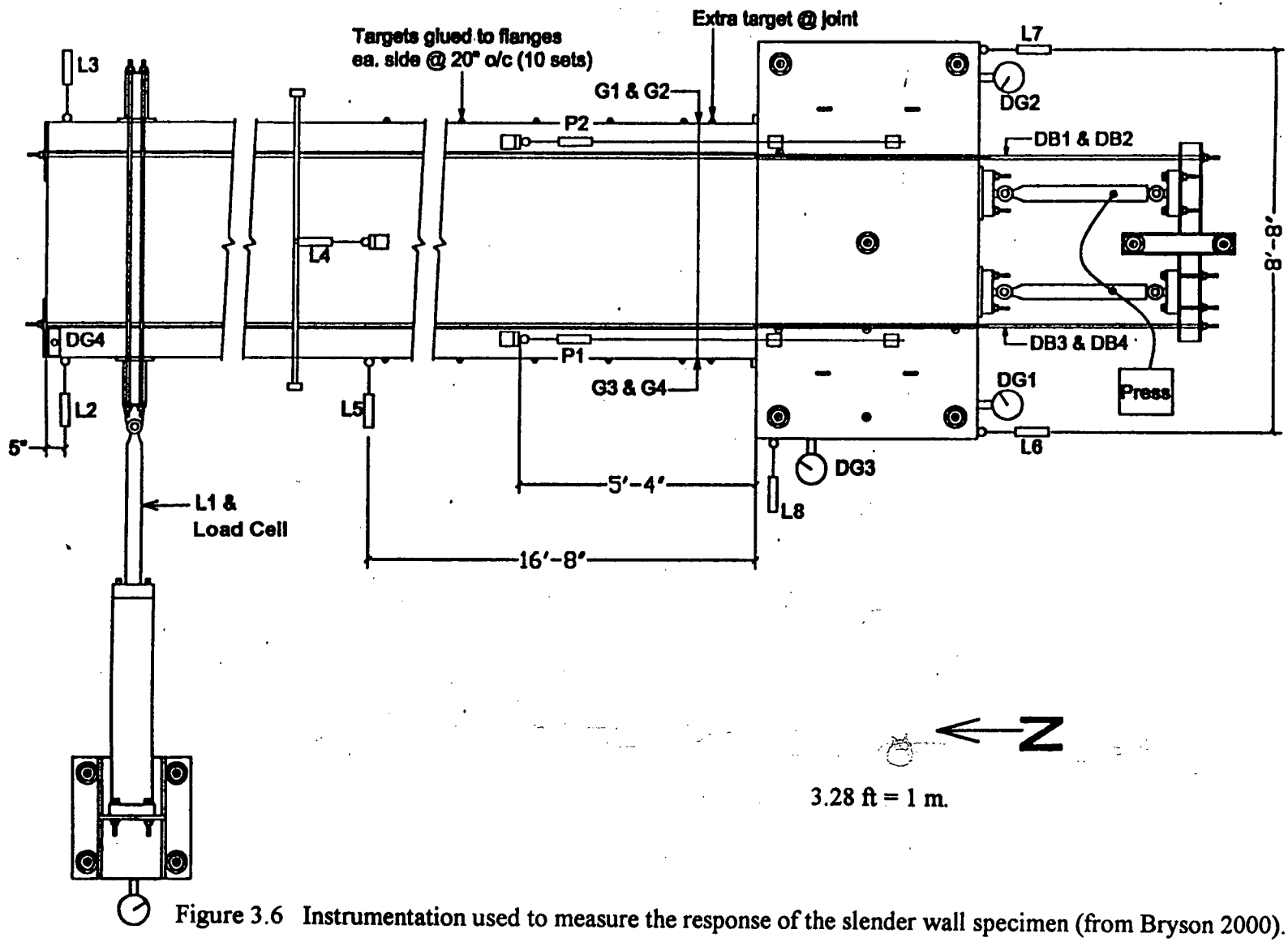

Figure 3.6 Instrumentation used to measure the response of the slender wall specimen (from Bryson 2000).

probable plastic hinge region. The LVDT's were attached to the fixed base block and extended over the wall flanges. Three LVDT's were used to monitor any movement of the base. A load cell was installed between the hydraulic actuator and the wall in order to measure the lateral load applied to the wall. The four Dywidag bars that were used to apply the axial load had been strain gauged to act as a load cells that measured the forces in these bars.

To measure the concrete strains at various locations along the wall length, specially designed metal targets were epoxyed to the concrete surface. These targets were shaped to fit a digital caliper device that was used to obtain accurate measurements of the displacement between the targets (see Figure 3.7). On each side of the wall, 11 targets were equally spaced at 20 in. to measure the strains over the region that was expected to be cracked (i.e., the lower 200 in. of the wall length). The first gage length was set to 16 in. in order to match the critical joint location. Additional targets were placed at the critical section (construction joint) to measure the deformations at this particular location. In addition to measuring concrete strains, four strain gages were attached to the longitudinal reinforcement (10M bars) at the critical section (construction joint) location.

The LVDT's, load cells and strain gages were linked to a data acquisition system that stored the data at a fixed sampling rate. The digital caliper readings were recorded manually.

3.5 Test Procedure

The axial load was held constant during the test, while the lateral load was progressively increased. The actuator that applied the lateral load was run in displacement control. The desired displacement level was input to the electronic wave generator (as a fraction of the actuator maximum stroke) and the corresponding period of the cycle was chosen to give the same rate of loading (1 mm/sec) used in all cycles. The displacement level was increased in small increments in the early stages of the test to capture the effect of cracking on the elastic deformation of the wall. At each displacement level, four complete cycles were performed. Figure 3.8 summarizes the sequence of testing cycles and displacement levels.

Digital caliper readings were taken at peak displacements in each direction at the first and the fourth cycle. Cracks were also marked and photographed at the peak displacement in each

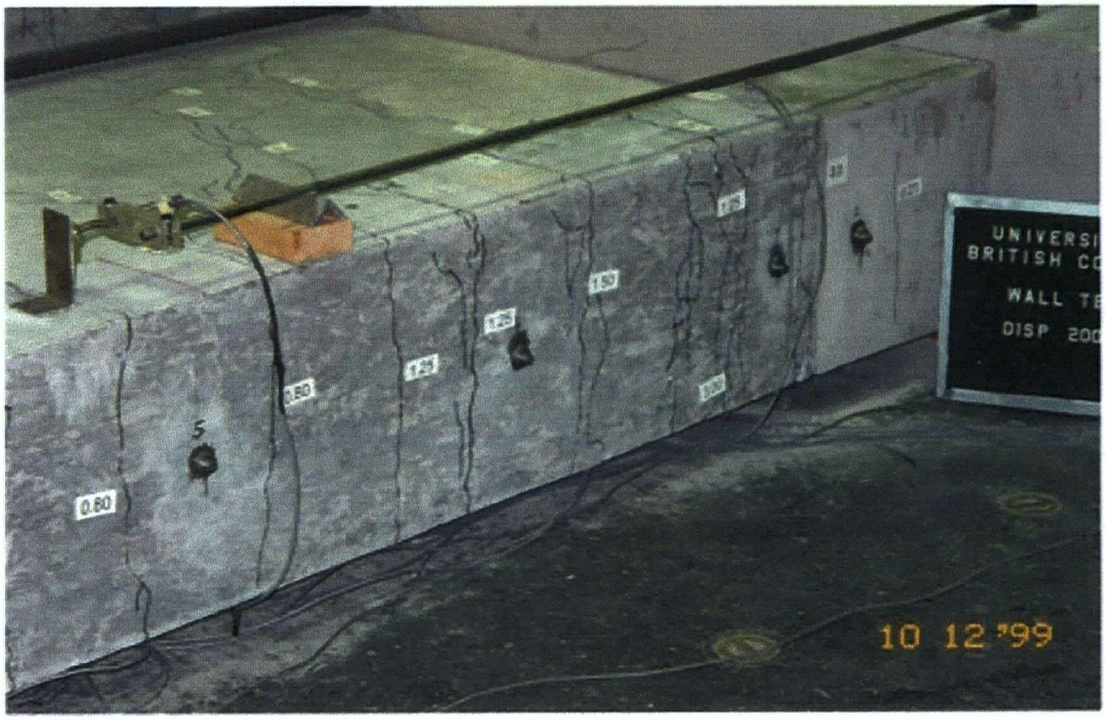

(a)

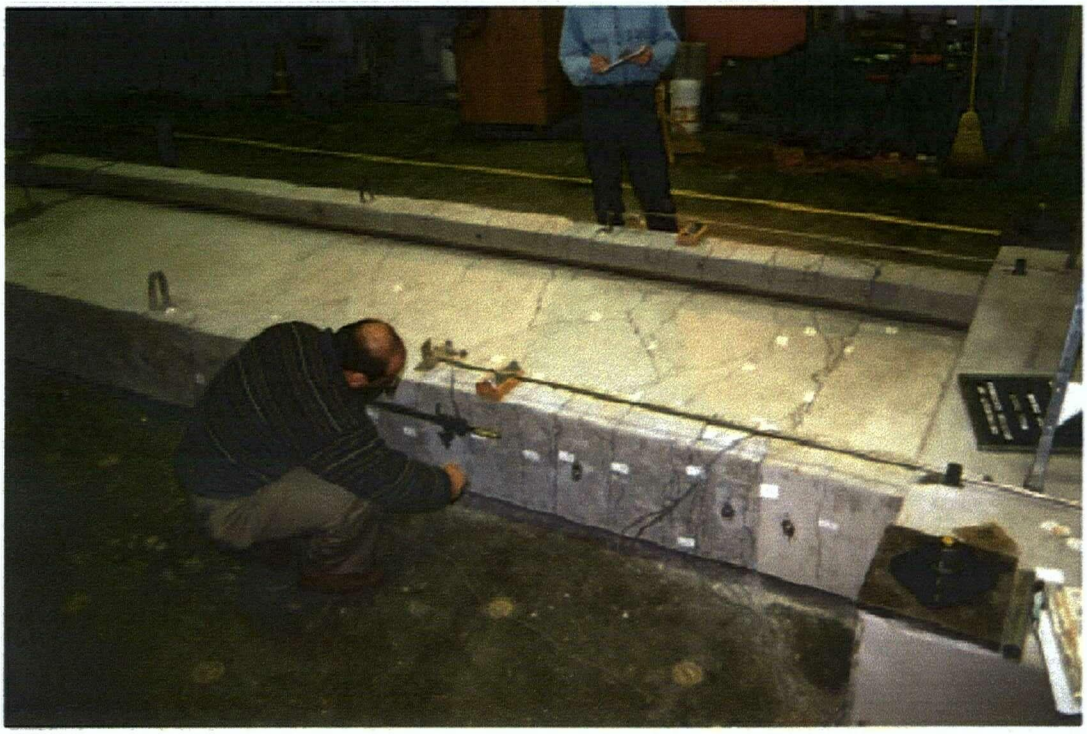

(b)

Figure 3.7 Measuring concrete strains at various locations along the wall height: (a) metal targets epoxyed to concrete, (b) digital caliper device.

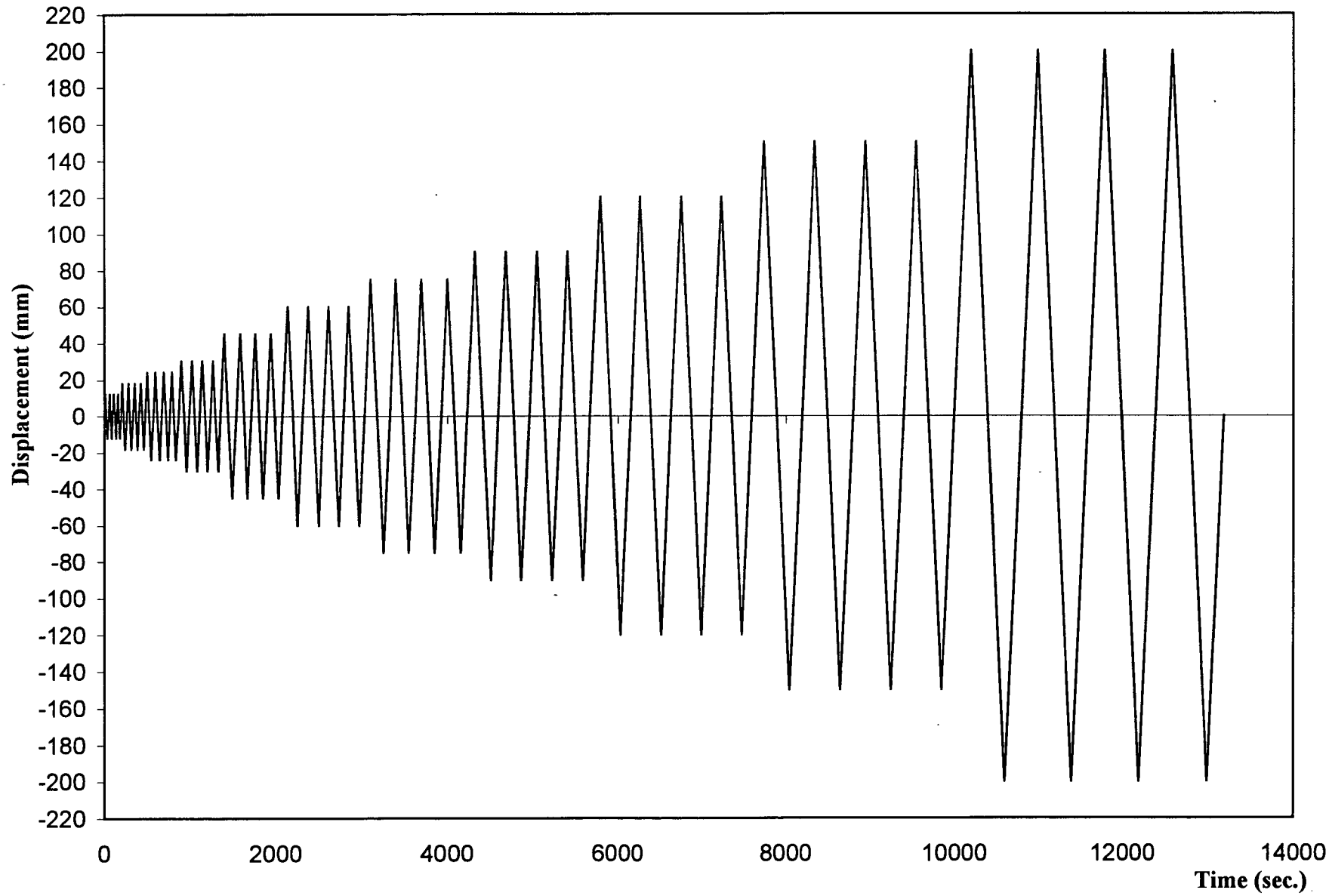

Figure 3.8 Sequence of imposed reverse cyclic lateral displacement at the tip of the wall.

direction at the first and fourth cycle. Readings from the LVDT's, strain gages, and load cells readings were recorded continuously by the data acquisition system at a sampling rate of 5 readings/sec.

3.6 Corrections to Measured Results

Figure 3.9 summarizes the measured (uncorrected) load-displacement relationship of the wall. Due to a problem with the data acquisition system, the test data for the 30 and 45 mm displacement cycles were not recorded. Therefore additional cycles to +/- 48 mm displacement levels were added.

During the test it was observed that the base of the wall did rotate somewhat. The measured displacement of the base was used to estimate the rigid body motion at the top of the wall, and the recorded displacement of the top of the wall was corrected to account for this effect. To estimate the displacement of the wall top due to rotation of the wall base, the center of rotation was assumed be at the middle bolt in the base (see Fig. 3.10-a). Displacement readings of LVDT 6 and 7 were used to compute the rigid body rotation of the base at any instant. The rotation of the base multiplied by the distance from the middle bolt to the location where the lateral displacement was measured at the "top" of the wall (11823 mm) gives the displacement that should be subtracted form the recorded data. Note that the base rotation times the short vertical distance from the middle bolt to LVDT 8 (711 mm), gives an estimate of the displacement readings of L8 if the center of rotation was at the center of the block as assumed. Several such checks were made and good correlation was found.

The lateral load was corrected for the friction force due to the Teflon bearings that supported the dead weight of the wall. The friction force for one complete cycle of loading was assumed to follow Coulomb friction model as shown in Fig 3.10-b. These forces were subtracted from the load recorded for each and every cycle. The corrected load-displacement relationship including the effect of base rotation and friction is shown in Figure 3.11.

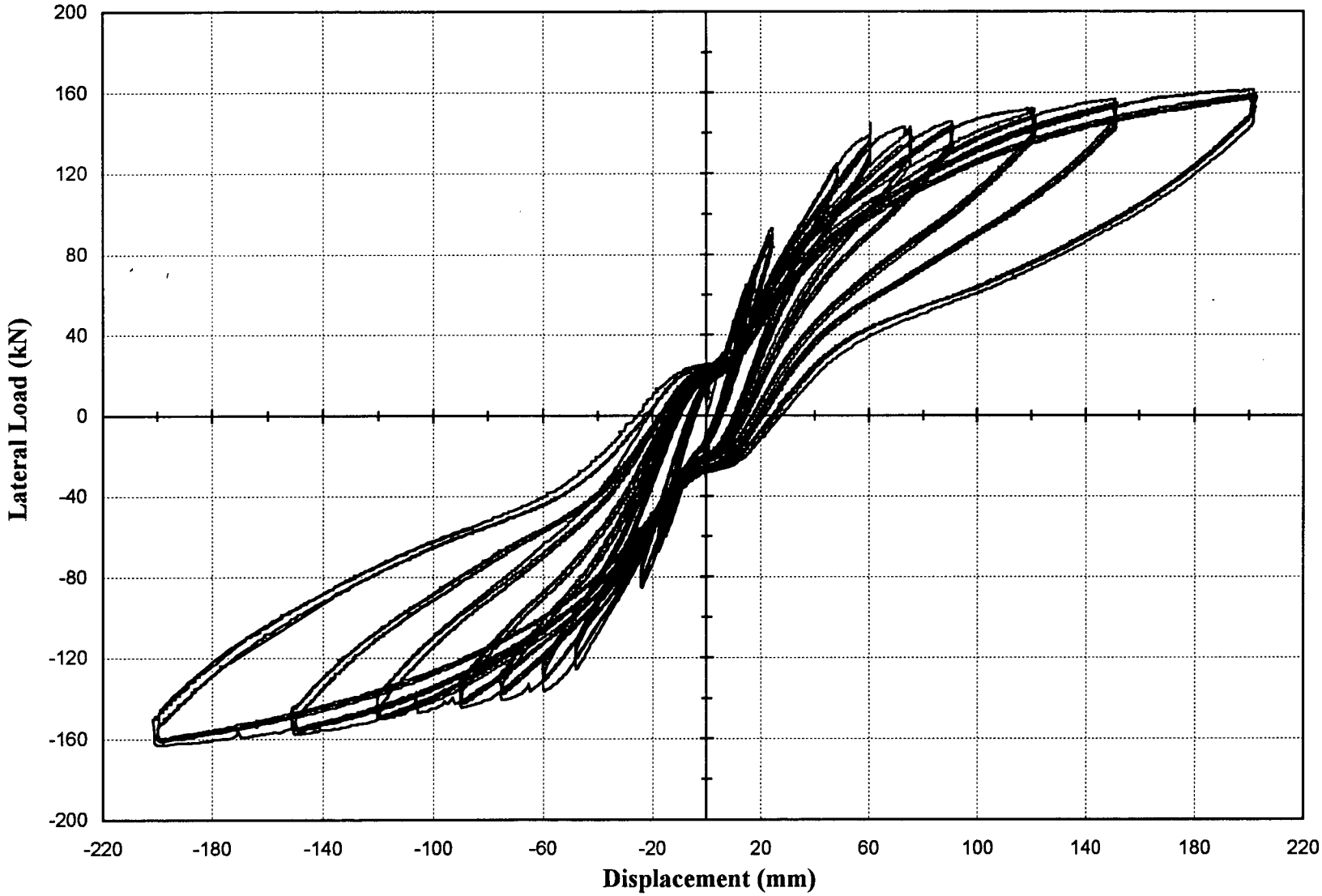

Figure 3.9 Measured lateral load-displacement response of the slender wall specimen.

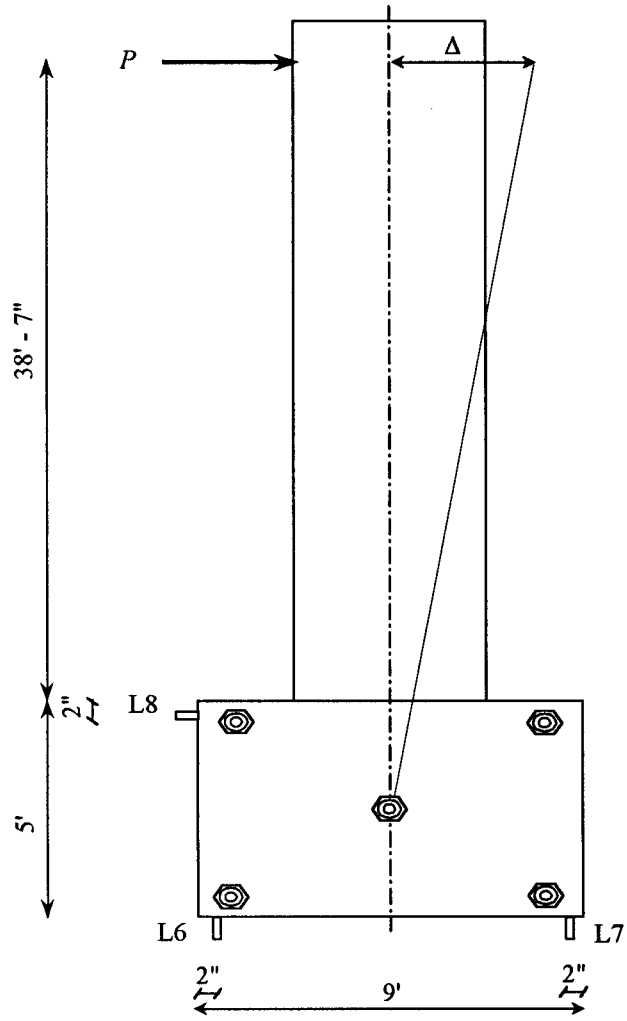

(a) $\Delta_{corrected} = \Delta_{measured} - \{(L6 - L7) / 8'\text{-}8''\} * (40'\text{-}11'')$

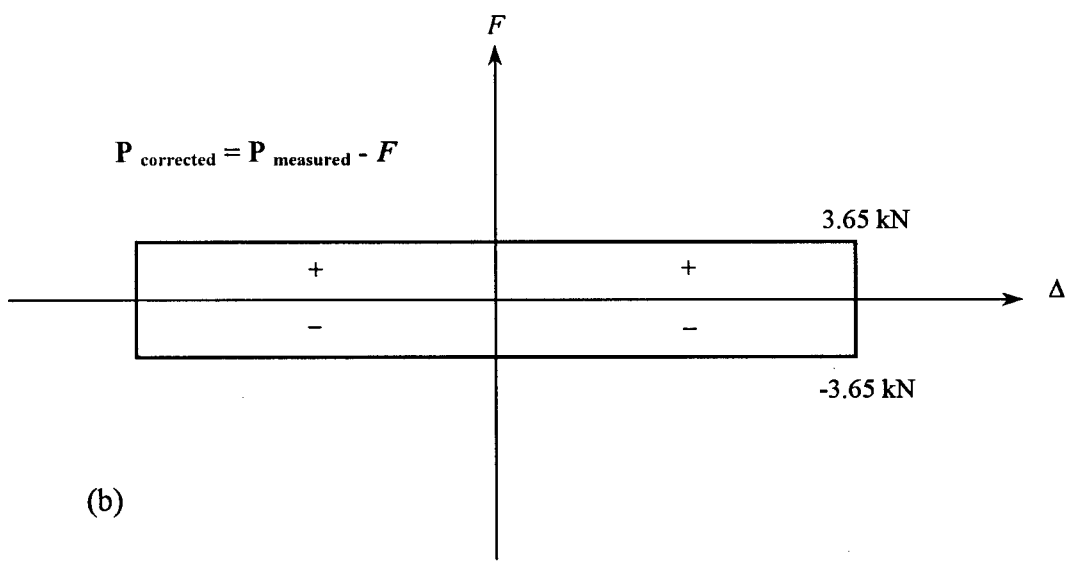

(b)

Figure 3.10 (a) Correction to measured displacement due to observed rotation of the base block during testing, (b) Correction to measured force due to Teflon sliding bearings.

3.7 Summary of Test Observations

As expected, flexural behavior dominated the response of the slender wall specimen. No early strength decay caused by lack of shear capacity or bond failure was observed. Significant diagonal cracking (flexure-shear cracking) was observed near the later stages of the test, however, these cracks did not appear to influence the overall response of the wall.

According to the strain gauge readings, first yielding of the longitudinal reinforcement occurred at the critical section at a lateral displacement of 48 mm.

Spalling of the cover at the critical joint location occurred at a displacement level of 200 mm and some metal targets were lost. To fail the specimen, further cycling was undertaken and the longitudinal reinforcement buckled at the critical section. Two longitudinal reinforcing bars were observed to have fractured.

3.8 Discussion of Test Results

As shown in Figure 3.11, the hysteresis loops reached the monotonic load capacity showing no strength decay within a realistic range of deformations. Strain hardening of the reinforcement in the post-yield deformation caused additional gain in strength (over-strength). This feature of stable hysteresis loops is typical of flexural dominant response.

The initial slope of the load-displacement response was essentially unchanged, even after cycling the specimen further into the inelastic deformation range, the initial slope remained close to the initial uncracked gross stiffness. Upon unloading from one direction and reloading in the other, the stiffness increased as the load approached zero. As the moment reduced, the axial compression closed the cracks and the wall responded nearly as an uncracked wall.

The small residual displacement at zero load and small residual load at zero displacement supported the inherent assumption in the trilinear bending moment-curvature model that the initial portion of any loading cycle will pass through the origin and follow the original uncracked response up until exceeding the lower-bound M_l, as discussed in Chapter 2, Section 2.5. (See also Chapter 5, Section 5.4.1).

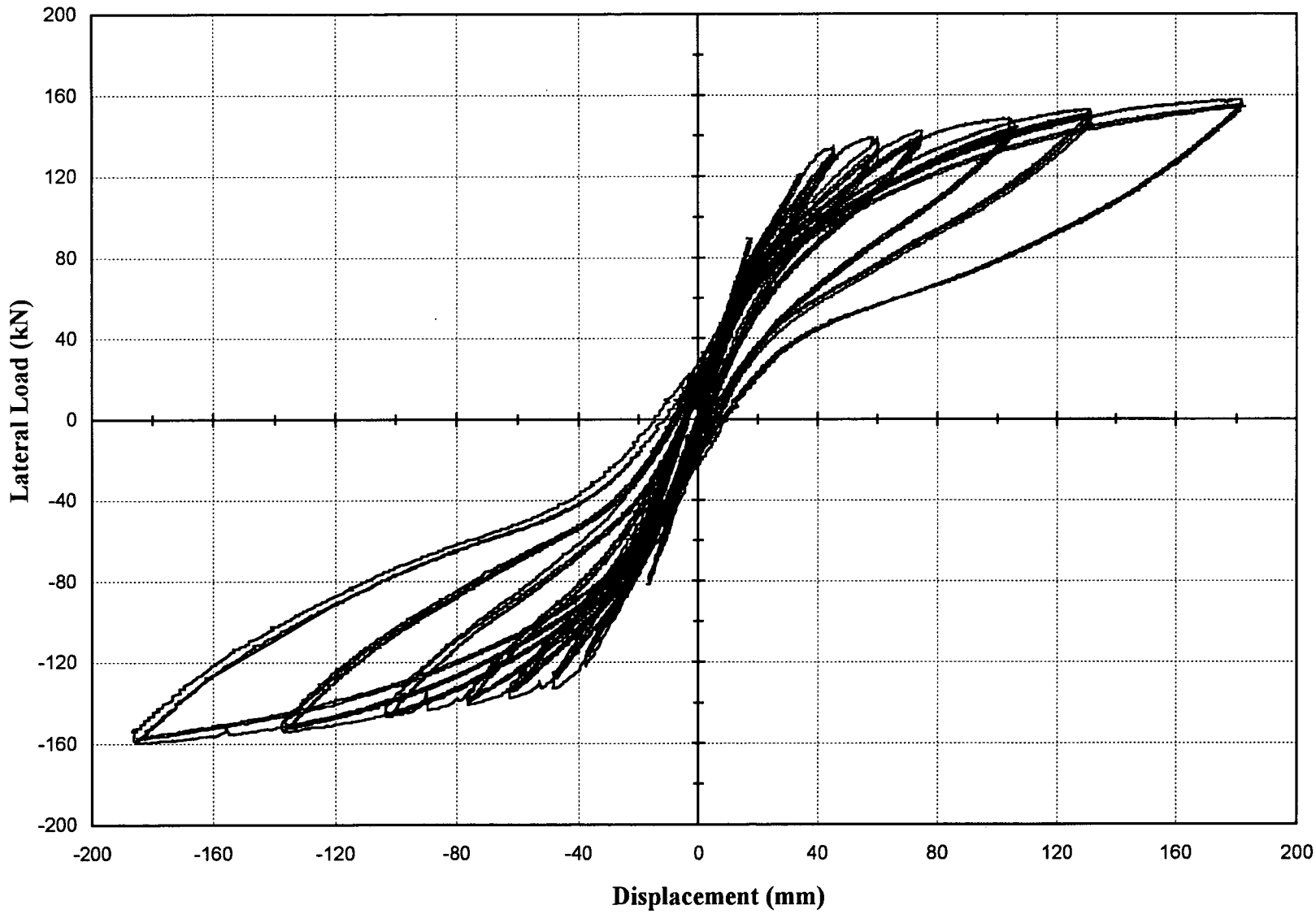

Figure 3.11 Corrected load-displacement response of the slender wall test.

Beyond the initial uncracked range, the slope of the curve reduced (secondary slope). With subsequent cycling of the specimen into larger displacements, the slope of the curve degraded further. The process of degraded slope with increased deformations is often termed stiffness degradation. Further cycling at the same displacement level showed little degradation in stiffness from the first to the second cycle. No degradation was observed due to cycling from the second cycle to the subsequent cycles.

Degradation of the secondary slope with moving from one displacement level to another agrees in principle with the analytical results shown for the bending moment-curvature relationship (Figure 2.7-a, Chapter 2).

Figure 3.12 shows, for clarity, the first cycle at each displacement level of the load-displacement relation. The concept of upper-bound and lower-bound response discussed for the bending moment-curvature relationship (Chapter 2) can also be used to represent the load-displacement response under cyclic loading as well. The upper-bound load-displacement relation is the response that may be obtained when loading the specimen monotonically to failure without having been damaged from a previous load cycle (or alternatively, previously uncracked response). The lower-bound load-displacement relation or severely cracked response is a function of the previously attained displacement or drift level. Figure 3.12 highlights the upper (monotonic) and lower-bound load-displacement responses. The upper-bound load-displacement response was drawn as the envelope to the hysteresis loops. The lower-bound load-displacement is the severely cracked response of the wall specimen when pushed to the maximum displacement level (i.e., 200 mm displacement cycles).

The relation between the bending moment calculated at the critical joint versus the measured rotation of the critical section is plotted in Figure 3.13. The moment-rotation relation provides an indication of the flexural deformations exhibited plus any slippage of the longitudinal reinforcement that may occur at the critical joint.

The bending moment at the critical section was calculated as the sum of the primary and secondary moments. The primary moment was calculated as the product of the applied lateral loading and the distance from the critical section location to the hydraulic actuator (37'-2.2", 11.333 m). The secondary moment was calculated as the sum of the vertical component of the

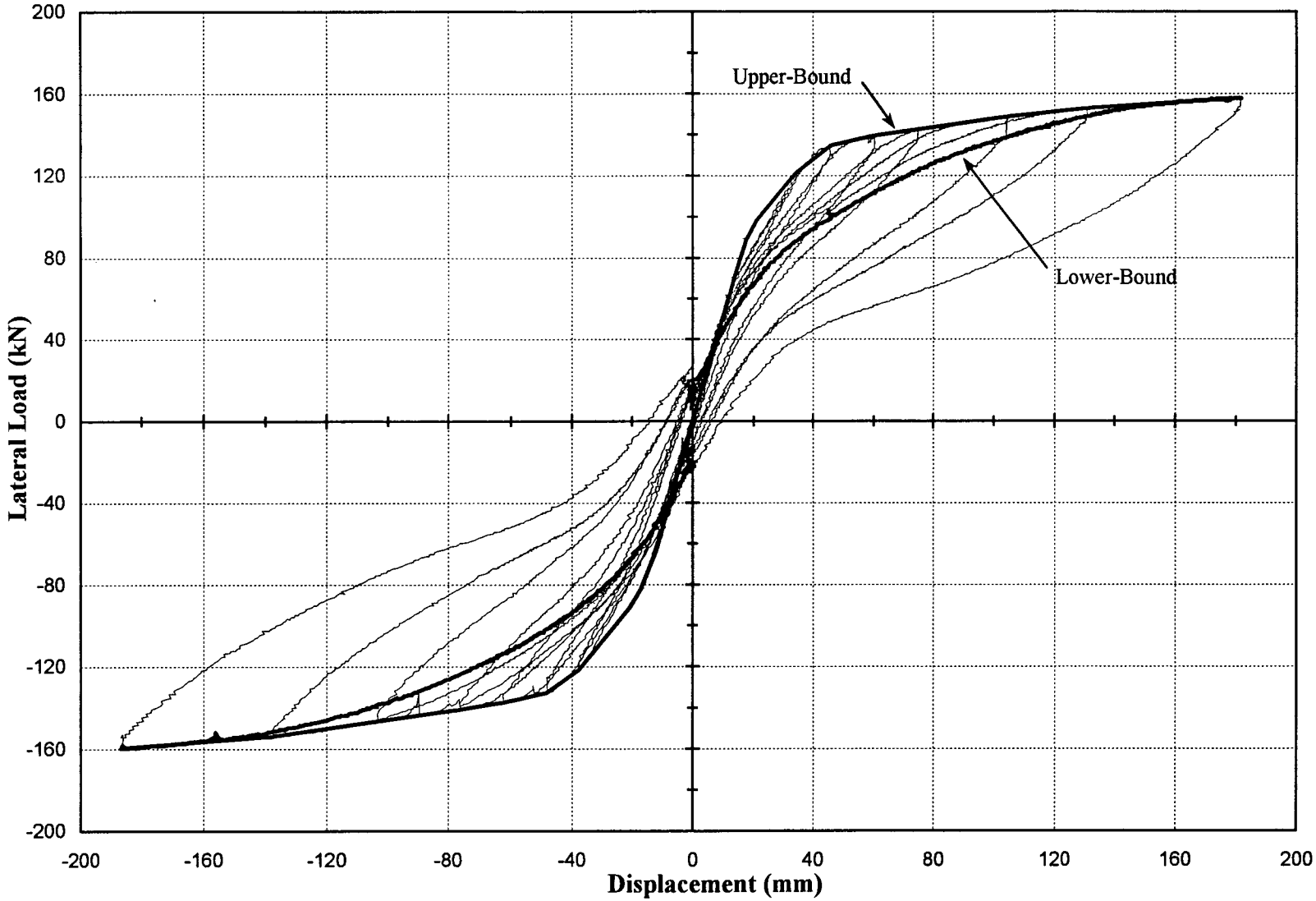

Figure 3.12 Upper-bound and lower-bound load-displacement response of the wall specimen under cyclic loading.

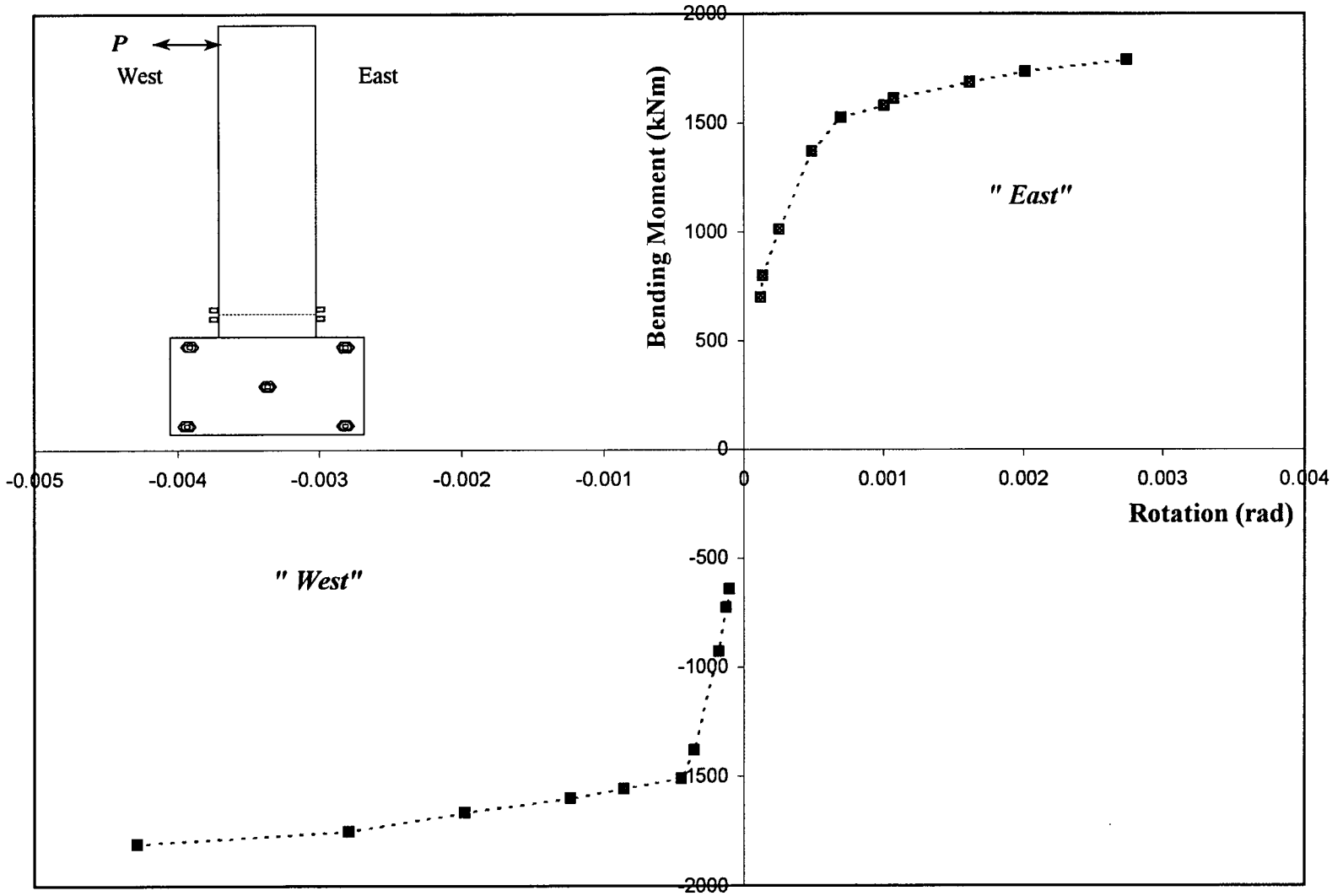

Figure 3.13 Measured bending moment-rotation response of the wall specimen taken at the peak lateral displacement.

axial compression multiplied by the lateral displacement and the horizontal component of the axial compression multiplied by the distance to the critical joint. Local drift angle at the tip of the wall, approximated as 1.5 times the corrected lateral displacement divided by the height of the wall, was used to obtain the vertical and horizontal component of the axial compression load.

Rotation of the critical joint was determined using the measurements taken for the two targets adjacent to the joint on each side of the specimen. Rotation measurements shown in Figure 3.13 were taken at the peak lateral displacement at the first cycle for each displacement level in each direction. Readings of the targets (displacement in mm) were divided by the width of the wall specimen (64 in., 1625 mm) to determine the rotation of the critical joint.

Moment-rotation relation resembled the shape of the monotonic upper-bound load displacement relation, shown in Figure 3.12, indicating that the specimen behavior is dominated by flexure response. Unsymmetry of the measured rotations indicated a local slippage of the longitudinal reinforcement (movement of the reinforcement relative to the surrounding concrete) at one side of the wall specimen. This observation is supported by the existence of a honeycomb void at the critical section in the east side of the specimen. As mentioned earlier, failure of the specimen ultimately occurred by fracture of two reinforcing bars at the east side of the specimen.

Readings of the targets along the length of the wall were converted into strain values and then divided by the width of the wall to give curvature measurements. These curvature measurements along the height of the wall are shown in Figure 3.14 for the different displacement levels in the East and West loading direction.

3.9 Comparison with the Trilinear Bending Moment-Curvature Model

To determine the relationship between the applied bending moment and the measured curvatures, the strain measurements taken at each location along the height of the wall (between any two targets) for the different displacement cycles are plotted (in terms of curvatures) against the calculated bending moment at that location in Figure 3.15. Note that the measured curvature values at each location are plotted individually and shifted horizontally by a fixed increment in order to observe the trend in each relationship.

The data shown in Figure 3.15 is summarized in a different way in Figure 3.16 where the measured curvatures at different locations over the height and at different displacement cycles are plotted versus the bending moment calculated at that location. The measurements were taken at the peak lateral displacements at the first cycle for each displacement level. No target readings were taken for the lower-bound bending moment curvature relationship (i.e., severely cracked response at 200 mm cycle). The predicted upper-bound bending moment-curvature relationships (both nonlinear and trilinear) are also shown in the figure. These were determined using the procedures described in Chapter 2. Comparison between the predicted and observed relationships show good agreement. It is interesting to note that the more complex nonlinear relationship compares no better to the experimental relationship than the simplified trilinear relationship.

It should be mentioned that the increase in strength due to strain hardening of the reinforcement as observed in the test is not captured in the proposed model. However, this increase in bending moment at high curvatures compensates for the assumption that the lower-bound includes the effect of some tension-stiffening beyond yielding of the reinforcement. See Section 2.6.4 (Case E in Fig. 2.7-a).

3.10 Concluding Remarks

The experimental study conducted on a large-scale slender wall validated the bending moment-curvature model. The experimentally calibrated bending moment – curvature model will now be used to develop a general method to determine the linear flexural stiffness of concrete walls.

Up to this point in the thesis, only the measured curvatures and the calculated bending moments were used in the comparison with the proposed analytical model. Where applicable in the following chapters, additional test results will be used to validate predictions from the proposed model.

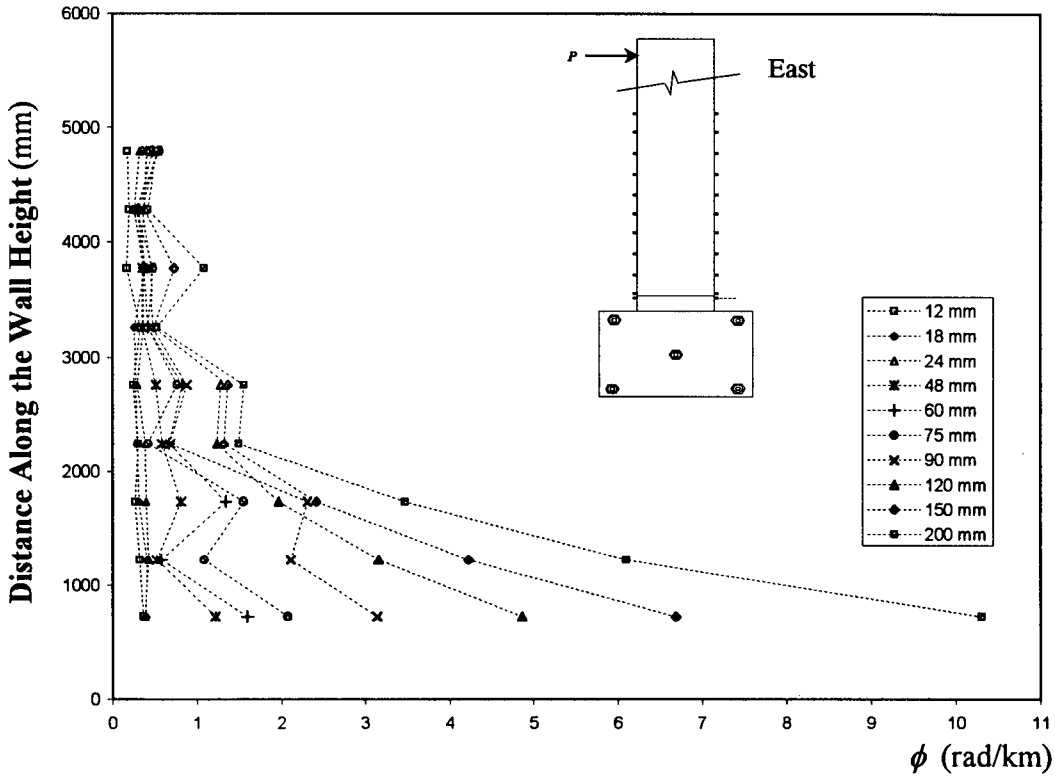

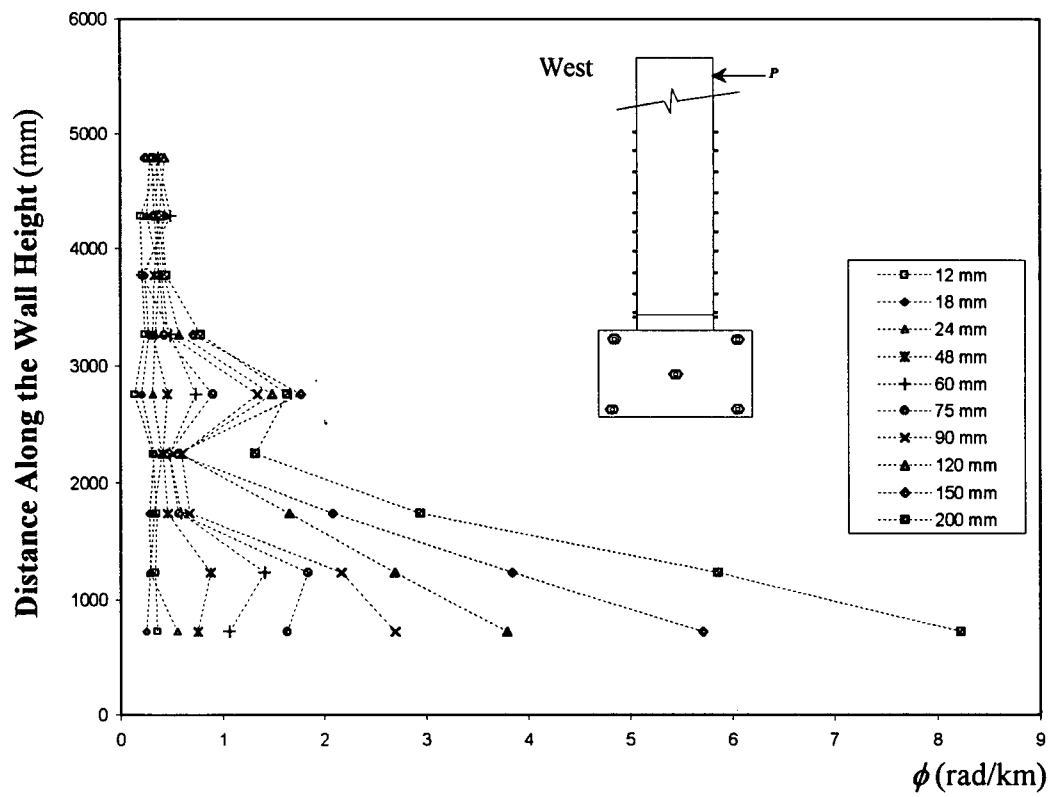

Figure 3.14 Measured curvature distribution along the wall height during the different lateral displacement cycles.

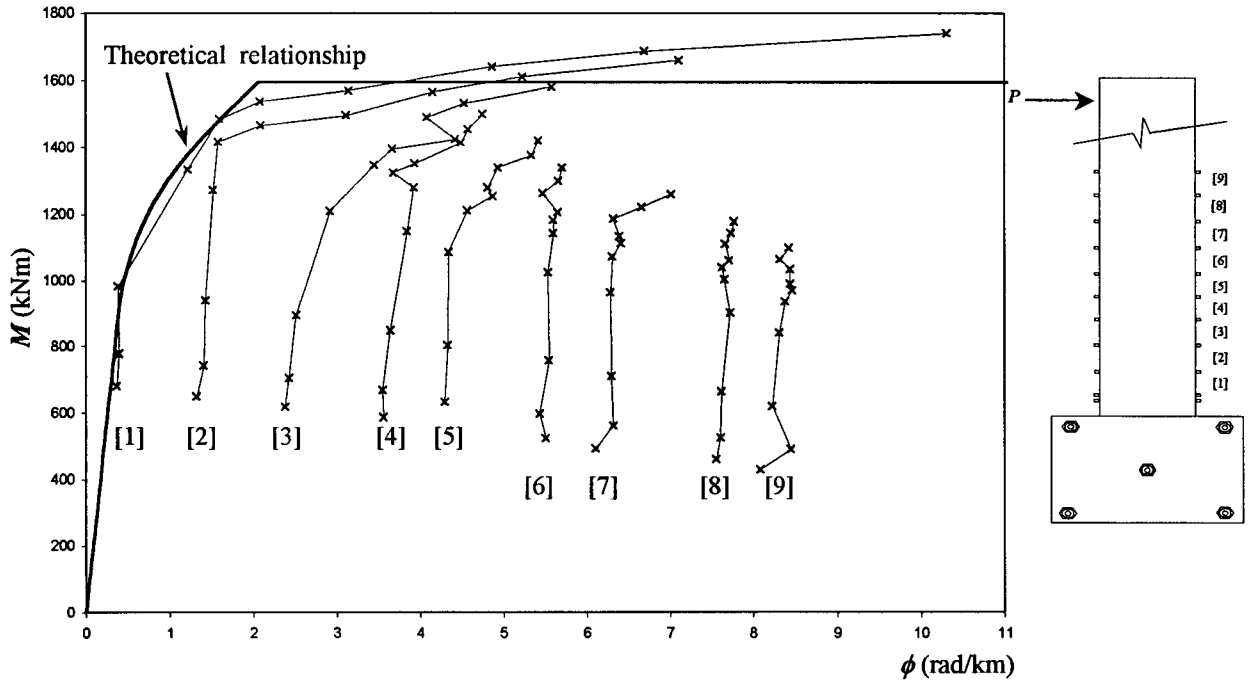

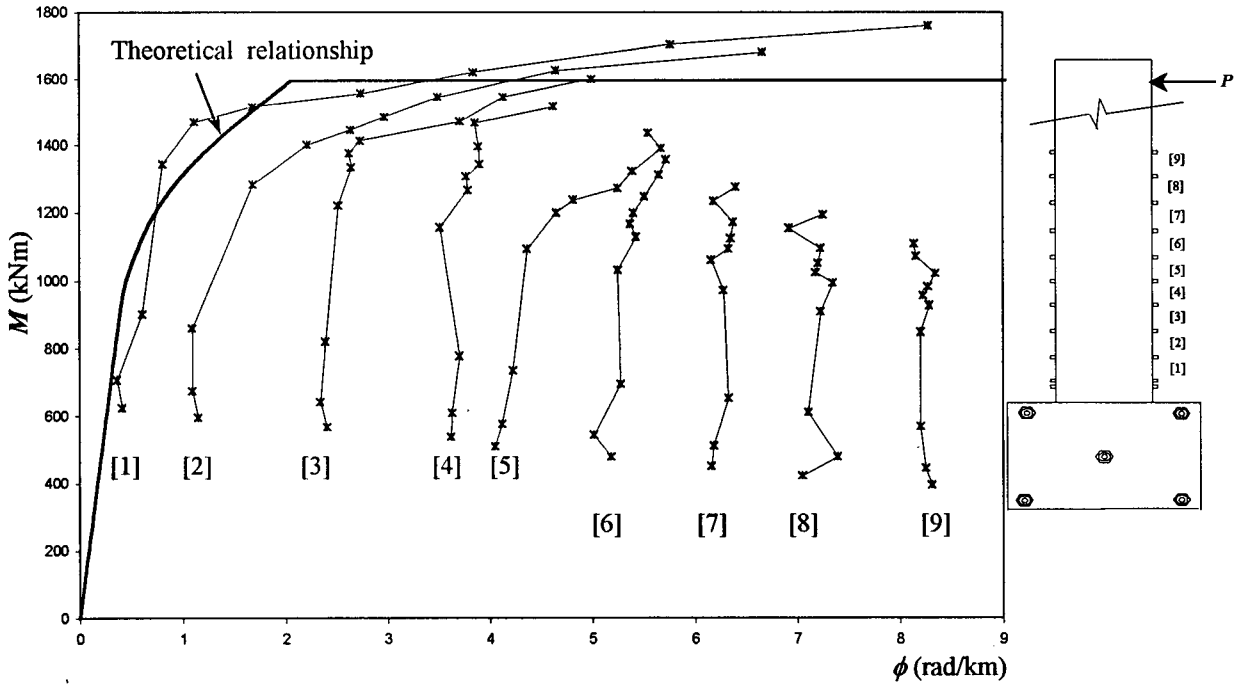

Figure 3.15 Trend of the measured bending moment-curvature relationship taken at various locations along the wall height during the different lateral displacement cycles.

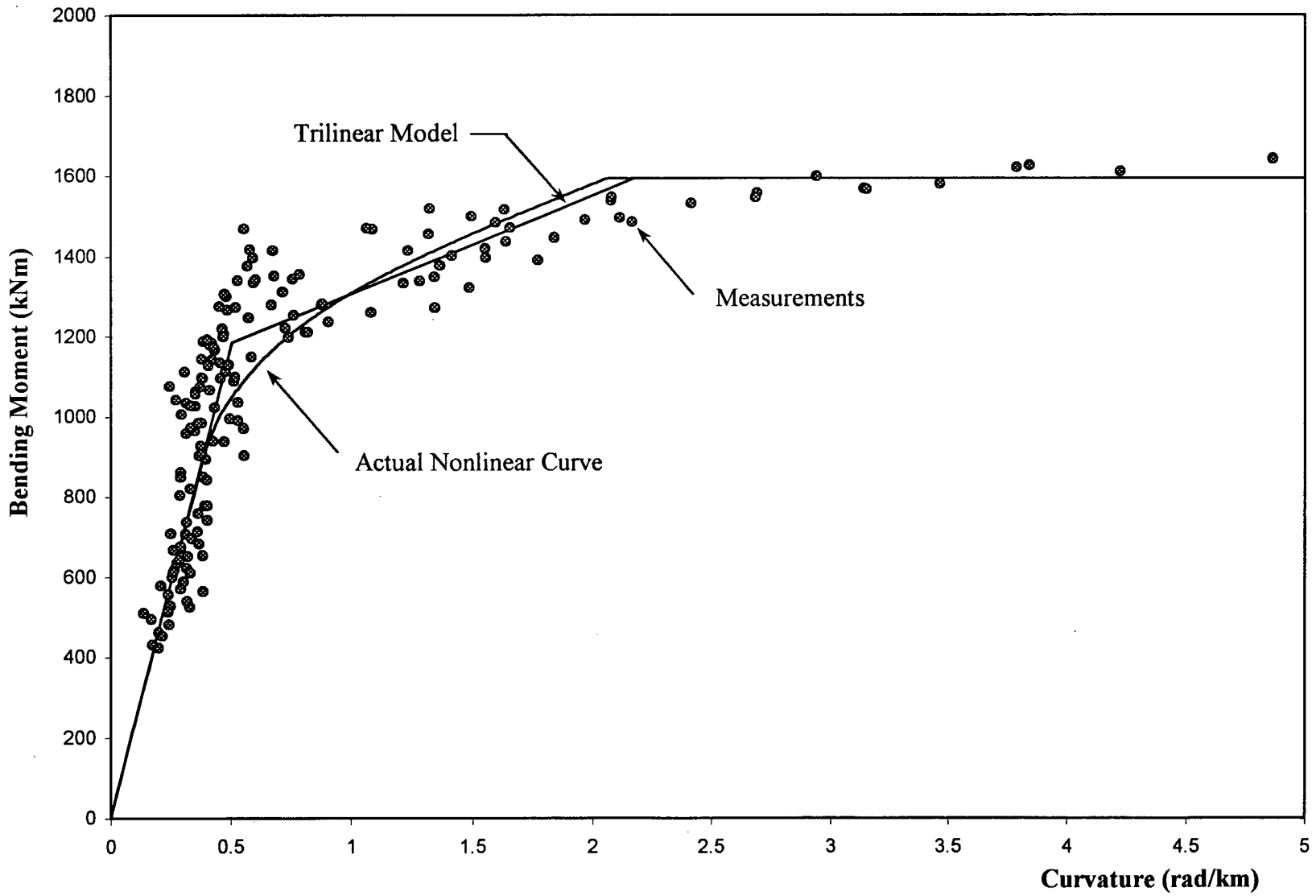

Figure 3.16 Comparison of the measured and predicted bending moment-curvature relationships.

Chapter 4

Effective Flexural Stiffness of Concrete Walls

4.1 Introduction

The trilinear bending moment-curvature relationship (i.e., nonlinear stiffness model) developed in Chapter 2, having been validated against the experimental results in Chapter 3, is used in this chapter to determine a "linear" flexural stiffness that can be used for the linear seismic analysis of concrete walls. The effective stiffness of a wall structure is determined by obtaining the linear elastic-perfectly plastic (bilinear) equivalent of the actual nonlinear load-displacement relationship. The effective stiffness is the slope of the linear elastic portion of the load-displacement relation.

As seen from the slender wall test results, once concrete cracks, the flexural stiffness of the wall reduces. Additional cracking due to cycling loading degrades the stiffness further and results in a substantial reduction in the flexural stiffness. Degradation of stiffness due to cracking during the cyclic motion of an earthquake is well recognized in the literature and known to increase the fundamental period of a building, see Figure 4.1.

To account for the degradation of stiffness and similar to the proposed bending moment-curvature model, the effective stiffness of the wall structure is expected to range from an upper-bound effective stiffness (which corresponds to a wall that is loaded monotonically without being previously cracked) to a lower-bound effective stiffness (which corresponds to a wall that is severely cracked from the previous load cycles).

In the following, the use of the trilinear bending moment-curvature relationship in predicting the actual nonlinear load-displacement relation of a wall structure is described. Characteristics of the load-displacement relation are discussed and the effective linear stiffness (both upper-bound and lower-bound) are determined. The influence of several important parameters on the predicted flexural stiffness is examined and a general as well as a simplified procedure to

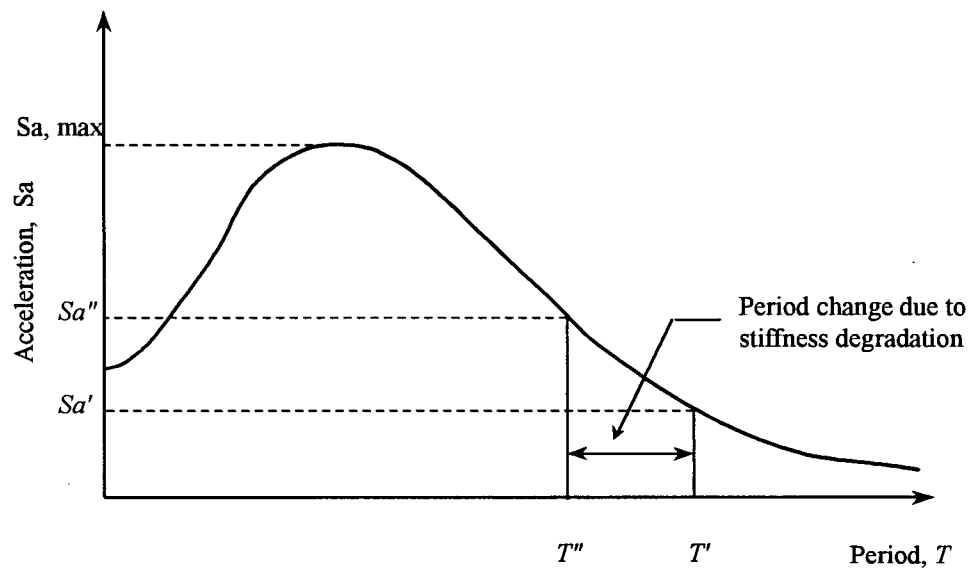

Figure 4.1 Typical lengthening of the fundamental period of a concrete wall due to the reduction in stiffness resulting from cracking during earthquake motion.

determine the effective flexural stiffness of concrete walls are presented. Finally, a comparison between the predicted stiffness of the slender wall test and the measured response is presented.

It is important to realize that while the objective is to predict the effective flexural stiffness of structural walls in high-rise buildings, the developed procedure is applicable to any structural wall that is dominated by flexural response.

4.2 Prediction of the Load-Displacement Relationship

Figure 4.2 summarizes the procedure used to predict the load-displacement curve of a wall and the assumptions used to simplify the calculations. A triangular lateral load distribution was assumed along the height of the building. The relevance of this assumption is discussed later (Section 4.3). The axial compression acting on the wall was assumed to vary linearly from zero at the top to a maximum value at the base. M_l is a linear function of the axial load and therefore also varies linearly over the height of the wall from the value at the base to a small value at the top of the wall. For simplicity, M_l was assumed to be zero at the top of the wall.

In many high-rise building, the geometry of the concrete walls are relatively uniform over the height of the building. Also, in those cases where only minimum reinforcement is required at the base of the wall, the amount of reinforcement will be uniform over the height of the structure. For simplicity, the concrete geometry and reinforcement arrangement were assumed to be uniform over the height of the wall and thus the gross moment of inertia, I_g, and the cracked section moment of inertia, I_{cr}, were assumed to be constant over the height of the wall.

The displacement, Δ, at the top level of a wall is given by the moment area theorem integral:

$$\Delta = \int_0^H \phi(h) \cdot h \cdot dh \qquad [4.1]$$

where ϕ_h is the curvature at level h distanced from the top level and H is the height of the wall.

The curvature at the base has the highest lever arm in the integral and hence has the largest contribution to the displacement at the top (i.e., the displacement at the top level is primarily the

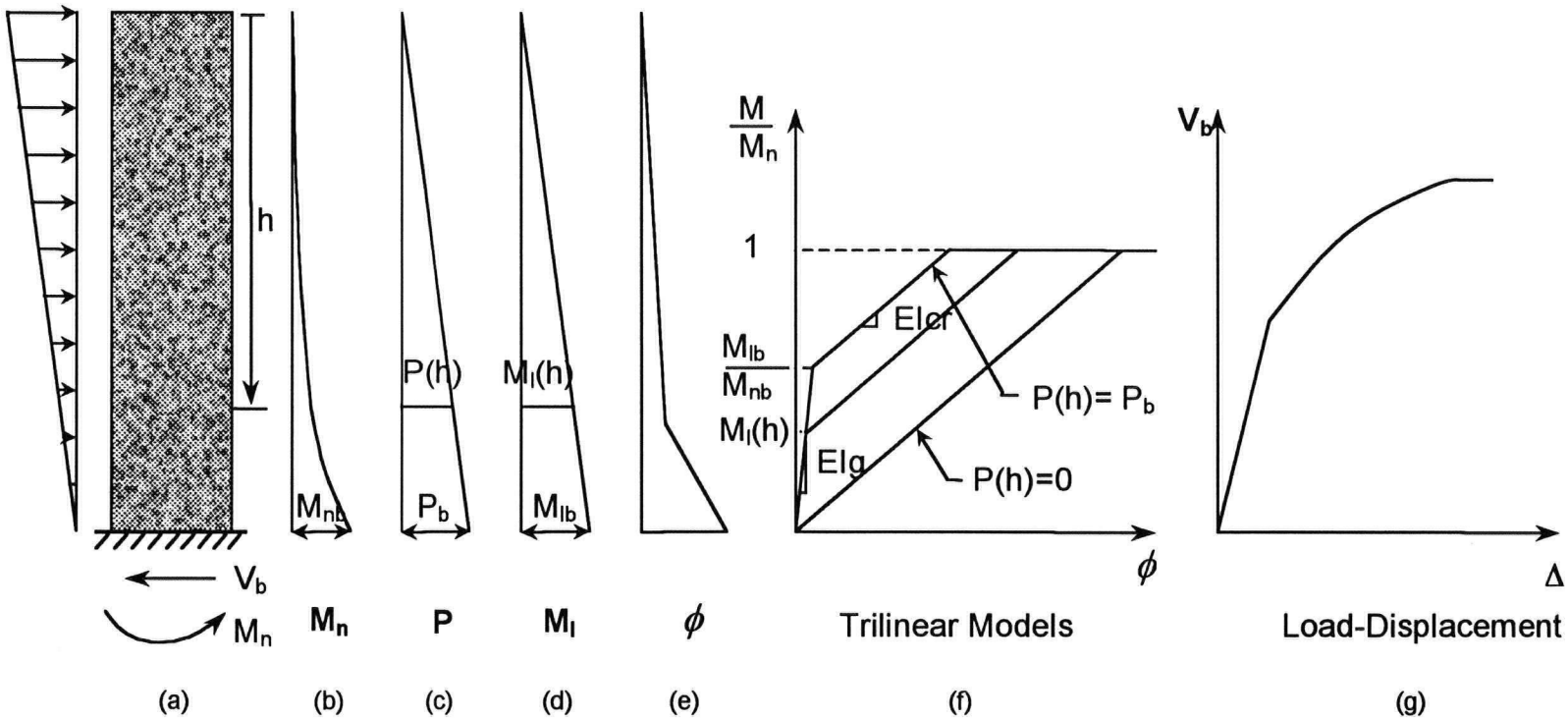

Figure 4.2 Procedure used to predict the load-displacement relationship: (a) assumed load distribution, (b) corresponding bending moment distribution, (c) assumed axial compression, (d) linear moment capacity, (e) resulting curvature distribution, (f) trilinear bending moment-curvature models, (g) complete load-displacement curve.

results of the curvatures near the base of the wall). Small error in the displacement results from using the characteristics of the cross section at the base when the wall characteristics vary over the height. Therefore, the load-displacement curve of a wall structure can be characterized by the two non-dimensional parameters that describe the bending moment-curvature relationship of the cross section at the base of the wall: the ratio of the cracked section moment of inertia to the uncracked section (gross) moment of inertia, I_{cr} / I_g, and the ratio of the linear bending moment to the capacity of the wall section at the base, M_l / M_n.

Prediction of a nonlinear load-displacement curve requires the application of Equation [4.1] to determine the top displacement, Δ, at different load steps. The height of the wall was discretized into several levels. Each level has its specific trilinear bending moment-curvature relationship according to the assumed axial load at that level (Figure 4.2-f). At each load step, the bending moment distribution along the height was computed, and the curvature at each level was determined from the corresponding trilinear bending moment-curvature relationship. Integration of the resulting curvature distribution gives the top displacement at this load step. The procedure was repeated for several load steps and the complete load-displacement curve was determined.

Note that even though the bending-moment curvature relationship is piecewise linear, the load-displacement relationship is nonlinear. Nonlinear curvature distribution along the height, resulting form the cubic distribution of the bending moment, is the main reason.

The above procedure was implemented in program *Wall-Tools* and the program was used to generate the load-displacement relationships shown in the following sections.

4.3 Characteristics of the Load-Displacement Relationships

The procedure just described was used to determine the load-displacement relationships of the walls shown in Figure 4.3. Two different cross sections at the base of the wall were considered in the example. The actual nonlinear load-displacement relations shown in the figure are for the monotonic upper-bound response. A somewhat secondary slope follows the initial linear uncracked gross section response of the load-displacement relation until the wall reaches its yield strength/displacement. Bilinear approximation of the actual nonlinear load-displacement

relationship is needed to estimate the effective stiffness of the response. The effective stiffness of the wall response is determined as the slope of the linear elastic portion of the bilinear idealization.

FEMA 273 (1997) suggests the use of the secant to 60% of the yield strength as the elastic slope of the bilinear idealization of the actual load-displacement curve when determining the fundamental period of a structure. Paulay and Priestley (1992) suggest the use of an effective secant stiffness to the nonlinear load-displacement curve that is based on 75% of the yield strength or nominal strength of the concrete member. French and Schultz (1991) used the secant to the load-displacement curve at 2/3 of the maximum load to idealize the actual nonlinear curve with a bilinear approximation when examining the displacement history of several beam tests. The secant to the nonlinear load-displacement curve at first yield of the reinforcement was used by Priestley and Hart (1989) to define the effective stiffness for period and ductility calculations of rectangular masonry walls.

For walls with a small amount of vertical reinforcement as shown in Figure 4.3 (common in high-rise wall buildings constructed in British Columbia), the uncracked section response of the load-displacement relationship is very significant. In addition, the secondary slope of the load-displacement curve is nearly flat. Considering the effective stiffness as the secant at 3/4 of the nominal/yield strength or alternatively at 2/3 or 3/5 of the maximum load results in a stiffness value that is very close to the initial uncracked response and underestimates the effective yield displacement of the wall response (see Figure 4.3).

While the equivalent bilinear idealization of the load-displacement relationship using the secant to the first yield of reinforcement may provide a more appropriate estimate of the yield displacement (Priestley and Hart,1989), it certainly gives a lower estimate of the effective stiffness needed for the calculation of the elastic fundamental period of the wall structure. Also, it has been shown (Section 2.2) that relating the stiffness to the yield curvature does not seem to capture the elastic deformations of such walls. Note that the low values of effective stiffness recommended in the commentary to the New Zealand concrete code (Figure 1.1) are based on the recommendation of Priestley and Hart (1989). The SEAOC Blue Book (1996) indicates that this stiffness recommendation "can yield unrealistically low values of stiffness".

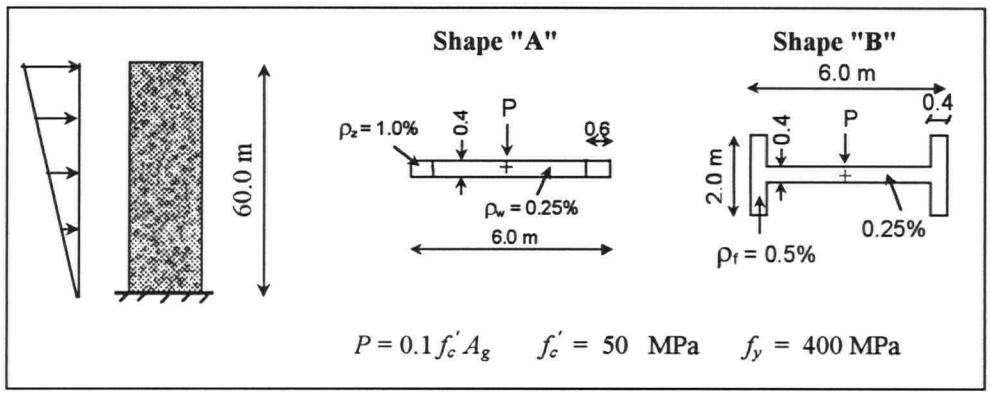

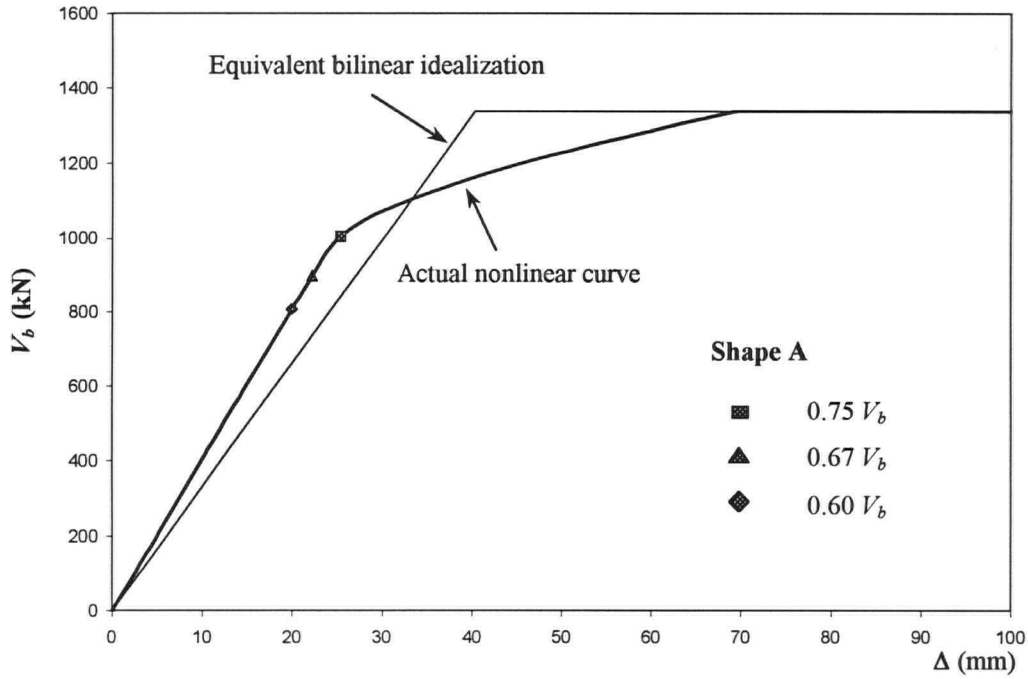

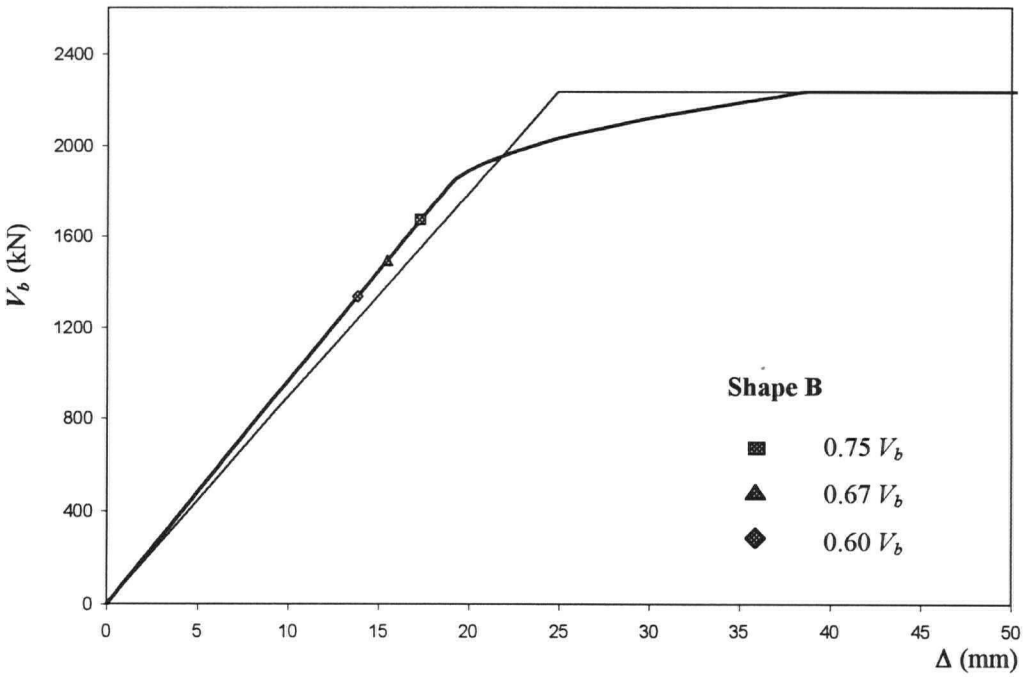

Figure 4.3 Load-displacement characteristics for typical wall sections.

Since a good representation of the nonlinear load-displacement curve should also involve a good representation of the actual energy absorbed by the real inelastic load-displacement curve (i.e., area under the curve) in addition to the provision of a realistic estimate of the effective yield displacement, it is suggested that the equivalent bilinear idealization of the actual nonlinear load-displacement curve is the one that has the same area under both curves (i.e., equal energy). FEMA 273 (1997) also stated that the use of the specified secant stiffness at 60% of the yield strength to determine the bilinear equivalent of the actual nonlinear load-displacement relationship is an approximate measure with the recommendation to evaluate the use of this criteria, "the best choice may be to have approximately equal area under both curves". This criterion of equal area under the actual nonlinear and the idealized bilinear load-displacement curves (equal energy under both curves) was used to determine the bilinear equivalent of the load-displacement curve. Further discussion and comparison of the different assumptions to determine the bilinear equivalent of the load-displacement curve are provided in Section 4.4.

Figure 4.4 shows the load-displacement curve of the wall example shown in Figure 4.3 (Shape A). Two different load distributions were used: the triangular load distribution (as shown previously in Figure 4.3 and repeated here for comparison) and the first mode lateral forces. The results of the analyses are shown in terms of the top displacement of the wall as well as the displacement at the center of lateral load. In each case, the equivalent bilinear idealization with the same area under the actual load-displacement curve is also shown. Note that the plots are presented with non-dimensional axes where the load is divided by the maximum load and the displacement is divided by the corresponding yield displacement.

The results of the analyses indicate that the stiffness of the elastic portion of the bilinear response of the wall or the "effective stiffness" as a ratio of the initial (uncracked) stiffness is reasonably independent of the assumed load distribution and the location of measured displacement. This stiffness value of 0.75~0.78 I_g is unique to the cross section characteristics of the specific wall.

4.4 Determination of Effective Flexural Stiffness of Concrete Walls

Both the upper-bound and lower-bound effective stiffnesses of a wall structure were determined by obtaining the bilinear equivalent of the actual load-displacement relationship. The load-

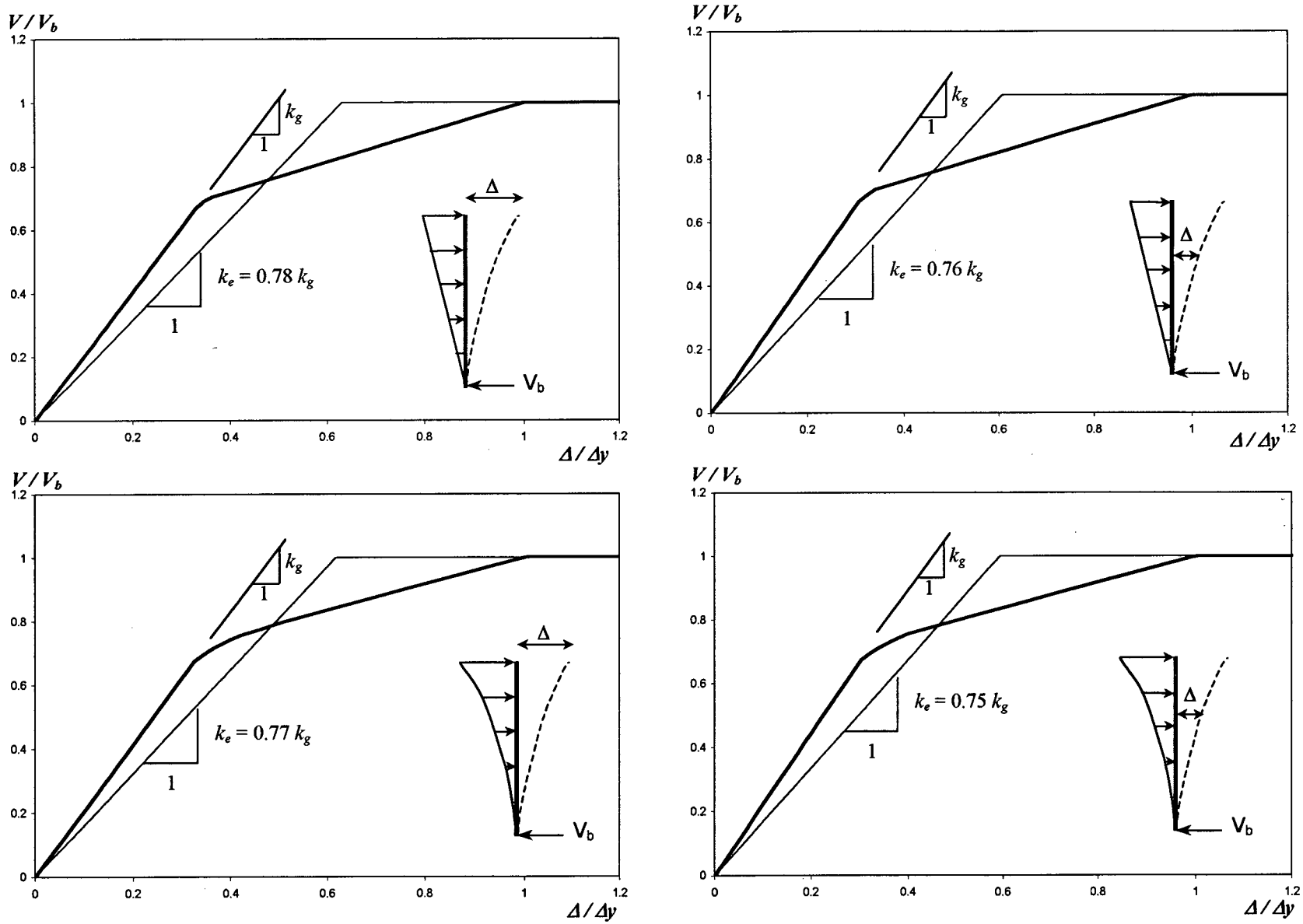

Figure 4.4 Independent bilinear idealization of the load-displacement relationship.

displacement relationship of a wall, characterized by the two non-dimensional parameters that describe the cross section at the base of the wall: I_{cr} / I_g, and M_l / M_n, was determined using the procedure described in Figure 4.2. The equivalent bilinear idealization of the load-displacement curve was determined with the same area under both curves and the effective stiffness was determined as the elastic stiffness of the idealized relation.

The effective flexural stiffness was determined for a variety of possible values of the two non-dimensional parameters that characterize the load-displacement relationship of a wall structure and the resulting effective stiffnesses (represented as a fraction of the gross moment of inertia, I_e / I_g) are plotted in Figure 4.5.

Figure 4.5 shows the variation of the effective stiffness with any possible variation in the characteristics of the section at the base of the wall. As shown, the effective stiffness can be anywhere between 0.0 and 1.0 and is influenced by the ratio I_{cr} / I_g and/or the ratio M_l / M_n.

The effective stiffness results shown in Figure 4.5 can be approximated by the following expression:

$$\frac{I_e}{I_g} = \frac{I_{cr}}{I_g} + \left(3\left(\frac{M_l}{M_n}\right)^a - 2\left(\frac{M_l}{M_n}\right)^b\right)\left(1 - \frac{I_{cr}}{I_g}\right) \qquad [4.2]$$

Where the exponent a, and b are defined in Table 4.1. Figure 4.6 compares results from the simple expression, Equation [4.2], with the curves of Figure 4.5. Very good agreement is found.

Before using the above procedure to determine the effective flexural stiffness for various wall structures and examine the influence of the important parameters that affect the stiffness, it is useful to use the fundamental approach illustrated in Figure 4.5 to confirm the premises of equal area criteria to approximate the nonlinear load-displacement relation with a bilinear curve. Figure 4.7 compares the effective stiffness values determined using the equal area criteria to those computed using a secant stiffness to a point on the actual load-displacement curve located at: 75%, 67% and 60% of the yield strength. As mentioned earlier, these have been used by others to determine the equivalent elastic stiffness. The different procedures yield very similar results for small values of M_l / M_n. On the other hand, very different results are obtained for

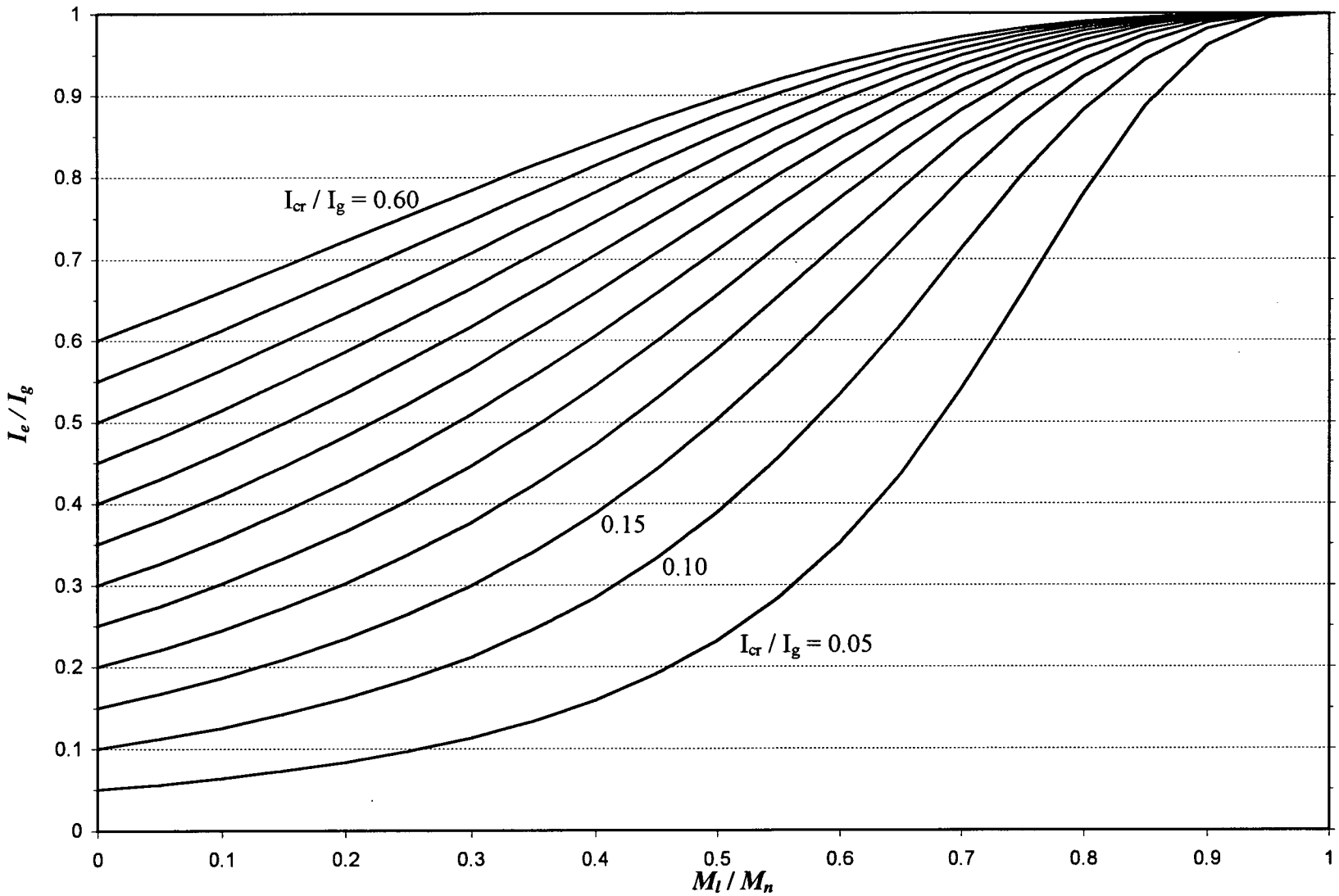

Figure 4.5 Determination of the effective flexural stiffness, I_e, for concrete walls.

Table 4.1 Values of the exponent *a* and *b* for Equation [4.2].

I_{cr}/I_g	*a*	*b*
0.05	3.8	6.0
0.10	2.8	4.4
0.15	2.3	3.6
0.20	2.0	3.1
0.25	1.9	3.0
0.30	1.8	2.9
0.35	1.7	2.8
0.40	1.6	2.6
0.45	1.5	2.4
0.50	1.4	2.2
0.55	1.3	2.0
0.60	1.2	1.8

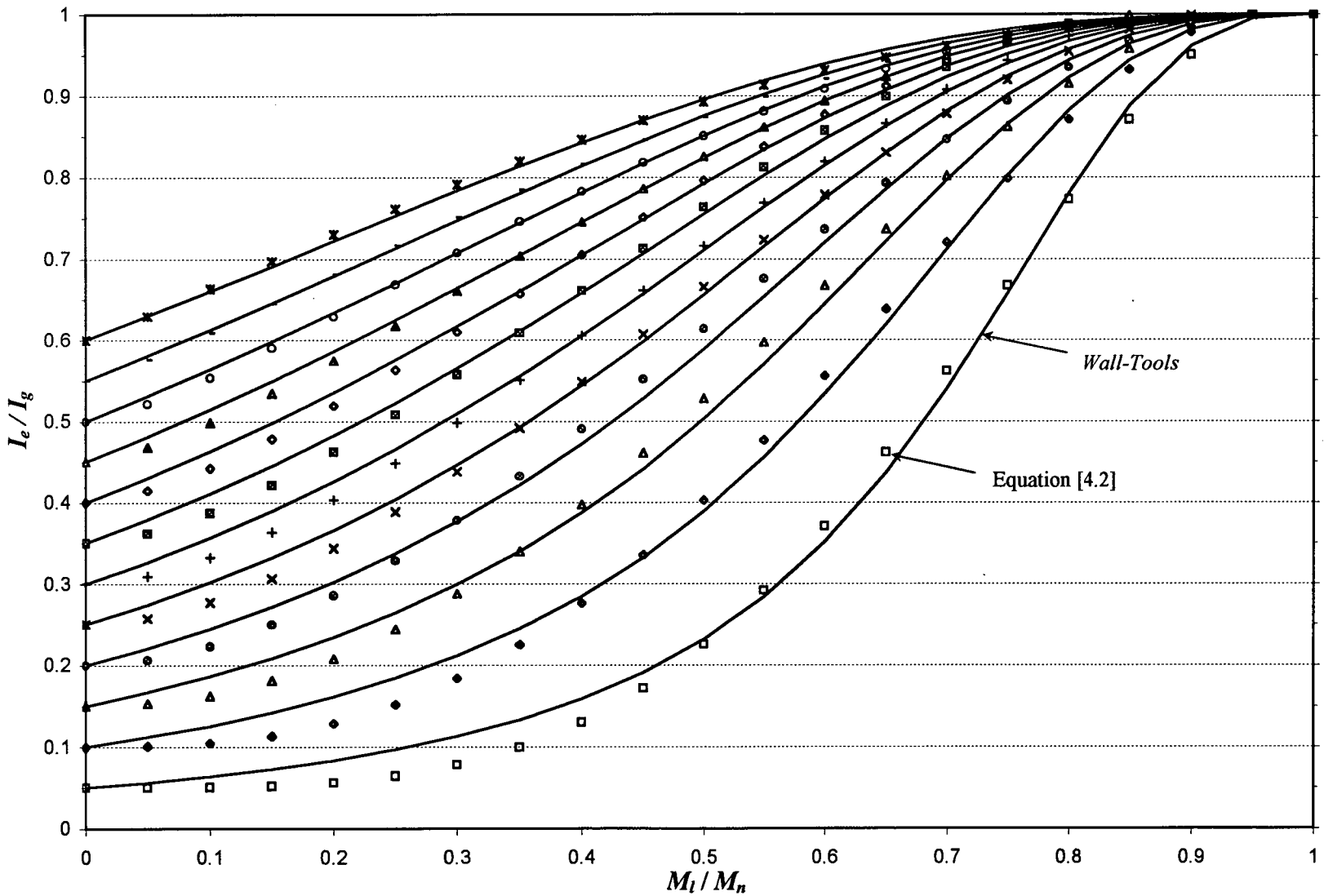

Figure 4.6 Comparison of the predicted effective flexural stiffness with the value estimated using Equation [4.2].

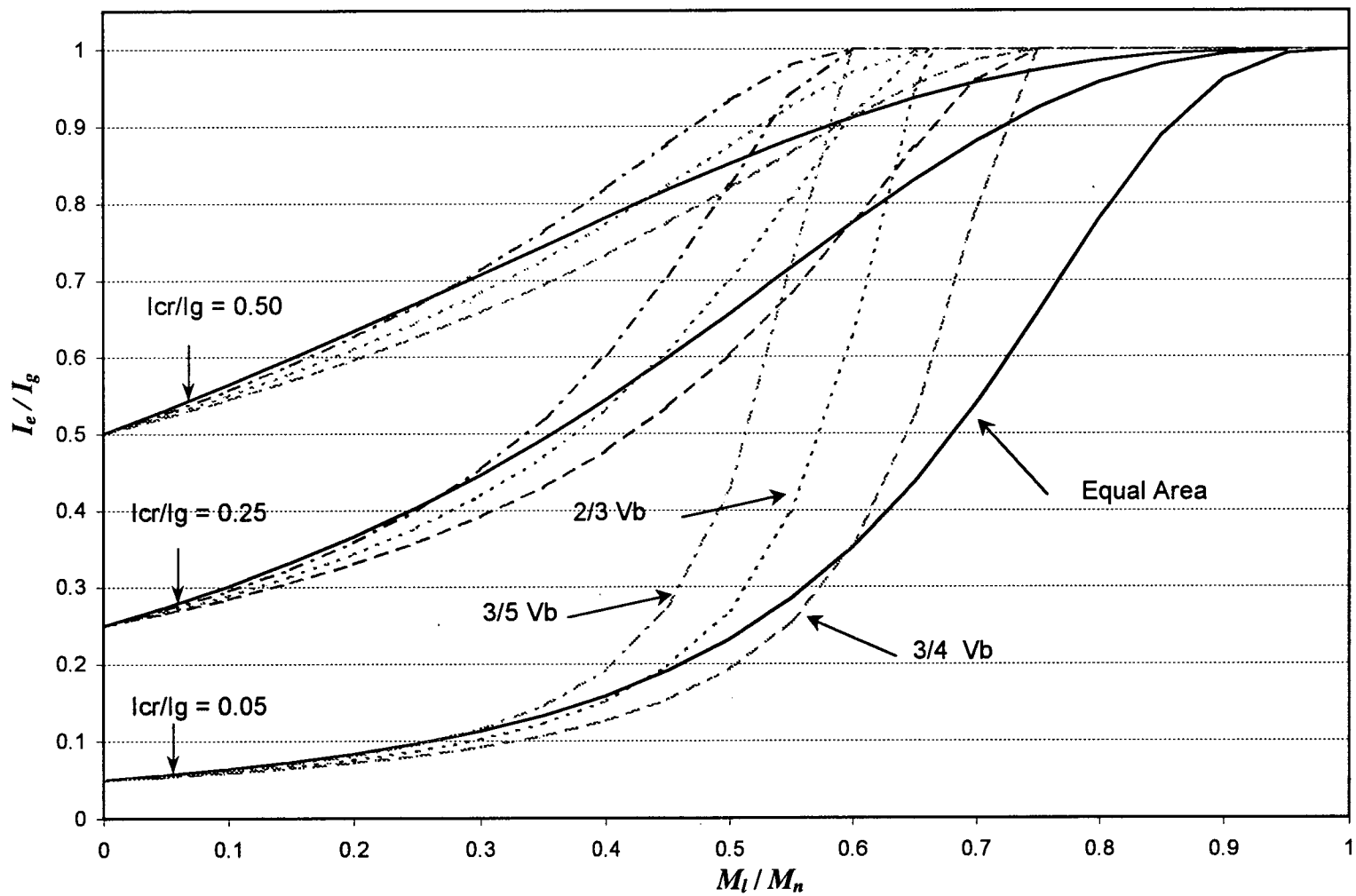

Figure 4.7 Comparison of the effective flexural stiffness determined using different methods to obtain the equivalent bilinear elastic stiffness.

large values of M_l / M_n (when the initial gross stiffness exceeds the prescribed portion of the yield strength on the load-displacement relation). Large values of the ratio M_l / M_n occur for example when there is a minimum amount of vertical reinforcement in the wall as shown previously in Figure 4.3. The equal area method provides more conservative, and it is believed more appropriate, values of the effective stiffness.

4.5 Trend of Stiffness Variation

Figure 4.5 provides a fundamental method to determine the effective stiffness of a wall structure knowing the four parameters that characterize the cross section at the base: I_g, I_{cr}, M_l, and M_n. Increasing the ratio I_{cr} / I_g and/or the ratio M_l / M_n increases the effective stiffness. A change in geometry or material property of the section at the base that affects any of the four parameters will have an influence on the predicted stiffness of the wall.

It is useful then to examine the influence of some important variables (that affect the four parameters) on the stiffness values of some typical concrete walls. The main variables are: the axial compression acting on the wall; the concrete geometry; the amount and distribution of vertical reinforcement; the concrete compressive strength; and the yield strength of the vertical reinforcement.

In the following, the influence of each of the main variables is examined and the significance of each variable on the variation of stiffness is illustrated. Results are shown for the upper-bound and lower-bound effective stiffness.

4.5.1 Axial Compression Acting on the Wall

Effect of the axial compression acting on the wall is widely recognized (e.g., Priestley and Hart 1989, Council, 1992) as an important parameter affecting wall stiffness. Figure 4.8-a shows the variation of the effective stiffness with the axial compression acting on a rectangular wall cross section. Increasing the axial compression results in an increase in both M_l and M_n.

The increase in M_l with axial compression is approximately linear (as discussed in Chapter 2). The corresponding increase in M_n is approximately linear as well for the low range of axial compression applied to a typical wall section. When the rate of increase of M_l with respect to the axial load exceeds the corresponding rate of increase of M_n (i.e., $M_{l,\mathrm{P2}} / M_{l,\mathrm{P1}}$ is greater than $M_{n,\mathrm{P2}} / M_{n,\mathrm{P1}}$), axial compression increases the effective stiffness (Figure 4.8-b).

4.5.2 Geometry of the Wall Section

Figure 4.9 demonstrates the variation of the effective stiffness of five different cross sections commonly used in wall structures. The wall cross sections have the same length and amount of reinforcement and are subjected to axial compression ranging from 2% to 20% of $f_c' A_g$.

Changing the geometry of the cross section influences all four parameters in Figure 4.5. Different wall cross sections with the same amount of reinforcement and subjected to the same axial load have a different flexural capacity, M_n. The shape and size of the compression side of the wall influence the depth of the neutral axis and hence the contribution of the concrete in compression. Gross moment of inertia, I_g, is a cubic function of the length of the section. Area of the flange and square the depth to the centroid also contribute to I_g. Geometry of the tension side of the cross section affects the calculation of the linear bending moment, M_l (Sectional modulus, S, in Equation [2.7]). The shape and size of the compression side of the cross section influence the cracked section moment of inertia, I_{cr} (besides the amount of reinforcement which plays a major role in the determination of I_{cr}).

As shown in Figure 4.9, the effective stiffness is very different from one shape to another. The recommendations for the effective stiffness from different documents are also shown in the figure. It is interesting to see that each recommendation is correct for a certain type of wall under certain conditions.

It is interesting to note that the T-shape section is the equivalent to the C-shape section when subjected to reverse bending (i.e., pushed in the other direction) and hence, unsymmetrical shapes have different stiffness depending on the direction of loading.

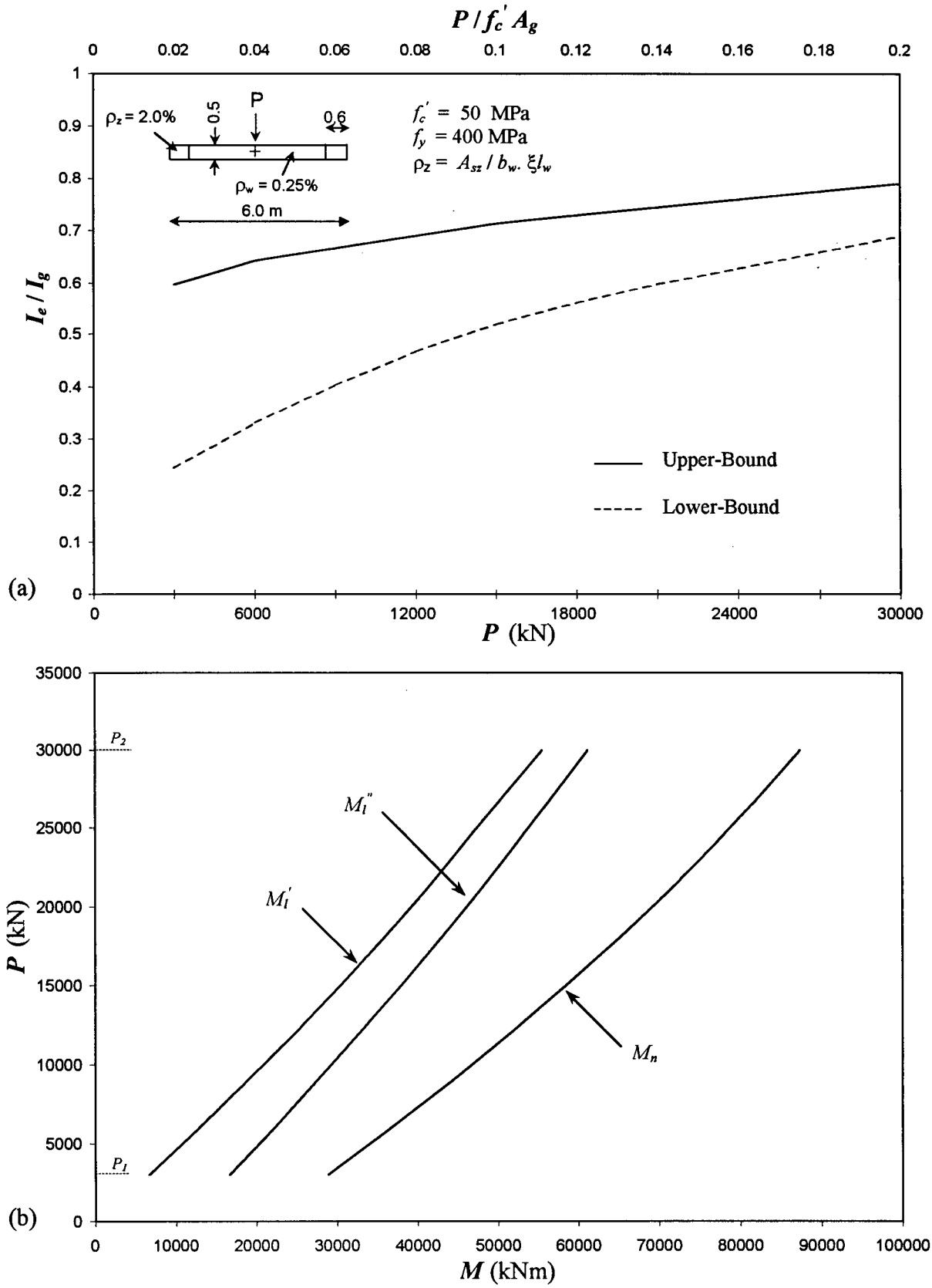

Figure 4.8 Variation of the effective flexural stiffness with the magnitude of axial compression.

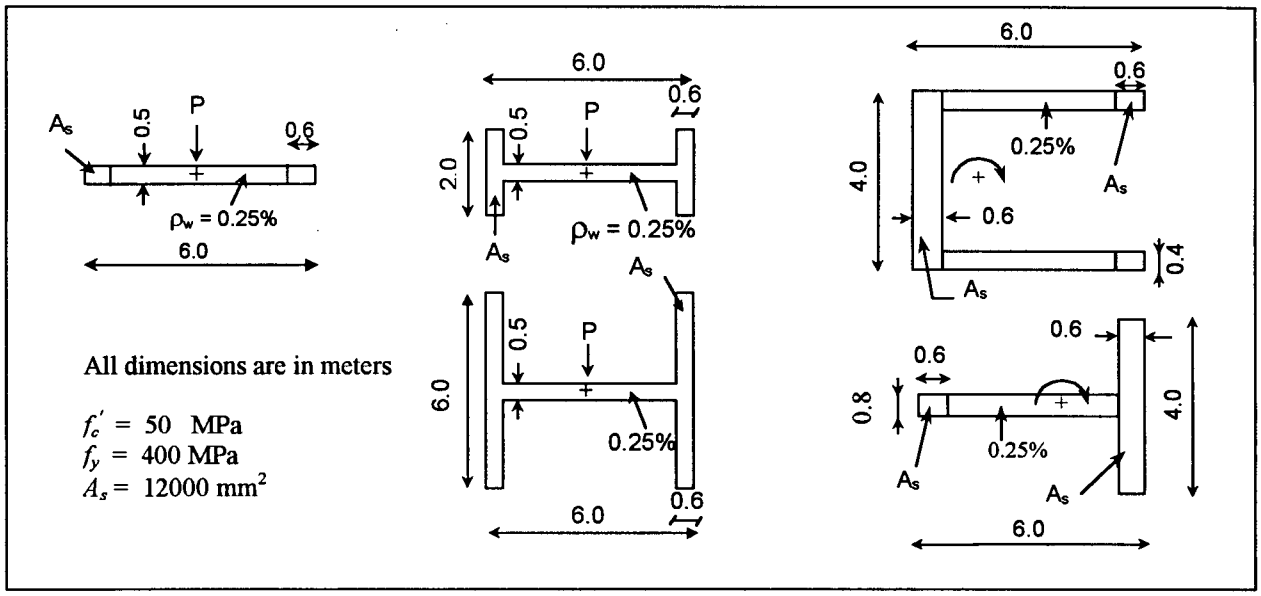

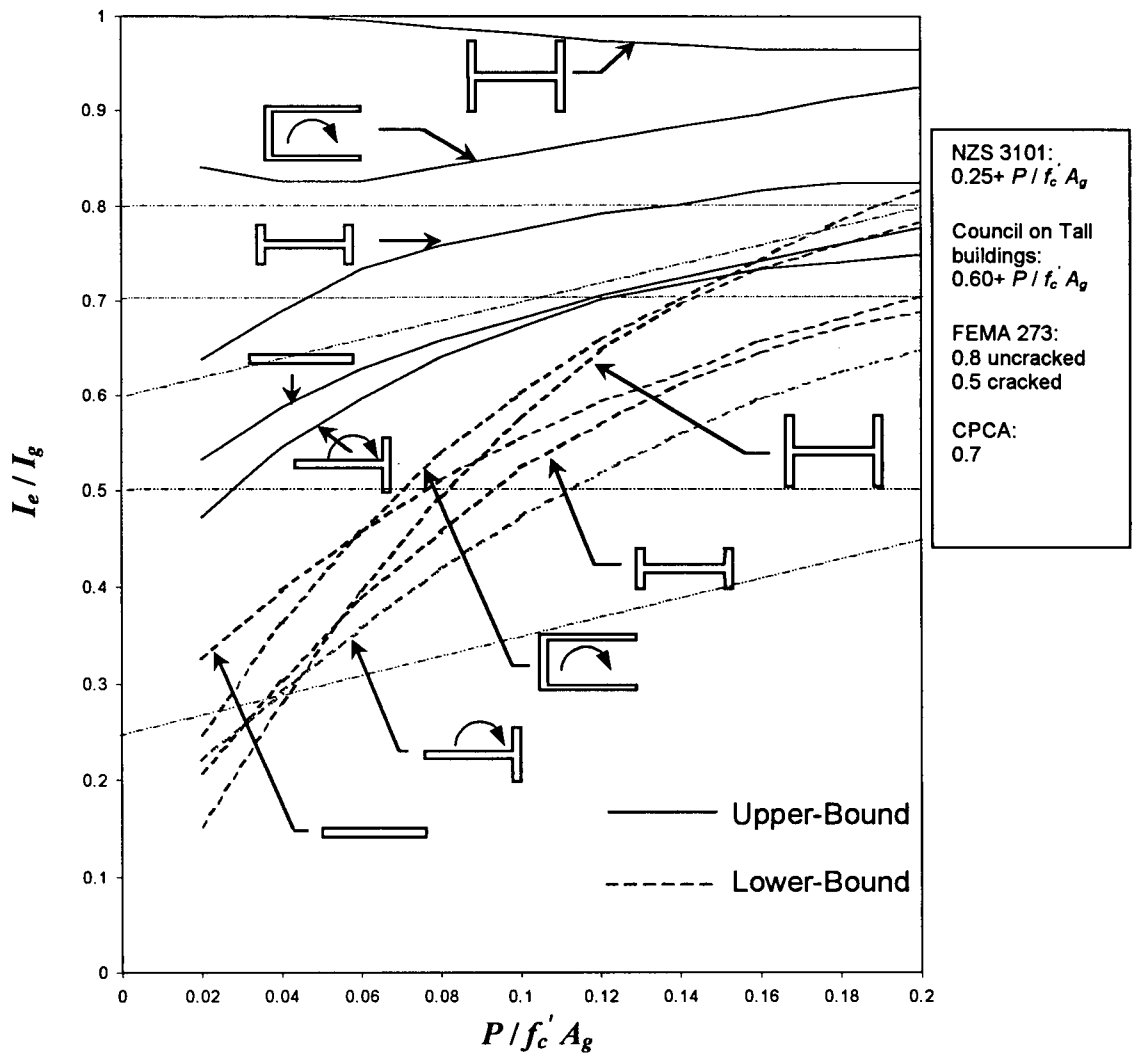

Figure 4.9 Variation of the effective flexural stiffness for different wall shapes.

4.5.3 Amount and Distribution of the Vertical Reinforcement

Figure 4.10 shows the variation of the effective stiffness for different amounts of vertical reinforcement concentrated in the boundary zone of a rectangular wall section. Increasing the amount of reinforcement increases the flexural capacity of the wall section, M_n, as well as the cracked section moment of inertia, I_{cr}. The increase in M_n reduces the effective stiffness whereas the increase in I_{cr} increases the stiffness value. Whichever of these two dominates the response will control whether there is an increase or decrease in the resulting effective stiffness.

For the rectangular wall shape, the upper-bound effective stiffness is reduced with the increase of the amount of vertical reinforcement whereas the lower-bound effective stiffness is increased with increasing the amount of the reinforcement (Fig. 4.10-a).

Note that the increase in the value of M_n and I_{cr} (when increasing the amount of reinforcement) is the same for both the upper and lower stiffness prediction, however, it is the range of the M_l / M_n ratio that makes the difference. Upper-bound stiffness prediction involves higher values of M_l / M_n ratios in which a small change of M_n and consequently M_l / M_n makes a drastic change in the stiffness value (see Figure 4.5). In other words, for high values of M_l / M_n (upper-bound stiffness prediction, M_l'' / M_n), the increase in M_n and the consequent reduction of M_l / M_n ratio dictate the predicted stiffness, whereas for the lower-bound effective stiffness prediction (lower range of M_l' / M_n values) the effect of increase in I_{cr} value with the increased amount of reinforcement controls the resulting stiffness value.

A reduction in the value of the upper-bound effective stiffness with an increasing amount of reinforcement should not be confused with the basic definition of stiffness where a stiffer structure is displaced less when subjected to the same force (or alternatively, stiffer response of the structure requires higher force to displace the same amount of deflection). The force-displacement characteristics of two cases of different amounts of reinforcement, for both the upper and lower-bound predictions, are shown in Figure 4.11. As the amount of reinforcement increases, the secondary slope of the curve becomes larger (which is a function of I_{cr}) and the amount of displacement is less for the same lateral force (i.e., stiffer response). However, the slope of the bilinear approximation that gives an equivalent area to the actual load-displacement curve is smaller when the amount of reinforcement is increased for the upper-bound predictions.

The opposite is true for the lower-bound stiffness. It is worth mentioning that the effective stiffness determined using a certain portion of the yield strength to approximate the actual load-displacement relation (secant to 75% of V_b for example) gives the same effect, i.e., a lower effective stiffness with a larger amount of reinforcement, for the prediction of the upper-bound stiffness (Figure 4.11-a).

Figure 4.12 shows the variation of the effective stiffness for flanged walls with two different flange sizes. The same trend observed in the case of a rectangular wall is also observed here with few exceptions. For example, the upper-bound stiffness of shape "B" is increased with the increase of the amount of reinforcement (ρ_f = 1.5% to ρ_f = 3.0%) for the low range of axial compression. The influence of M_n on reducing the effective stiffness is overcome by the contribution of I_{cr} to increase the stiffness value.

The exceptionally high effective stiffness of the flanged wall section with a small amount of vertical reinforcement (see Figure 4.12) is due to the fact that sections with a very small amount of reinforcement have a small increase in strength after cracking and therefore the effective stiffness is essentially the gross concrete stiffness. This remark is also true for the case of big-size flanged wall shown in Figure 4.9, where the amount of reinforcement considered in the example (As = 12000 mm^2, ρ_f=0.35%) is very small with regard to the big size of the flange.

Figure 4.13 shows the effect of distributing the amount of reinforcement over a different length in the boundary zone of the cross section. A slight increase in M_n is compromised with a small increase in I_{cr}, and the change in the effective stiffness value is insignificant.

4.5.4 Concrete Compressive Strength

The concrete compressive strength, f_c', influences the modular ratio, n, and hence I_{cr}, the tensile strength of concrete and hence M_l for upper-bound case only (i.e., M_l''), and to some extent M_n.

Figure 4.14 shows the effect of varying f_c' on the effective stiffness of flanged and rectangular wall sections. The lower-bound effective stiffness is always reduced with increasing the concrete compressive strength. The slight increase in M_n, while M_l' stays the same, reduces the

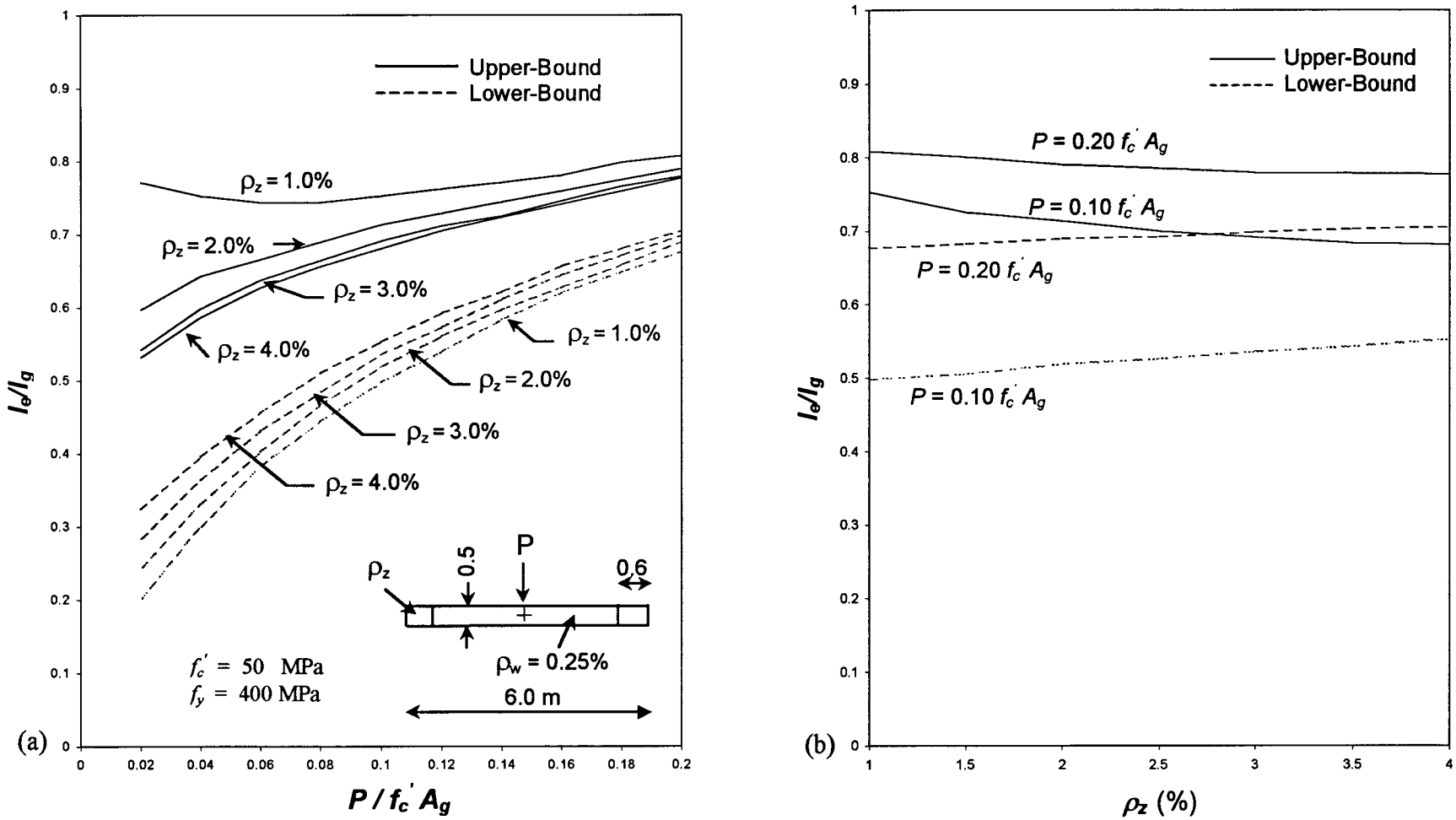

Figure 4.10 Variation of the effective flexural stiffness with different amounts of vertical reinforcement in a rectangular wall.

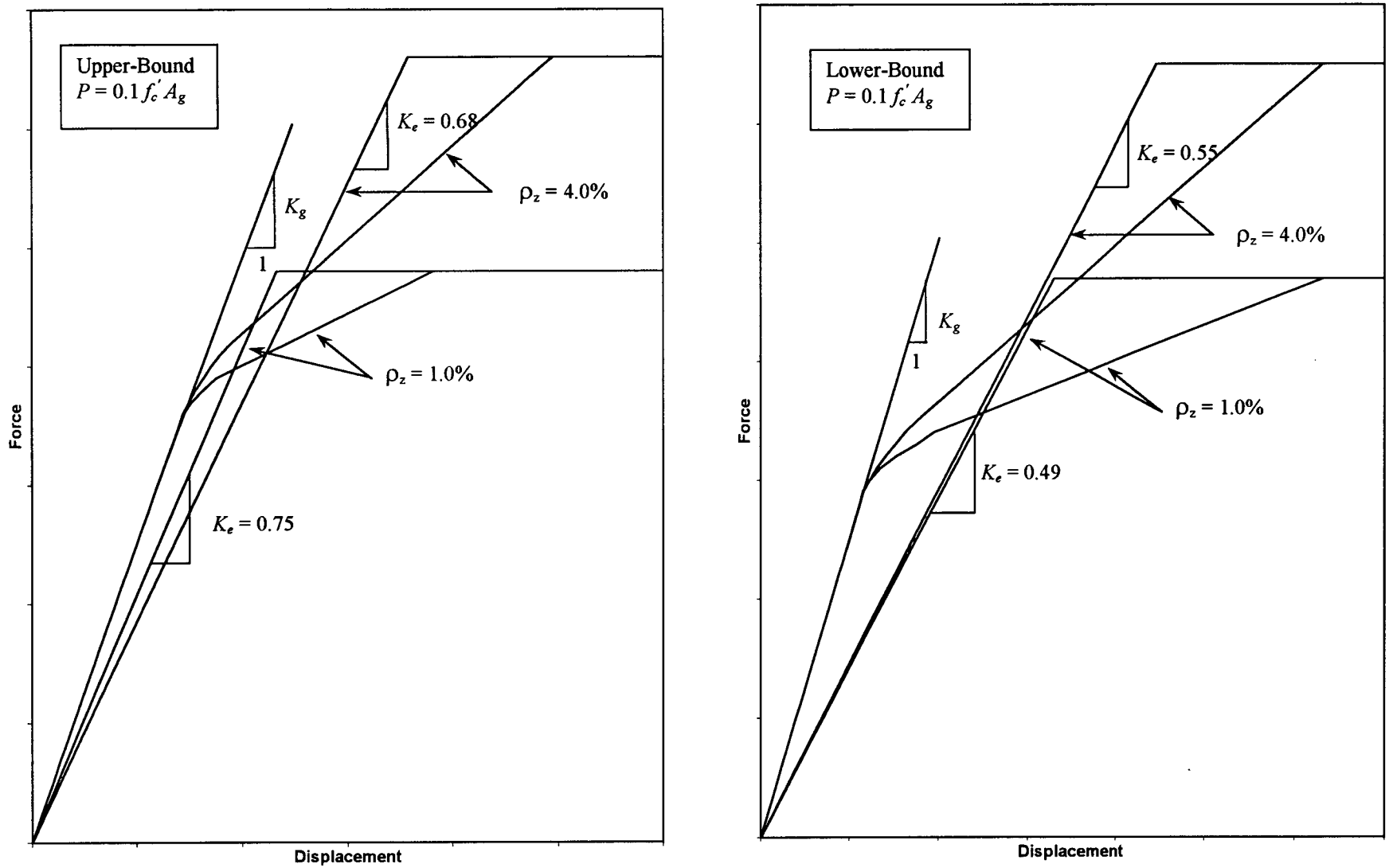

Figure 4.11 Load-displacement characteristics of a rectangular wall with different amounts of vertical reinforcement.

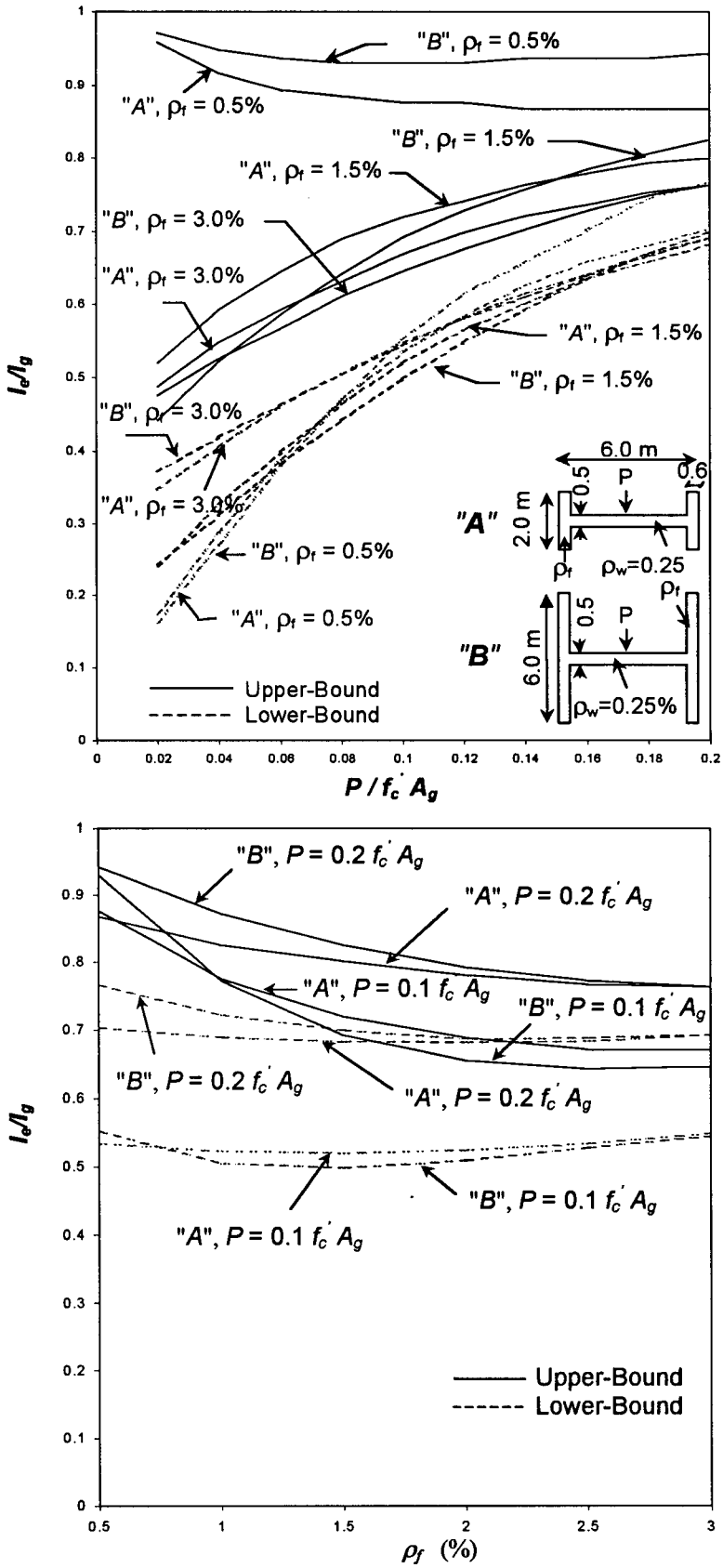

Figure 4.12 Variation of the effective flexural stiffness for flanged walls with different amounts of vertical reinforcement.

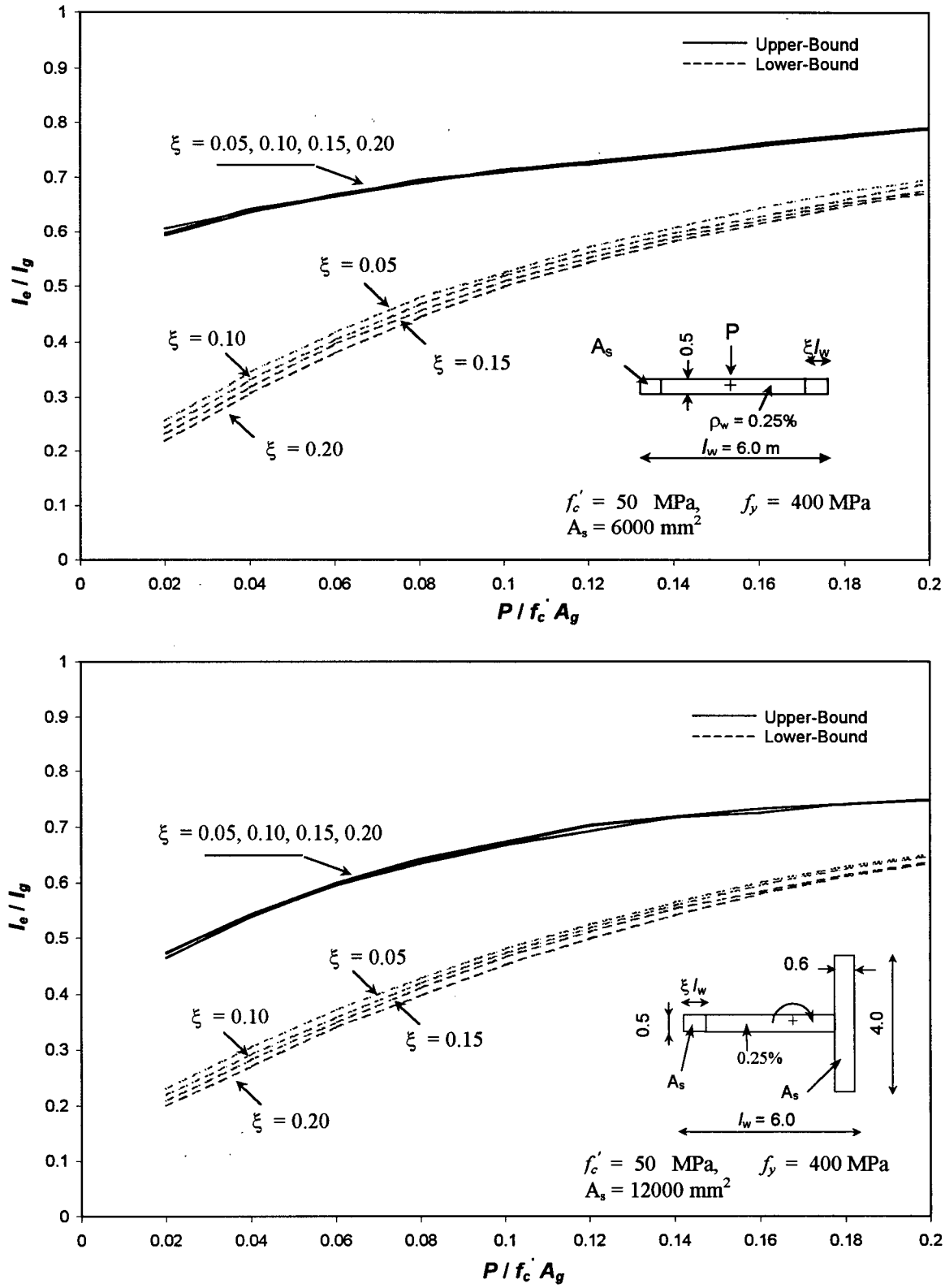

Figure 4.13 Variation of the effective flexural stiffness with different distributions of the vertical reinforcement in the boundary zone of the cross section.

ratio of M_l / M_n. The modular ratio, n, is also reduced (due to higher value of E_c) and hence I_{cr}. The upper-bound effective stiffness is influenced by both M_l and M_n. Increasing f_c' will increase M_l'' (due to higher concrete cracking strength) and M_n (due to stronger concrete in compression) while reducing I_{cr}.

Higher M_l'' value results in higher effective stiffness whereas higher M_n and/or lower I_{cr} result in lower effective stiffness. When the effect of the increased M_l'' exceeds the combined effect of higher M_n and lower I_{cr}, the result is higher upper-bound effective stiffness with increasing f_c' as seen for the flanged wall shown in Figure 4.14-a. The reverse effect is seen for rectangular walls shown in Figure 4.14-b where the upper-bound effective stiffness is mostly reduced with increasing f_c'.

4.5.5 Yield Strength of the Vertical Reinforcement

The yield strength of the vertical reinforcement influences only the capacity of the wall cross section, M_n. Increasing the yield strength of the reinforcement results in higher M_n and hence a lower ratio of M_l / M_n. The resulting effective stiffness is therefore reduced with an increase in the yield strength. Figure 4.15 demonstrates the effect of changing the yield strength of the vertical reinforcement on the effective stiffness of both rectangular and flanged wall sections.

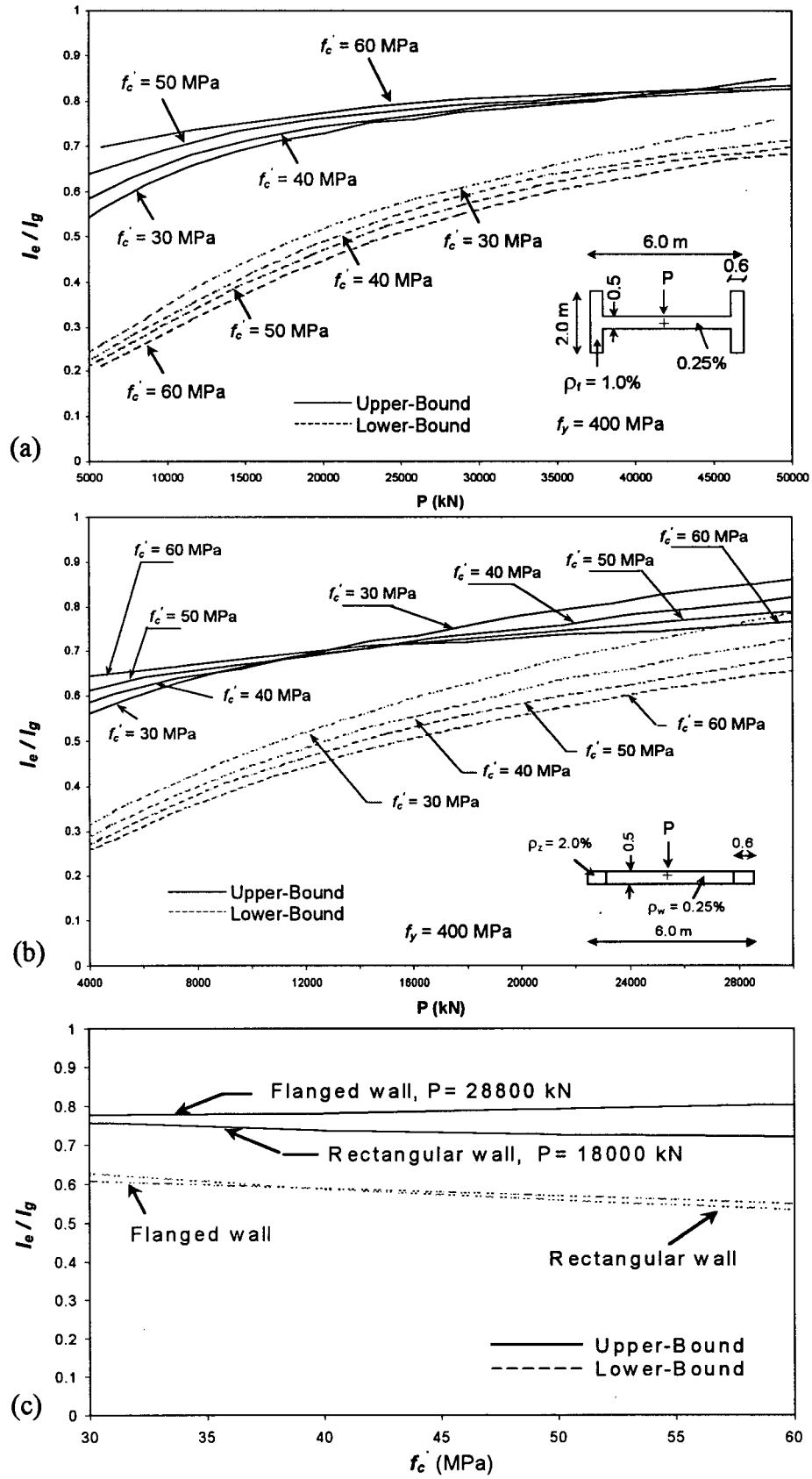

Figure 4.14 Variation of the effective flexural stiffness with varying concrete compressive strength.

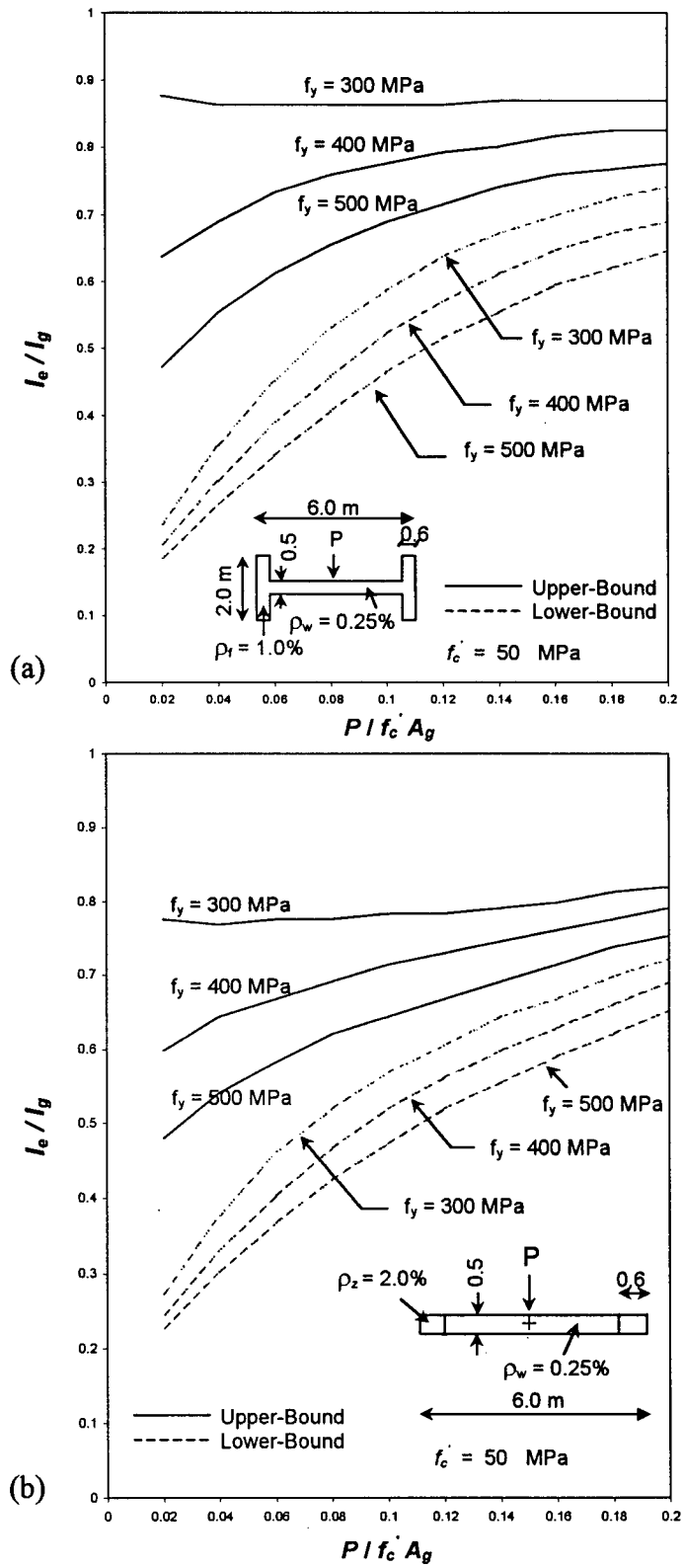

Figure 4.15 Variation of the effective flexural stiffness with varying yield strength of the vertical reinforcement.

4.6 Recommendations for Effective Flexural Stiffness of Concrete Walls

Results shown in the previous section indicate that the effective flexural stiffness of concrete walls can vary greatly (from as little as 0.1 I_g to as high as 1.0 I_g) depending on several parameters: magnitude of axial compression, geometry of the cross section, amount of vertical longitudinal reinforcement, yield strength of the reinforcement and the concrete compressive strength. The very large variation in effective stiffness that is recommended by the various documents (see Section 1.3) does actually exist in different wall types. The challenge is to identify which walls have what effective stiffness.

In this section, two methods to predict the effective flexural stiffness are presented: a general method and a simplified method. The general method captures the influence of all the various parameters that affect the stiffness value and provides an accurate estimate of the effective flexural stiffness. To determine the effective stiffness using the general method, the reinforcement and material properties of the cross section at the base of the wall are needed. As the amount of reinforcement is not normally known at the start of the analysis, designers need a quick estimate of the effective flexural stiffness to initiate the design process. The simplified method is intended to provide an estimate of the effective flexural stiffness of a wall structure.

4.6.1 General Method for Determining Effective Flexural Stiffness

An accurate estimate of the effective flexural stiffness of concrete wall building (both the upper-bound and lower-bound) can be determined using the following procedure considering the cross section near the base of the wall building:

- Determine the ratio of cracked section moment of inertia I_{cr}, and the uncracked (gross) section moment of inertia I_g. The value of I_{cr} for typical wall sections can be determined using Figure 2.9. For other wall shapes, use program *Wall-Tools*.
- Determine the ratio of linear bending moment M_l and the flexural capacity M_n of the cross section near the base of the wall. M_l can be determined using Equation [2.7]. To determine the upper-bound response and consequently the upper-bound stiffness of the wall, use $\beta = 1.5$ in Equation [2.7], while to determine the lower-bound stiffness use $\beta = 0$.
- Determine the effective stiffness of the wall I_e / I_g from Figure 4.5 or from Equation [4.2].

Figure 4.5 along with Equation [4.2] and Table 4.1 are reproduced together in Figure 4.16 for convenience. It is worth mentioning that Figure 4.16, besides providing an accurate estimate of the stiffness considering the effect of all important parameters, is a fundamental procedure and is not based on the assumptions involved in the development of the specific trilinear bending moment-curvature relationship presented in Chapter 2. Any theoretical bending moment-curvature relationship can be approximated using any convenient trilinear idealization (i.e., a bilinear idealization of the elastic deformations), and the two ratios of the idealized response (secondary slope to initial slope, and bending moment at the end of the first linear segment to the plastic moment capacity) can be used to determine the effective stiffness based on the equal area approach from Figure 4.16.

4.6.2 Simplified Method for Determining Effective Flexural Stiffness

As mentioned, a complete description of the cross section at the base of the wall must be known in order to accurately determine the effective stiffness using the general method. This is in general the case for the design checker (checking the completed design) or for a design peer review which is a common practice among structural design jurisdictions throughout the world. Reinforcement details of the wall cross sections are not known until the design is completed and hence to establish the design process and carry out the structural analysis of the building, an estimate of the effective flexural stiffness of the wall sections is needed. The intent of the simplified procedure is to capture the influence of the several parameters, previously discussed in Section 4.5, on the effective stiffness in an approximate way and provide a quick estimate of the flexural stiffness that can be used to start the design process.

A simple approximate estimate of the ratio of effective stiffness to gross stiffness can be a single number similar to what is currently recommended in many documents. However, based on the results presented earlier, it is more appropriate to link the effective stiffness to the axial compression acting on the wall since it is a major factor that affects the stiffness and has been recognized and used by others (Priestley and Hart 1989, Council 1992).

To develop simple expressions for both the upper-bound and lower-bound effective stiffness values of wall structures, several common practical configurations of the cross section at the base

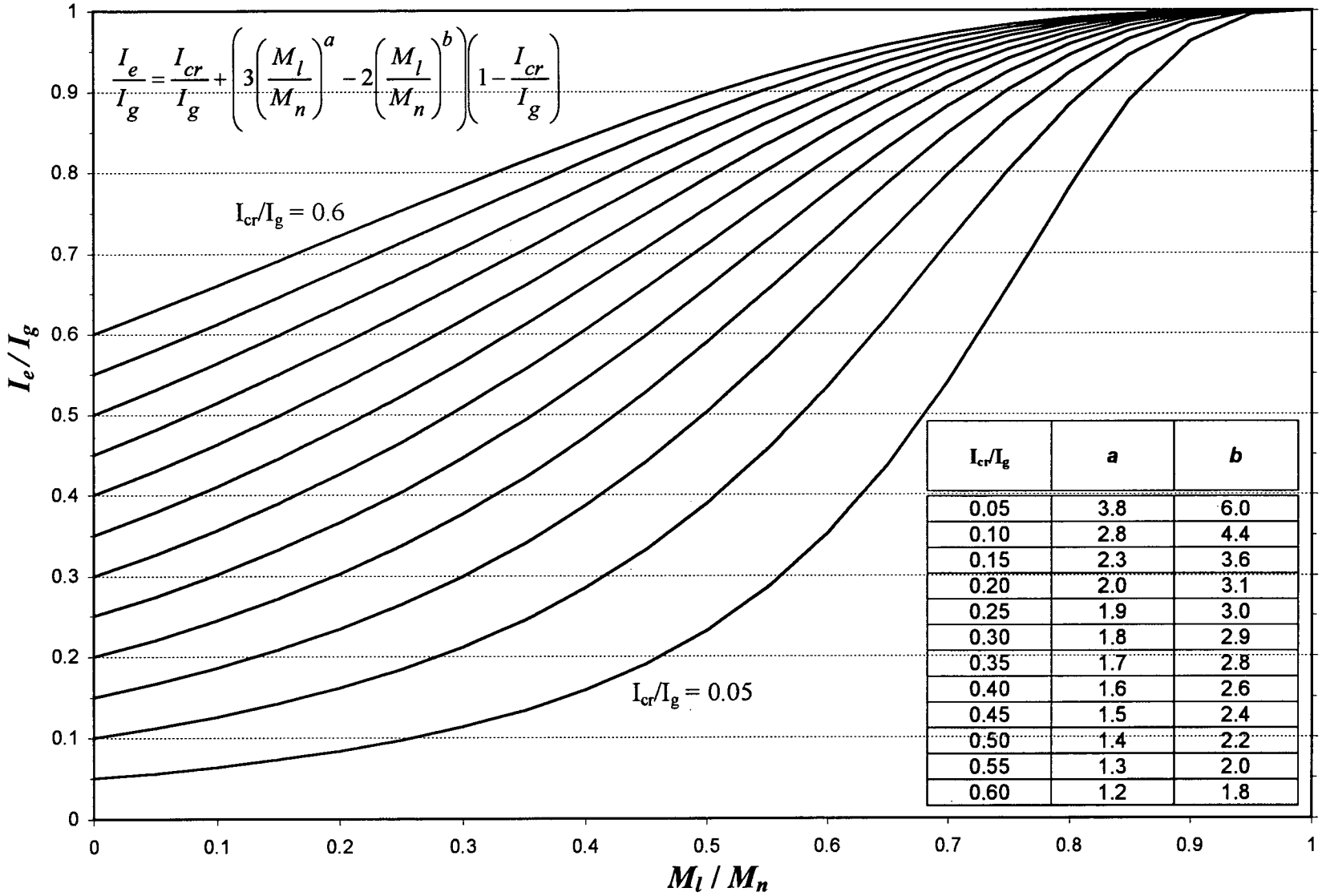

I_{cr}/I_g	a	b
0.05	3.8	6.0
0.10	2.8	4.4
0.15	2.3	3.6
0.20	2.0	3.1
0.25	1.9	3.0
0.30	1.8	2.9
0.35	1.7	2.8
0.40	1.6	2.6
0.45	1.5	2.4
0.50	1.4	2.2
0.55	1.3	2.0
0.60	1.2	1.8

Figure 4.16 Design chart for the determination of the effective flexural stiffness, I_e, for concrete walls using the general method.

of the wall were examined and these are shown in Figures 4.17 through 4.22. In each configuration (shape), the practical minimum and maximum amounts of vertical reinforcement in the boundary zones or the flanges were considered. Concrete compressive strength that ranges between 40 to 60 MPa (and the corresponding E_c and f_{cr}) were varied in each shape. For each geometry, upper and lower-bound effective flexural stiffness were determined for an applied axial compression ranging from 2% to 20% of $f_c' A_g$. Variation in the yield strength of the vertical reinforcement was not considered in this study since the majority of reinforced concrete structures currently built in North America have 400 MPa or 414 MPa (Grade 60) yield strength steel.

It is seen from the figures for the different geometries considered in this study that, despite the scatter, the upper-bound effective stiffness can be reasonably approximated by the expression suggested by Paulay (Council 1992):

$$\frac{I_e}{I_g} = 0.6 + \frac{P}{f_c' A_g} \qquad [4.3\text{-a}]$$

The lower-bound effective flexural stiffness shows less scatter particularly for rectangular and flanged wall sections. A steep increase in the effective stiffness is found when increasing the applied axial compression. The following simple expression is proposed for the lower-bound effective stiffness:

$$\frac{I_e}{I_g} = 0.2 + 2.5\,\frac{P}{f_c' A_g} \qquad [4.3\text{-b}]$$

Note that the upper-bound effective stiffness shall be less or equal to the gross section stiffness. The lower-bound effective stiffness shall never be taken higher than the upper-bound effective stiffness value. The two simple expressions (Eq. [4.3] a and b) are shown in Figures 4.17 to 4.22 for comparison.

While the proposed simplified expressions provide a reasonable approximation for most walls, there are certain conditions (e.g., flanged walls with an amount of the vertical reinforcement in the flange that is less than 1%) when the actual stiffness deviates considerably from the simple expressions. For this reason, it is suggested that the general method be used whenever necessary to estimate the effective stiffness of concrete walls. A more elaborate and extensive analyses for different wall shapes with various geometrical dimensions are provided in Appendix E.

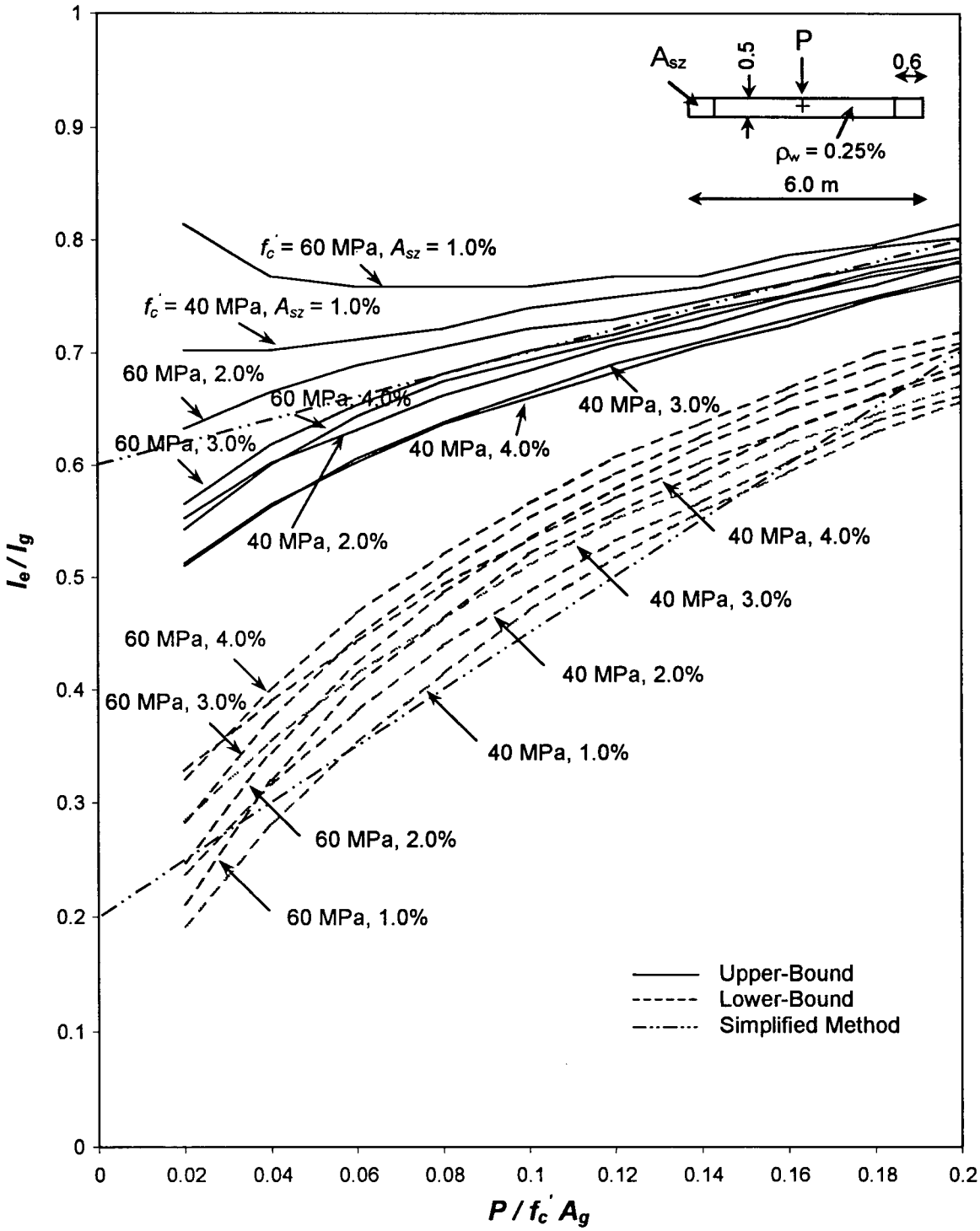

Figure 4.17 Comparison of the suggested simplified expressions for determining the effective flexural stiffness with a variety of results for rectangular walls.

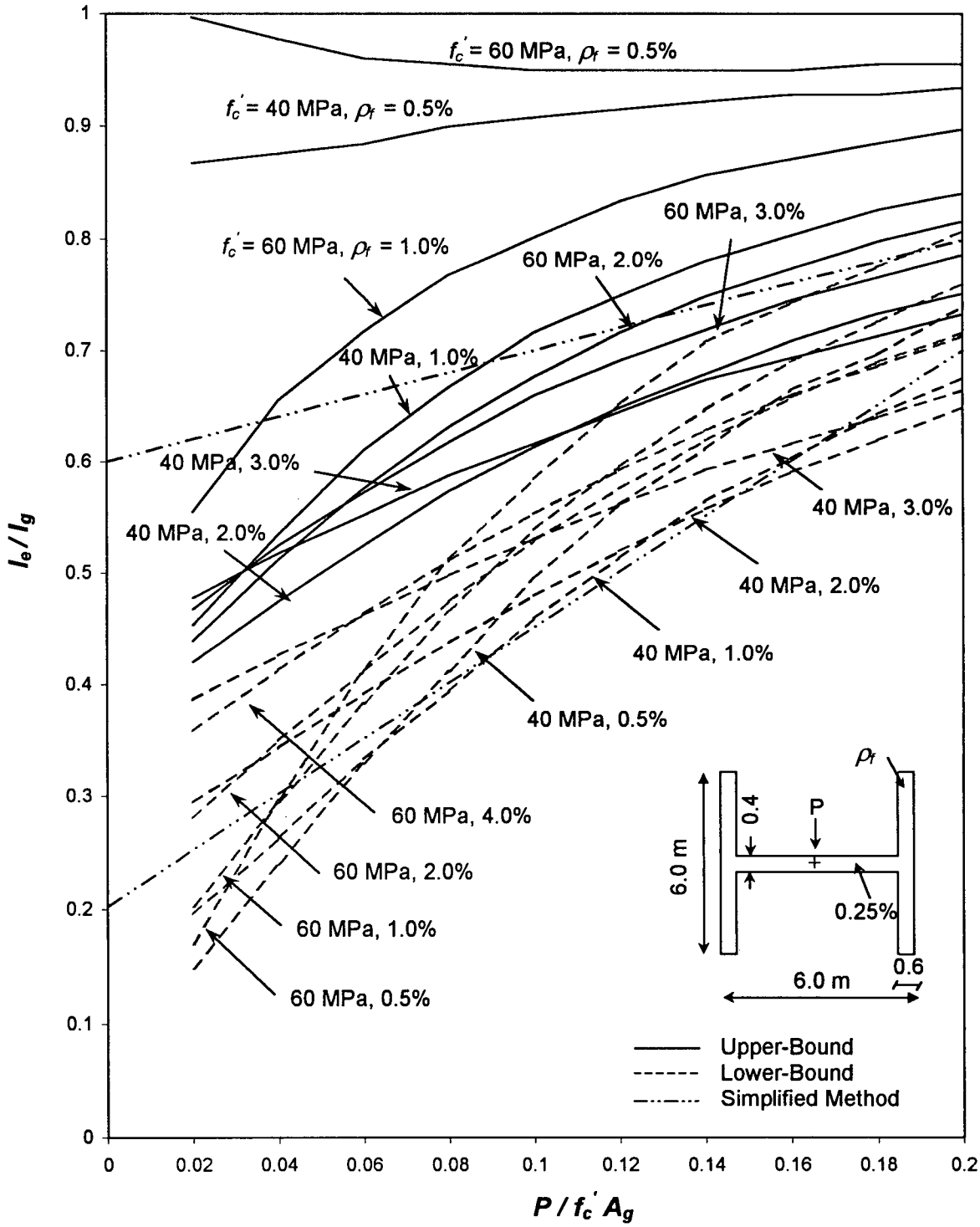

Figure 4.18 Comparison of the suggested simplified expressions for determining the effective flexural stiffness with a variety of results for flanged walls.

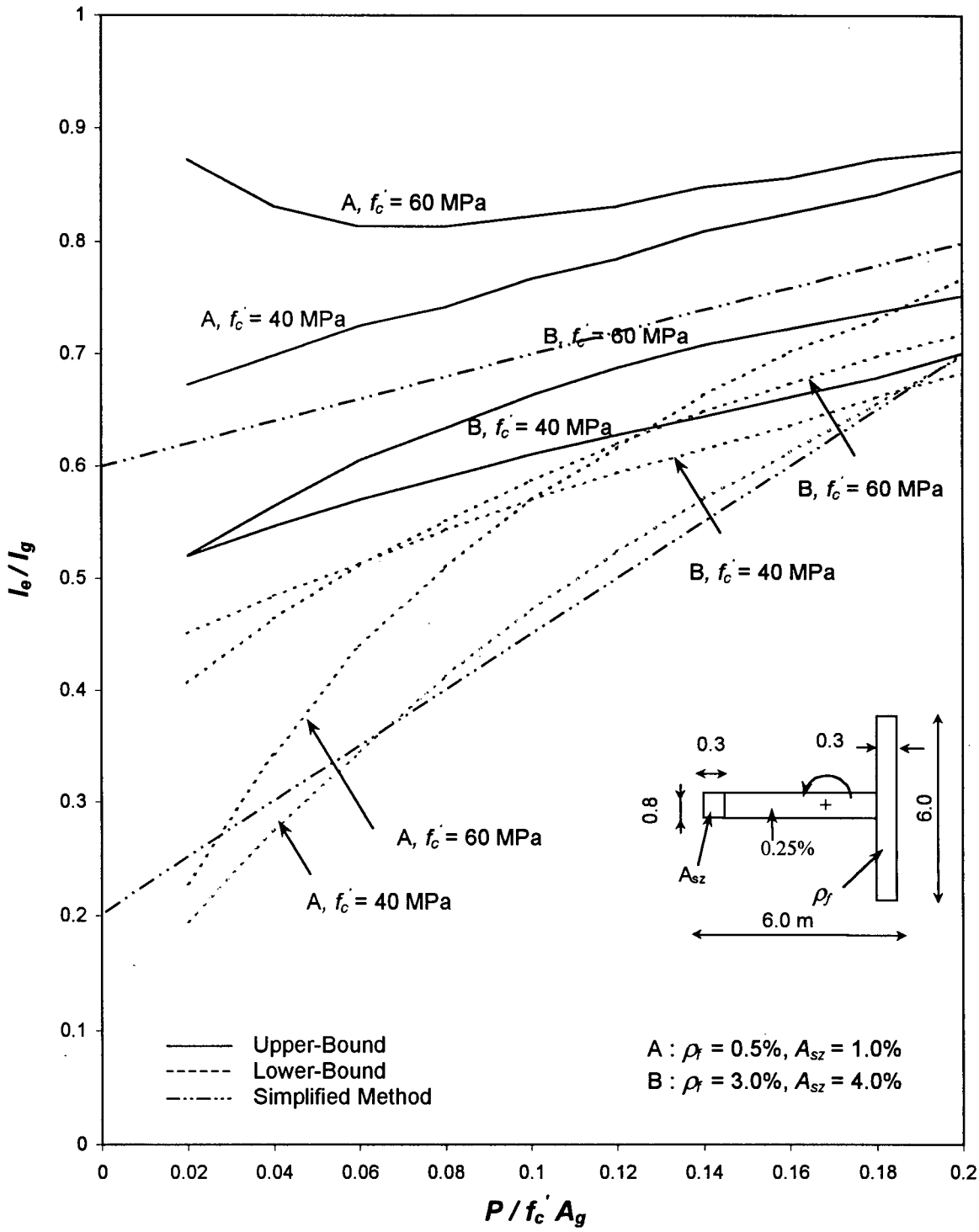

Figure 4.19 Comparison of the suggested simplified expressions for determining the effective flexural stiffness with a variety of "T" shaped walls (flange in tension).

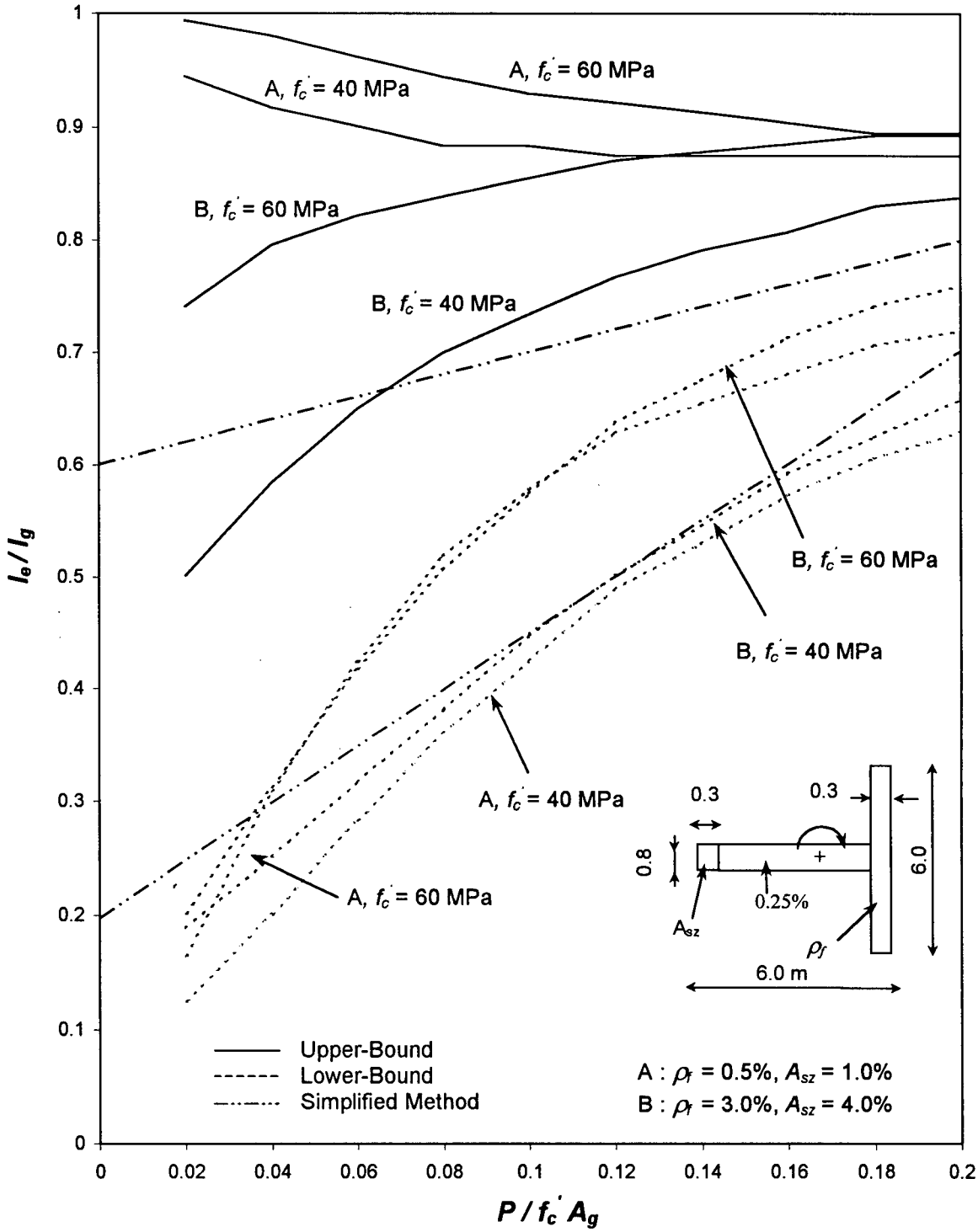

Figure 4.20 Comparison of the suggested simplified expressions for determining the effective flexural stiffness with a variety of "T" shaped walls (flange in compression).

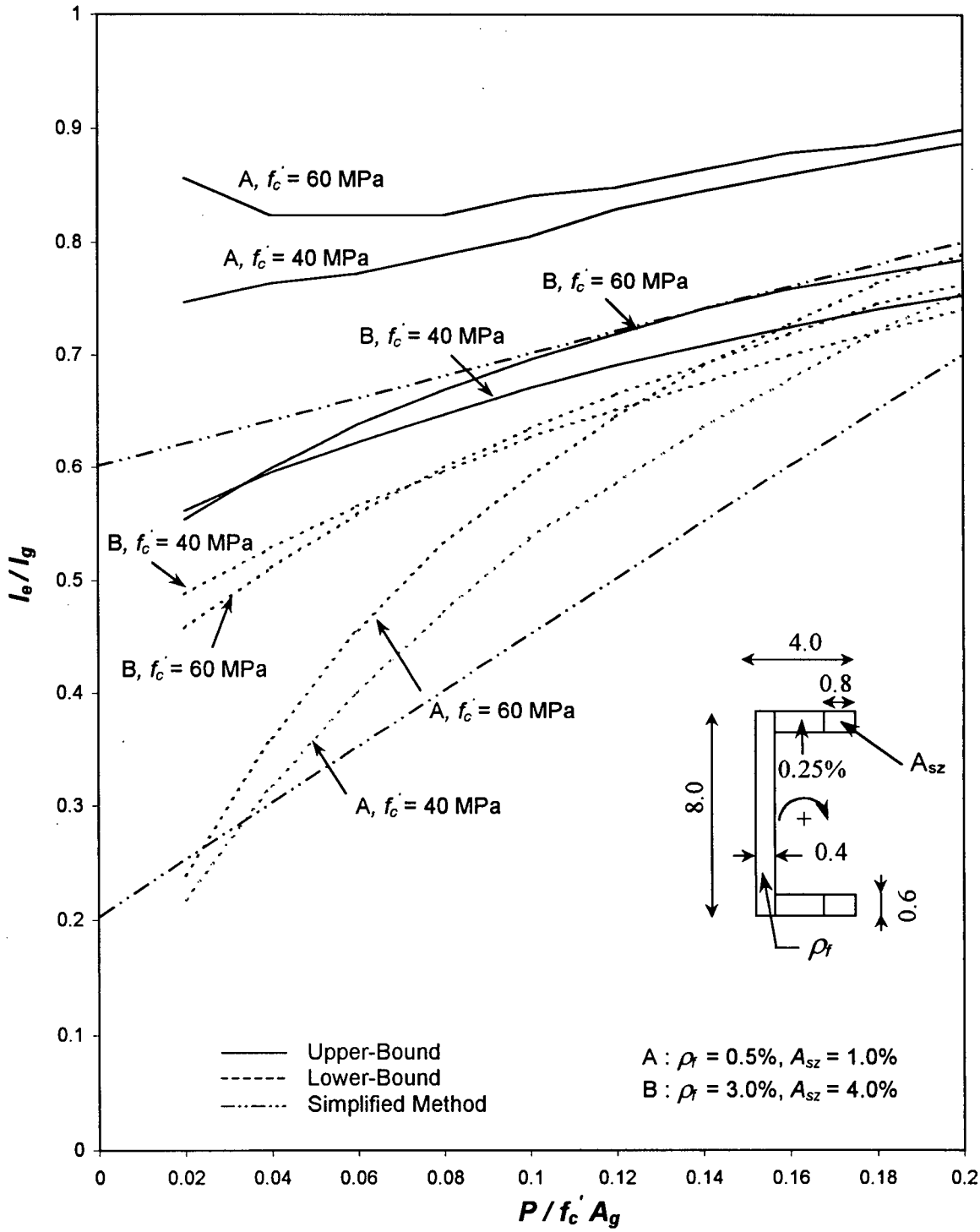

Figure 4.21 Comparison of the suggested simplified expressions for determining the effective flexural stiffness with a variety of "C" shaped walls (flange in tension).

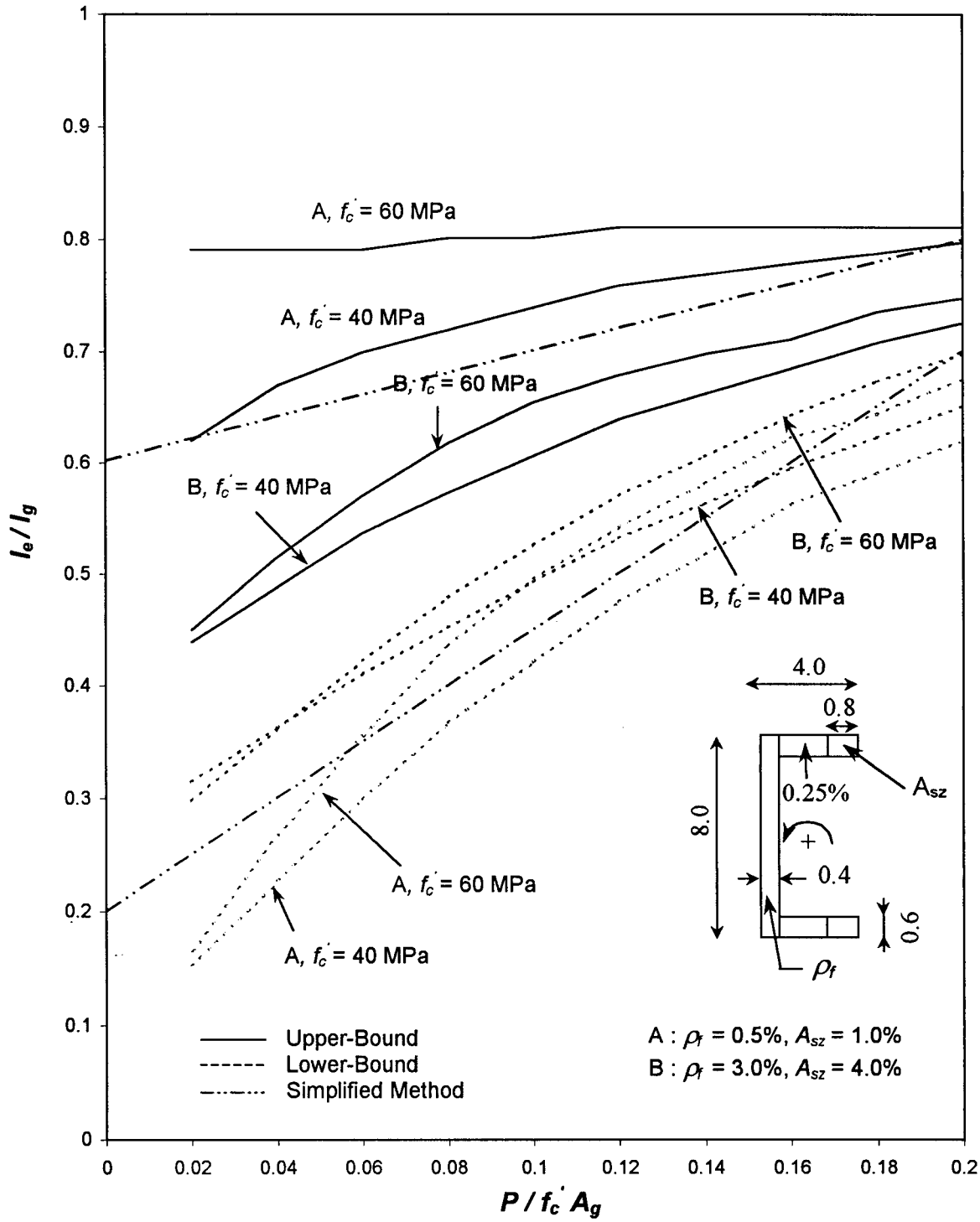

Figure 4.22 Comparison of the suggested simplified expressions for determining the effective flexural stiffness with a variety of "C" shaped walls (flange in compression).

4.7 Comparison of Predicted Stiffness with Slender Wall Test Results

The upper-bound load-displacement relation of the slender wall specimen, shown previously in Chapter 3, Figure 3.12, is compared with the predicted bilinear load-displacement relation in Figure 4.23. The effective elastic stiffness (I_e = 0.79 I_g) was determined using the general method.

The predicted lower-bound effective stiffness is compared with the ascending ramp of the hysteresis loops for each of the last four displacement/drift levels in Figure 4.23-b. Again, the general method was used to predict the elastic effective stiffness (I_e = 0.39 I_g). Because of the observed degradation in stiffness from the first cycle to the second cycle, the loading portion of the second cycle, rather than the first cycle, at each displacement level is shown in the figure. The lower-bound effective stiffness is related to the severely damaged and degraded response. Each cycle is labeled with the maximum drift ratio attained during the first cycle. The global drift ratio is the maximum displacement divided by the height of the wall.

The bilinear load-displacement relations shown in Figure 4.23 are estimated from the elastic analysis of a cantilever wall of 11.333 m subjected to a single concentrated lateral load at the top. The yield displacement, Δ_y, is estimated from the equation:

$$\Delta_y = \frac{F\ H^3}{3\ E_c\ I_e} \qquad [4.4]$$

where, H, is the height of the wall and, F, is the maximum lateral load computed as the capacity of the flanged wall specimen over the height of the wall (i.e., M_n / H). I_e distinguishes between the upper and lower-bound bilinear load-displacement relations.

It is interesting to compare the measured load displacement relationship (for both the upper-bound and lower-bound) with the bilinear load-displacement relation determined using the recommended stiffness from the Commentary to the Canadian concrete code (CPCA 1995) in Figure 4.24, and the Commentary to the New Zealand Standard (NZS 3101 1995) in Figure 4.25.

The two codes use a very similar philosophy for the seismic design of concrete walls and yet these documents differ by a factor of two regarding the effective stiffness.

It is clear that the 70% of I_g suggested in the CPCA Handbook (Fig. 4.24) compares well to the upper-bound response (or previously uncracked response) of the wall specimen but not very well to the lower-bound response. The recommendation of the commentary to the NZS, on the other hand, gives a conservative estimate of even the lower-bound stiffness at high drift levels.

4.8 Concluding Remarks

It is suggested that when estimating the maximum expected drift of a building, designers should estimate the period and the corresponding forces and displacements using the lower-bound effective stiffness for a severely cracked response of the wall. The upper-bound effective stiffness may be used when estimating the seismic design actions (bending moments and shear forces). A lower estimate of the fundamental period is preferred so as to get higher estimates of the seismic design forces (as shown previously in Figure 4.1). In short, the former is suitable for a displacement-based design while the latter is appropriate for a force-based design procedure.

The above suggestion is supported, conceptually, in the FEMA 274 document (1997) where the aim of getting a low estimate of the fundamental period is emphasized when the objective is to get a larger design forces to be applied to the building. On the contrary, a higher estimate of the fundamental period is preferred when the objective is a larger target displacement. Wallace and Moehle (1992) also suggested the use of two different stiffness values, I_g and 0.5 I_g, for estimating two fundamental periods of the building used for determining the seismic design forces and displacements, respectively.

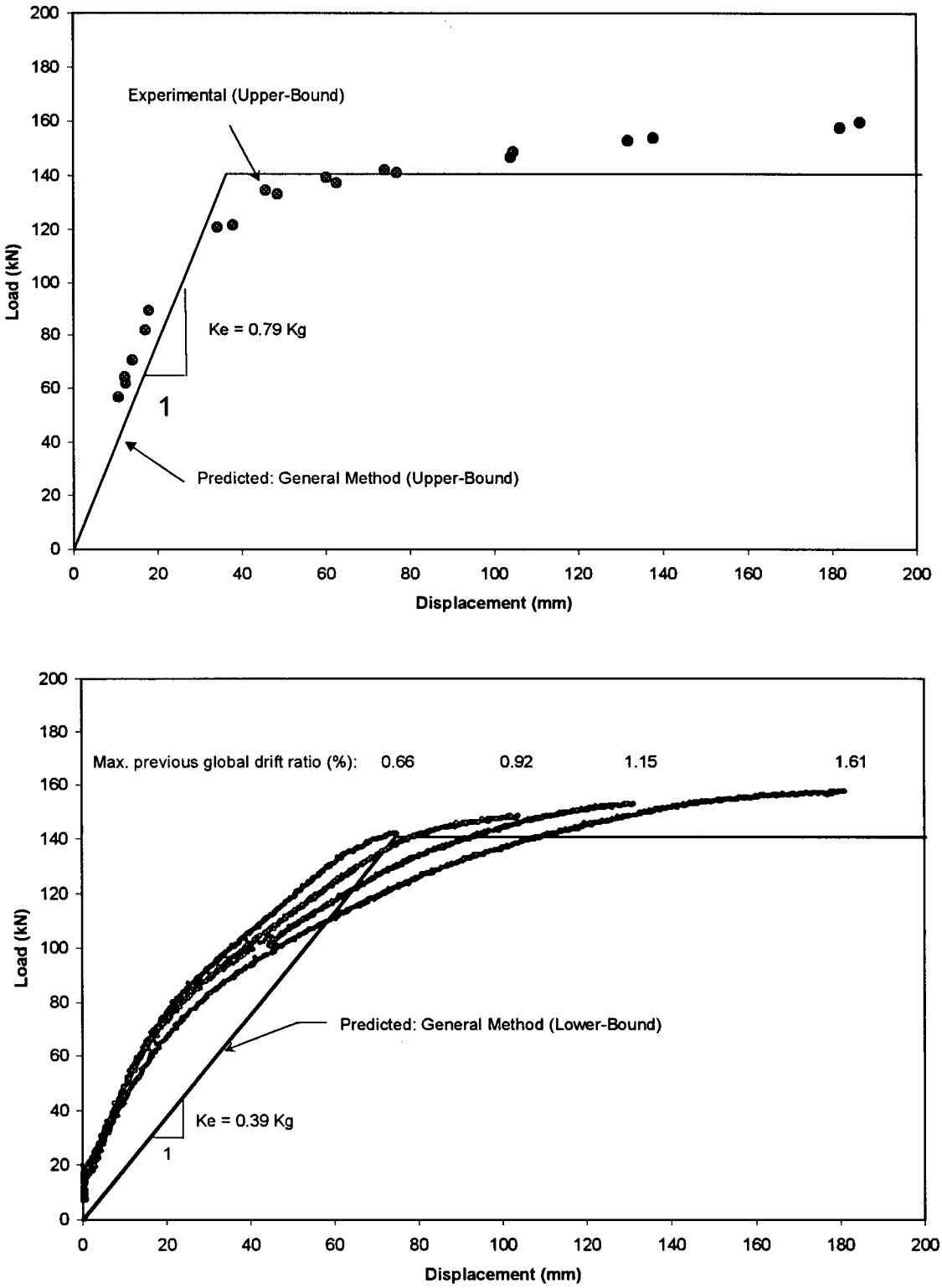

Figure 4.23 Comparison of the experimentally measured load-displacement relationship with the one predicted using linear elastic stiffness as proposed by the general method.

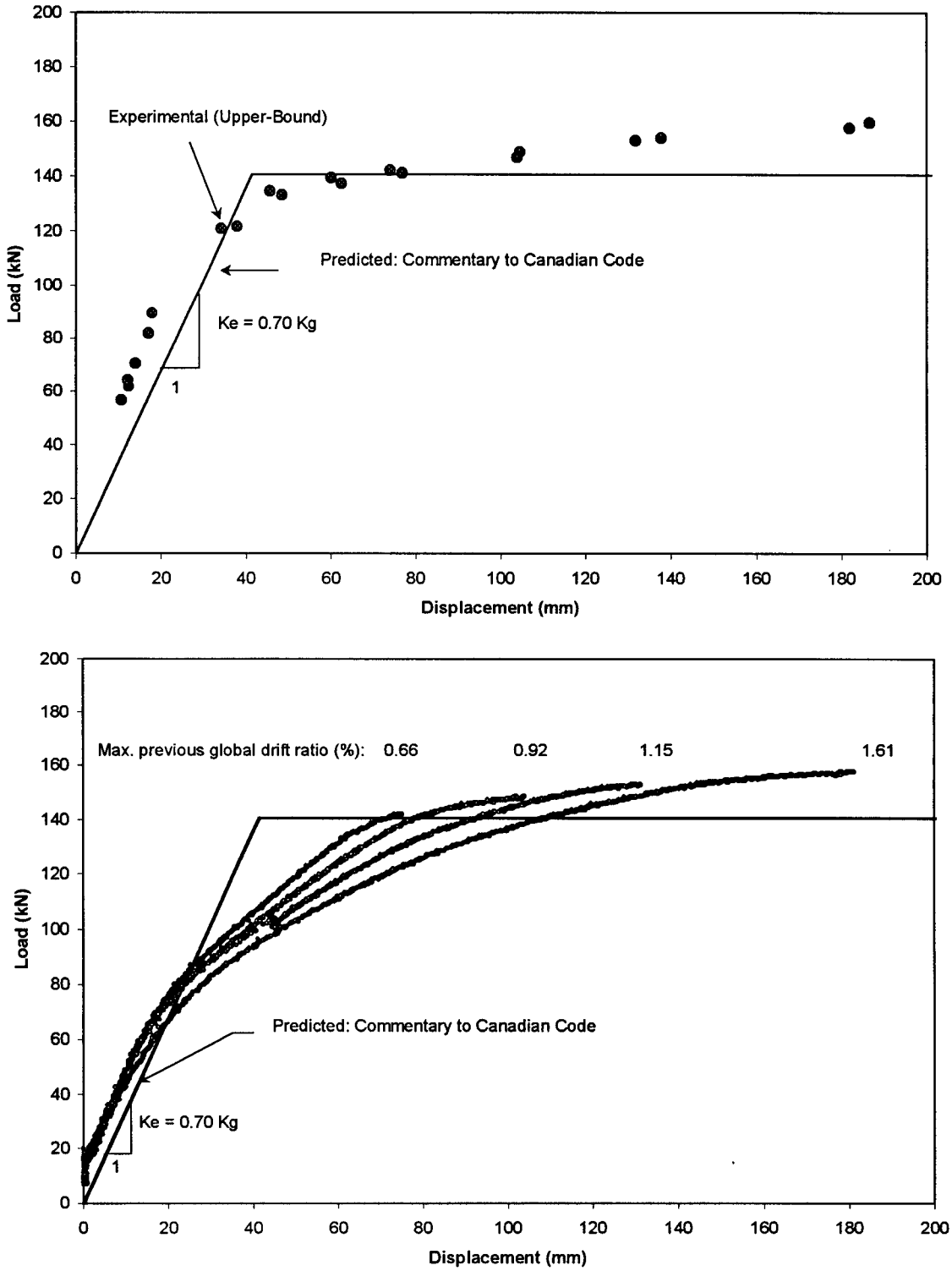

Figure 4.24 Comparison of the experimentally measured load-displacement relationship with the one predicted using the linear elastic stiffness suggested in the CPCA Handbook (1995).

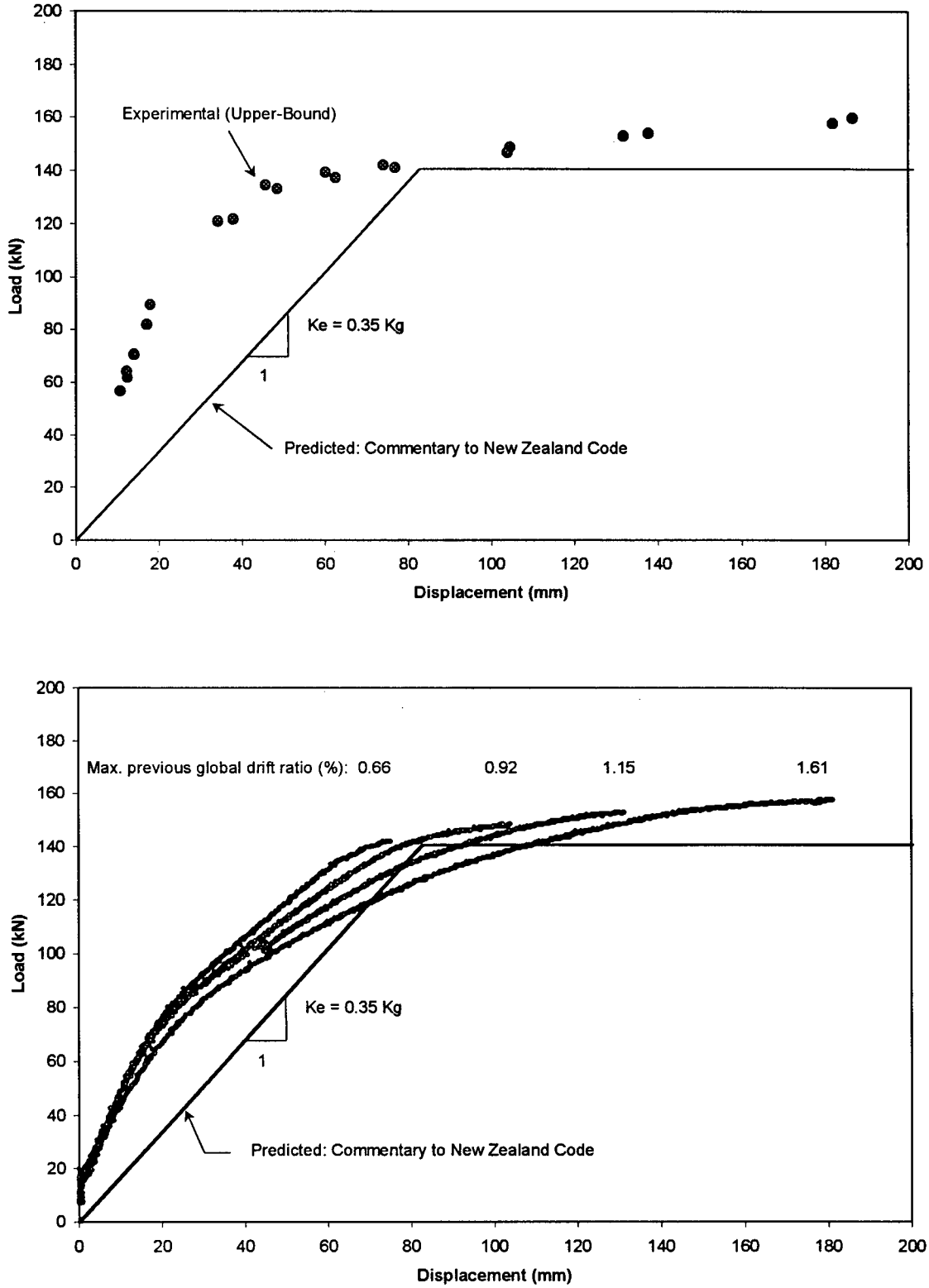

Figure 4.25 Comparison of the experimentally measured load-displacement relationship with the one predicted using the linear elastic stiffness suggested by the commentary to NZS 3101 (1995).

Chapter 5

Nonlinear Static Analysis of Concrete Walls

5.1 Introduction

One application of the proposed trilinear bending moment-curvature model is in nonlinear static analysis procedure commonly known as pushover analysis or sequential yield analysis. Pushover analysis is becoming increasingly popular and a necessary part of the design verification. It is one of the three analysis methods recommended by the NEHRP Guidelines for Seismic Rehabilitation of Existing Buildings (FEMA 273, 1997). It is also a main component in the Capacity Spectrum method developed by Freeman et al (1975) and recommended by the Applied Technology Council (ATC-40, 1996) to determine the displacement demand imposed on a building that is expected to experience inelastic deformations.

The pushover analysis provides valuable insight into the performance of a structure under earthquake loading, can be used to identify the weak elements in a structure, and to determine inelastic rotation demands which are needed to assess the system ductility. A key component to perform the pushover analysis procedure is the bending moment-curvature/rotation response of the elements of a building (frame model, wall panels, etc.). Proper modeling of the material properties is essential to obtain a useful result from the pushover analysis.

For a proper modeling of a wall element, and if the effect of cracking on the elastic deformations of a wall structure is to be accurately modeled, the trilinear bending moment-curvature model should be used. This flexural model, when combined with other models that capture the post-yielding behavior (strain hardening-softening), shear failure mechanism, P-Δ effect, bond and anchorage failure, etc., can provide a comprehensive representation of the structure performance under the applied loading.

The pushover analysis, besides its advantages, does not seem to capture the displacements due to higher modes of vibration, which are known to be of significance to the deflection of tall wall

structures. However, recent application of the pushover analysis to include the higher mode effects has been developed and reported (Paret et al., 1996; Bracci et al., 1997).

In the following, an overview of the basic procedures used in the pushover analysis are presented. Implementation of the trilinear model in a computer program to perform the nonlinear static analysis is described. Necessary features required to perform the analysis and to incorporate it into the computer program are also described. Finally, two example applications of the model in analyzing a wall and a coupled wall structure are presented.

5.2 Overview of Pushover Analysis Procedure

The pushover analysis is a useful procedure to identify the weak links in the seismic performance of a structure. A series of design iterations are usually carried out, during which the structural deficiencies are observed and corrected (Naeim and Lobo, 1998). The iterative analysis and design process continues until the design satisfies a pre-established performance criteria. The performance criteria for the pushover analysis (as detailed in FEMA 274, 1997 and ATC-40, 1996) is generally established as the desired state of the building given the roof top displacement (usually referred to as the target displacement).

The pushover analysis may be carried out using either force control or displacement control or a combination of both. In force control analysis, the structure is subjected to an incremental distribution of lateral forces to represent the seismic effects. In displacement control, the structure is subjected to a prescribed displacement profile where the relative displacements of key joints are constrained by simple geometric relationship. Since the deformed profile of displacement is not easily defined, and a distributed load pattern to represent the seismic forces are known and codified, force control is commonly used for building structures.

The analysis procedure usually involves modeling (subdividing) the structure into frame and beam-like elements. The model is subjected to a lateral loading pattern such as a uniform distribution, inverted triangular distribution, or fundamental mode of vibration (first mode) distribution.

During a typical pushover analysis, the vertical (gravity) loads on the structure are held constant, while the lateral loads are increased in small increments. At each load increment, the well known system of simultaneous equations are assembled and solved:

$$K \; u \; = \; F \qquad [5.1]$$

Where K is the global stiffness matrix, u is the joint displacement and rotation vector, and F is the applied load vector.

The vector of applied loads on each element is formed and assembled into the global load vector. Both gravity and lateral loads are considered. The element stiffness matrix (function of $E_c I_g$) is derived from the bending moment-curvature relationship defined for each element and then assembled into the global stiffness matrix. Since the element end moments are not known yet, the element stiffness matrix cannot be determined (i.e., K depends on u), the problem becomes nonlinear and an initial guess for the element end moments are required in order to calculate the stiffness.

Solution of this system of nonlinear equations requires an iterative scheme in which the initial guess is refined and the stiffness is recalculated until the solution has converged arriving at the correct stiffness values for each element. The analysis is continued for another load step (increment) until the maximum (full) specified lateral load or the target displacement is reached, or else the structure becomes unstable.

The correct element stiffness and end moments determine the state of cracking, yielding or plastic hinge formation in each element at this load level. Inaccurate material modeling can lead to an erroneous estimate of the structure performance.

When it is required to capture the strain hardening or softening characteristic of the building after it reaches instability (i.e., formation of plastic hinges at all the supported nodes), the force control is followed by a displacement control analysis provided that these effects are accounted for in the material model.

5.3 Implementation of Trilinear Bending Moment-Curvature Model in Pushover Analysis

A linear two-dimensional frame analysis program developed by Mutrie (1998) was modified to perform the nonlinear static analysis. The original program "*2Frame*" uses the stiffness method to analyze a frame-type building subjected to a static loading. The modified program "*2Frame-NL*" makes use of the trilinear bending moment-curvature relationship developed herein to model the nonlinear flexural behavior of a wall element.

Program *2Frame-NL* uses the existing subroutines and original input file of *2Frame* program and has additional subroutines and input data required to carry out a force controlled nonlinear static analysis. Output of the program includes the effective stiffness of each member at any instant in the loading history, sequence of yielding of the different members and the joint forces and displacements at each load increment. In the following, the necessary features added to *2Frame-NL* program to perform a nonlinear static analysis are briefly described.

5.3.1 Material Modeling

Nonlinear analysis requires the definition of the material type and nonlinear properties for each member of the structure model that is expected to yield or crack. For each wall member which has the same concrete geometry and reinforcement details, the family of idealized moment-curvature relationships, as shown in Figure 5.1-a for different axial loads acting on the wall member, are input in terms of two slopes E_cI_g and E_cI_{cr} and two interaction diagrams P - M_l , P - M_n (Fig. 5.1-b).

The axial gravity load applied on the member and held constant during the analysis, in addition to any axial load that may result from the lateral loading (as in the case of coupled walls) are used to determine the specific trilinear bending moment-curvature relationship for this particular member at a particular load step.

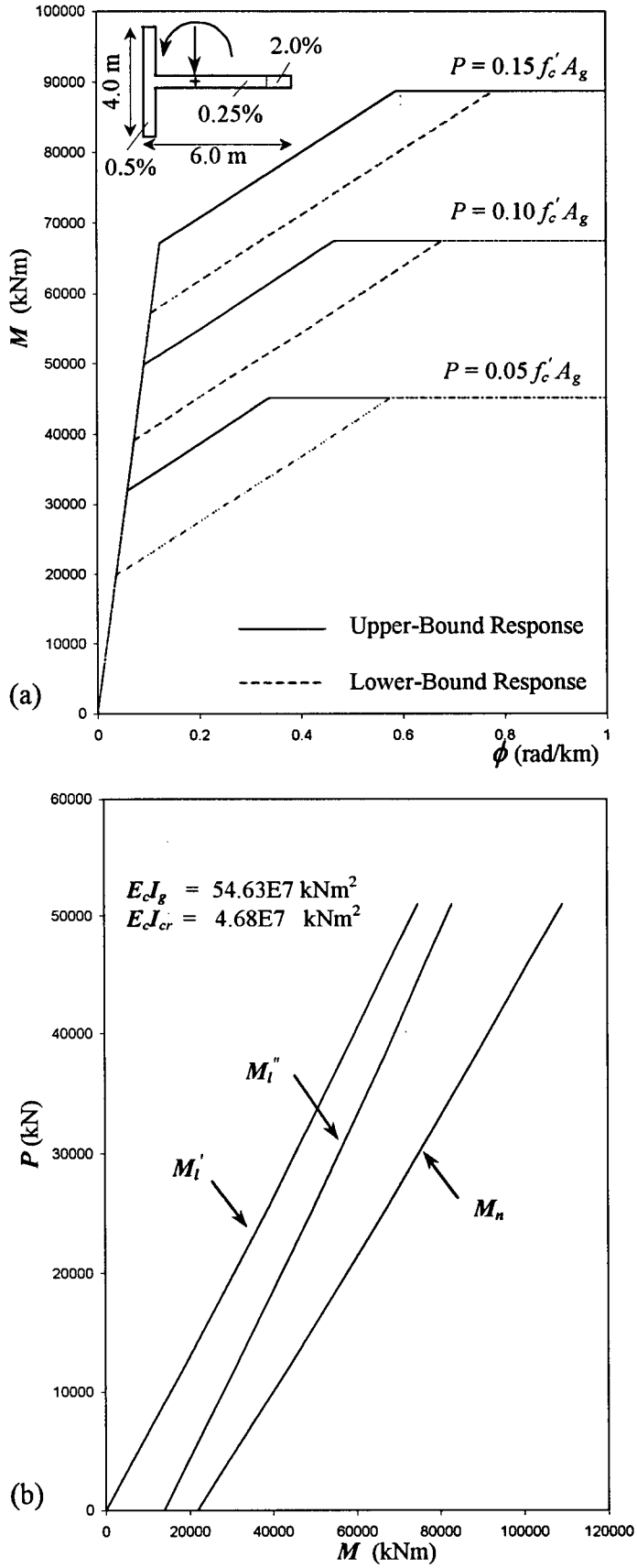

Figure 5.1 (a) Family of idealized bending moment-curvature relationships, (b) interaction diagrams input to nonlinear pushover program.

5.3.2 Determination of Effective Member Stiffness

During the iterative process to solve the system of nonlinear simultaneous equations, the effective stiffness of each member is updated (re-calculated) whenever there is a change in the end moments (i.e., nodal rotations). The effective stiffness is determined as follows (Figure 5.2): the bending moment distribution along the member length is determined from the member end forces (assuming linear distribution between the two nodes); the trilinear bending moment-curvature relationship, defined for each member as described above, is used to determine the curvature distribution along the length of the member; the effective member stiffness E_cI_e is that which gives the equivalent rotation between the two ends of the member (i.e., equal area under both actual and idealized linear curvature distributions).

The effective member stiffness E_cI_e is in general described as $\psi\, E_cI_g$, where a new value of ψ cannot be taken greater than the ψ_{max} reached in the previous load increment. Figure 5.2 shows the application of the above procedure on a typical wall segment for a general case of bending moment distribution. Four cases are identified for the computation of the effective member stiffness depending on the curvature distribution along the length of the member and are illustrated in Appendix F.

The computational procedure to determine the effective member stiffness using the equal rotation concept is also illustrated in Appendix F.

5.3.3 Solution of the Nonlinear Equations

Successive approximation technique (also known as direct iterations) is used to solve the system of nonlinear simultaneous equations (Eq. [5.1]) during each load increment. Since the joint displacements and rotations are not known at the first load increment, an initial estimate of the stiffness is based on the gross section properties of each member. The system of equations are then solved to obtain a set of values for joint displacements and rotations, and the end moments for each member can then be computed from the basic principles of the stiffness method.

The computed end moments are used to determine the updated member stiffness matrix, as described in the previous section, and thus the global stiffness matrix is updated (if necessary).

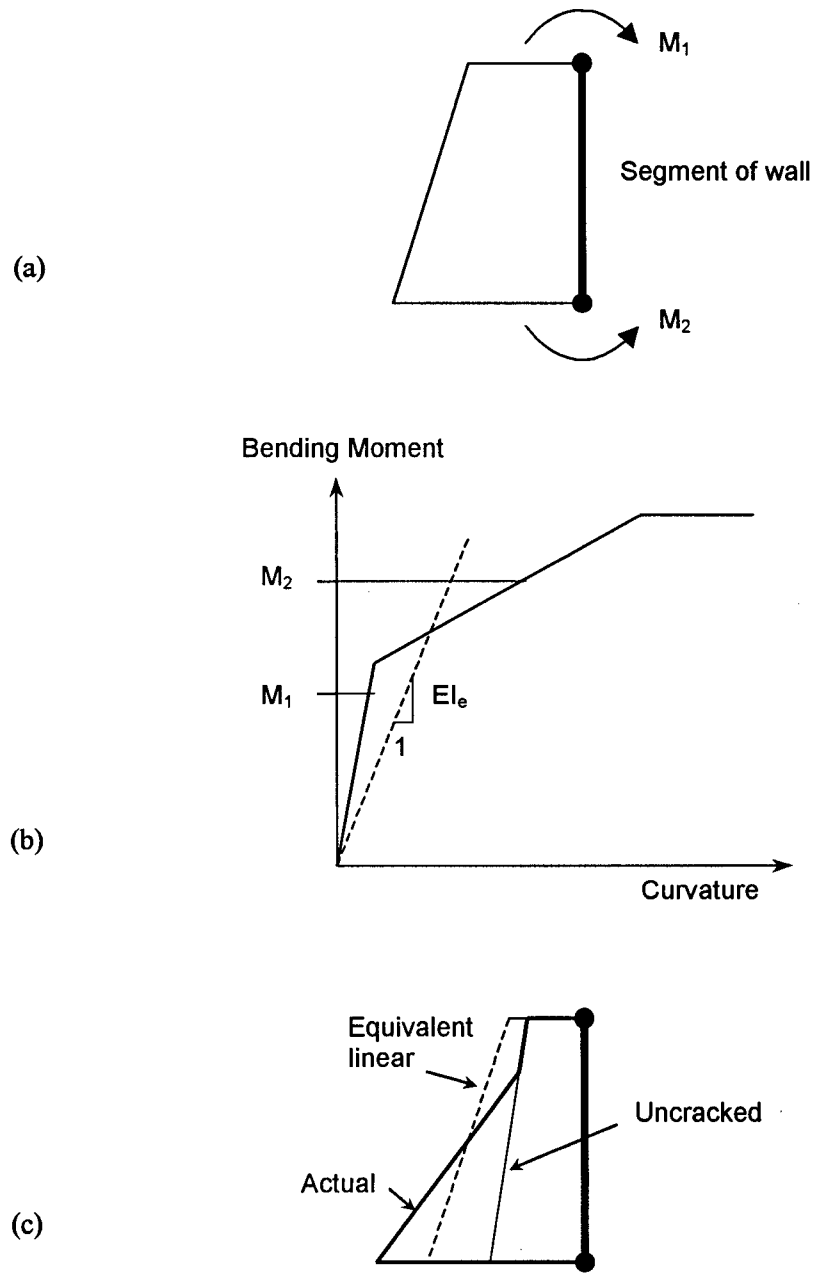

Figure 5.2 Application of trilinear bending moment-curvature model in non-linear static analysis: (a) bending moment distribution in a wall element, (b) trilinear bending moment-curvature model, (c) curvature distribution in a wall element.

The system of equations are solved again to obtain another set of values for the joint displacements and rotations.

Figure 5.3 shows diagrammatically the iterative procedure for a single variable problem. The iterative procedure is stopped or the solution has converged when a certain measure of the change in the unknowns (end moments, member stiffnesses, or joint displacements and rotations) between the successive iterations becomes less than a tolerable margin (acceptable level of accuracy). The norm of the u vector is considered as the tolerance measure between the successive iterations.

$$\frac{\left\| \sqrt{u_n^2} - \sqrt{u_{n-1}^2} \right\|}{\sqrt{u_n^2}} \leq Tolerance \qquad [5.2]$$

Care is taken regarding the convergence when using this iterative technique. The technique is generally slower and less convergence when compared with other well-converged iterative techniques such as Newton-Raphson, and Modified Newton-Raphson (Owen and Hinton 1980). However, this technique is preferred in this course of work since it gives a meaningful member stiffness (secant stiffness) at any particular instant of the analysis. This useful feature is demonstrated later in the example applications (Figure 5.11). A simple technique used to ensure the convergence between the successive iterations is to increase the number of loading steps (i.e., loading increments are decreased to about 5% of desired load).

5.3.4 Plastic Hinge Formation

A lumped plasticity approach was adopted to simulate the yielding of a wall element. This approach assumes that yielding takes place only in concentrated plastic hinges located at the element ends. When the bending moment at one end of a member reaches the yield (ultimate) capacity defined in the bending moment-curvature relationship, a hinge is inserted in the structure model and a joint moment is applied to simulate the plastic moment resisted by the member.

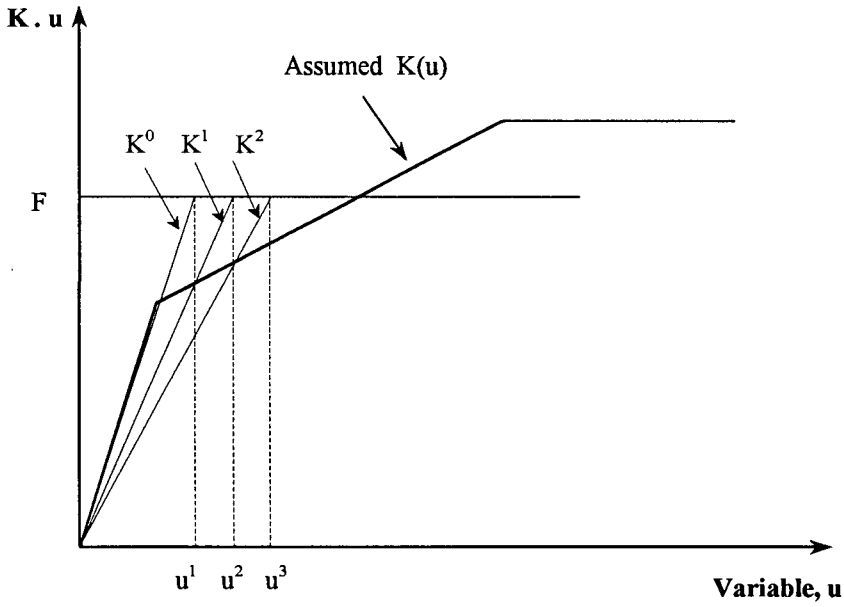

Figure 5.3 Successive approximation method for a single variable.

Since the plasticity is lumped at a single joint and to enhance the accuracy of the modeling, care needs to be taken when subdividing the structure so as to increase the number of members in the region where plastic deformations may take place, usually at the base of the wall structure.

When all the members connected to the same joint reach the yield capacity, a single step correction procedure is implemented to ensure the equilibrium of the joint.

5.4 Example Applications of the Pushover Analysis

Two examples are presented to demonstrate the application of the developed trilinear bending moment-curvature model in predicting the flexural response of a wall structure using a static pushover analysis. Program *2Frame-NL* was used to perform the nonlinear static analysis for the two examples.

In the first example, the load-displacement measurements taken from the wall test are compared with the pushover analysis results predicted using the trilinear bending moment-curvature model. In the second example, the pushover analysis is performed on a 32-story office tower with a reinforced concrete coupled wall core system and the results are compared with the maximum displacement demand on the structure. This example also serves to study the behavior (assess the performance) of the coupled wall system when subjected to a simulated earthquake loading.

Results of the examples show the advantages of using the trilinear bending moment-curvature model when predicting the flexural response of a wall structure over other models such as the bilinear relation that is suggested by Priestley and Kowalsky (1998).

5.4.1 Wall Test Example

A static pushover analysis was carried out on the wall test specimen to predict the monotonic load-displacement relationship. The wall test specimen was subjected to a constant axial compression of 1500 kN. A single lateral load applied at the tip of the wall was used to apply a reverse cyclic lateral displacement. Details of the specimen geometry and reinforcement were given in Chapter 3.

The wall specimen was modeled as a cantilever stick and subdivided into members and joints. The trilinear bending moment-curvature model used in the analysis for both the upper and lower-bound response are shown in Figure 5.4. The analysis was run incrementally and the program stopped when a plastic hinge formed at the base of the wall.

Figure 5.5 shows the computed load-displacement relation using the upper-bound trilinear response. The measured upper-bound load-displacement response of the wall test is plotted on the same figure for comparison. Also shown in the figure, is the load-displacement relation that is predicted using the bending moment-curvature model suggested by Priestley and Kowalsky 1998. This prediction is based on a linear curvature distribution along the height of the wall and a yield displacement of ($0.33\ \phi_y H^2$) where the yield curvature is estimated as ($2\ \varepsilon_y / l_w$). The yield strain, ε_y, of the 455 MPa reinforcing steel is equal to 0.00228. Note that this yield curvature was originally suggested for rectangular wall shapes, whereas the wall test had flanged shape. It is clear that the trilinear bending moment-curvature relationship describes the upper-bound response of the wall test specimen much better than the Priestley and Kowalsky bilinear relationship which is probably meant as a lower-bound response.

The pushover analysis was repeated for the wall test specimen using the predicted lower-bound bending moment-curvature response. Figure 5.6 shows the predicted and experimental load-displacement relationships. The experimental load-displacement relations are shown for only the ascending ramp of the hysteresis loops for various displacement/drift levels. Each cycle is labeled with the maximum drift ratio attained during the first cycle of loading. Because of the observed degradation in stiffness from the first cycle to the second cycle, the second hysteresis cycle for each drift level is the one shown in the figure as was done in Chapter 4.

The global drift shown in the figure is computed similar to the procedure outlined in Chapter 4. The local drift ratio was estimated as the sum of the elastic drift ($1.5*\Delta_y / H$) and plastic drift ($\{\Delta - \Delta_y\} / H$) at each load level, where H is the height of the wall and Δ_y is the yield displacement computed from the measured monotonic response and found to be 33 mm. The displacement ductility estimated for each load cycle is also shown on Figure 5.6. The displacement ductility was computed as the maximum displacement reached at each cycle divided by the estimated yield displacement.

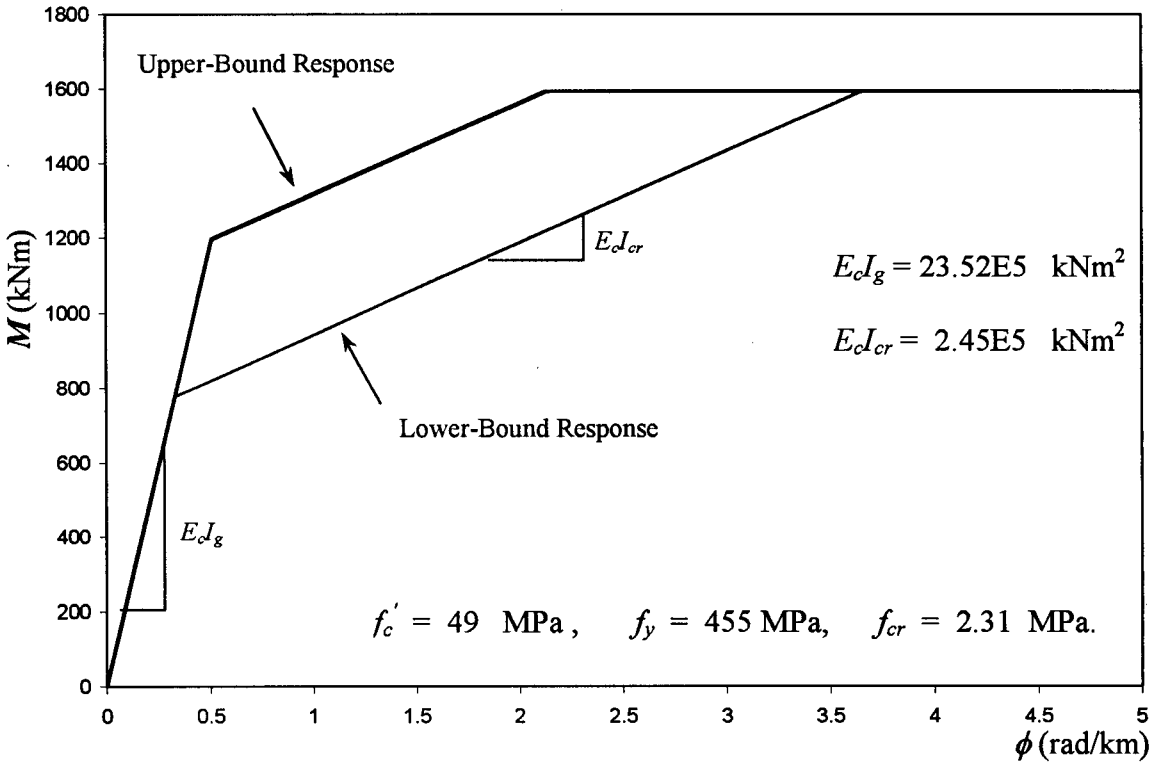

Figure 5.4 Trilinear bending moment-curvature relationship used for the analysis of the slender wall specimen.

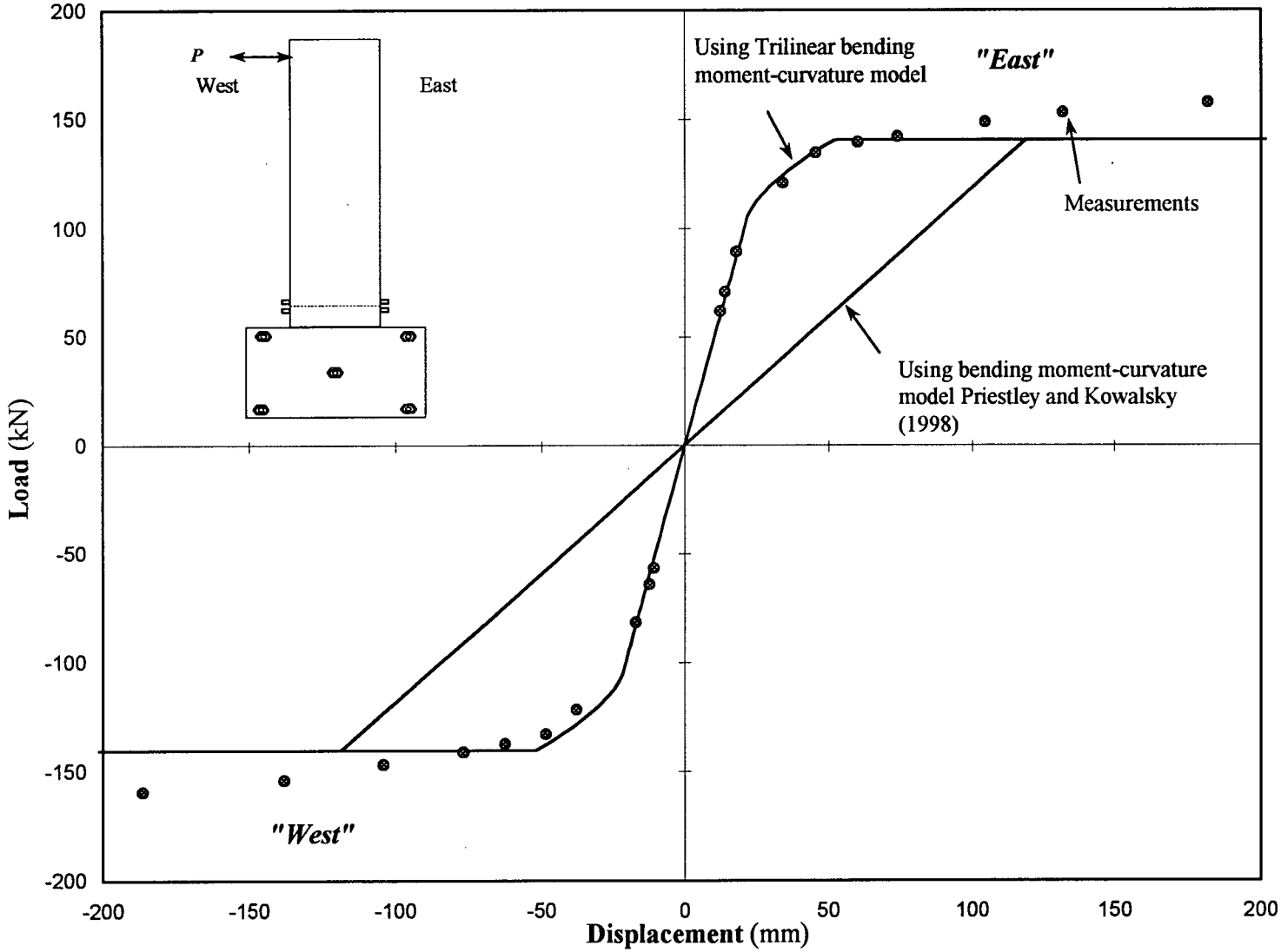

Figure 5.5 Comparison of predicted and observed upper-bound response of the slender wall specimen.

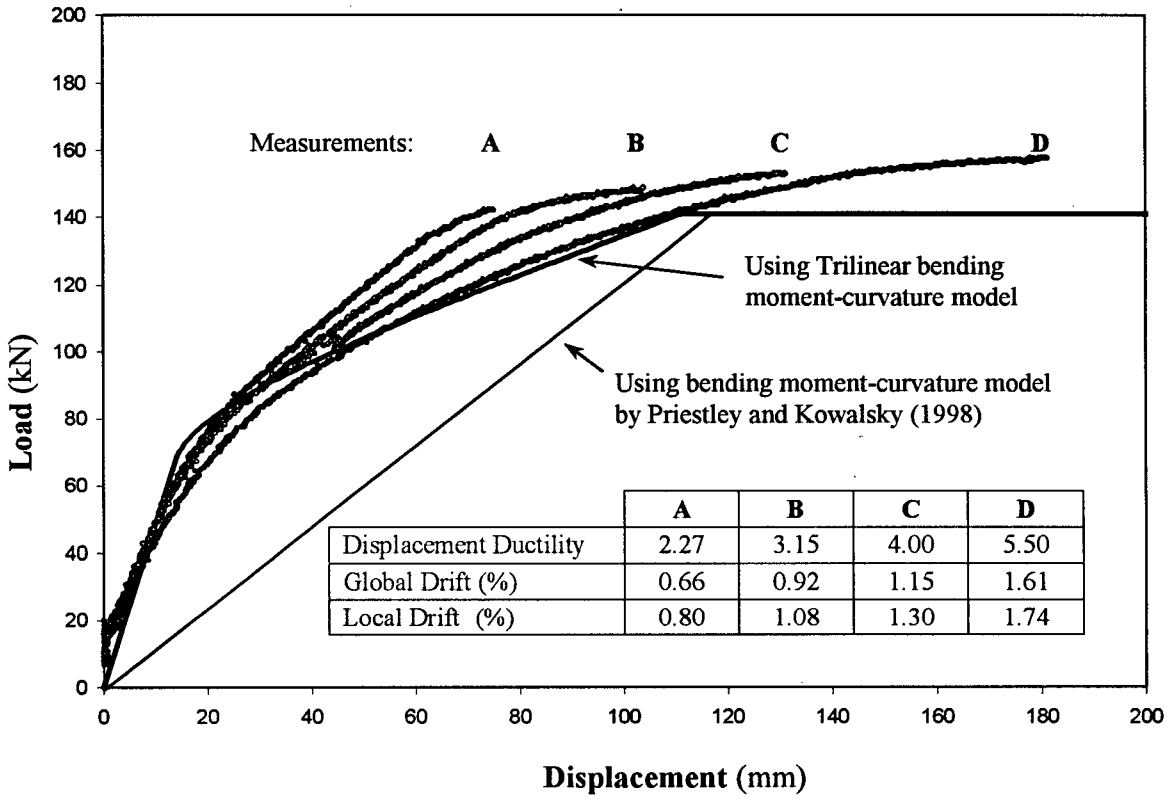

	A	B	C	D
Displacement Ductility	2.27	3.15	4.00	5.50
Global Drift (%)	0.66	0.92	1.15	1.61
Local Drift (%)	0.80	1.08	1.30	1.74

Figure 5.6 Comparison of predicted and observed lower-bound response of the slender wall specimen.

It is seen that the lower-bound trilinear bending moment-curvature model predicted a reasonable lower-bound estimate of the load-displacement relation. The load-displacement relation predicted using the Priestley and Kowalsky bilinear model significantly over-estimates the elastic deflections.

5.4.2 Coupled Wall Example

A coupled wall structure example is presented to illustrate the use of the trilinear bending moment-curvature model in determining the elastic deformations of wall members. The example was done as part of the design of Lincoln Square, a 1.6 million square ft development in the City of Bellevue, Washington. The objective was to better understand the behavior of a coupled wall structure when subjected to an incremental loading (by means of a static inelastic analysis) in addition to evaluating the system performance under a given maximum displacement demand.

Description of the project example:

The core wall structure is a 32-story office tower with an overall height of 450 ft above grade. Figure 5.7-a shows a three dimensional isometric view of the coupled wall core. Details of the cross section geometry are shown in Figure 5.7-b.

The core structure was analyzed in the long (coupled) direction. Additional openings were subsequently added to make the core coupled in the short-direction as well (Mutrie et al., 2000), but these are of no interest in this two-dimensional example. The example shown here is for the east-west direction only despite the unsymmetrical shape of the cross section.

The two-dimensional model of the structure in the long direction is shown in Figure 5.8. The four walls were modeled as column-like members located at the gross section centroid. The coupling beams were modeled as a beam-like elements connected to the columns using infinite stiffness extensions (rigid links). The nodes (joints) at each floor level were constrained to have the same horizontal displacement simulating rigid diaphragm action.

Prior to undertaking the two-dimensional nonlinear static analysis, a three-dimensional linear dynamic analysis of the structure was done by others (Adebar et al., 1999) to determine the first mode distribution of forces and the shear demand on the coupling beams; as shown qualitatively

in Figure 5.8. Due to the numerous coupling beams over the height of the structure, the degree of coupling was found to be 94%. The linear dynamic analysis was also used to establish the maximum inelastic response displacement for the structure during an earthquake that has a 10% probability of occurrence in 50 years and during an earthquake that has a 2% probability of occurrence in 50 years multiplied times a factor of 2/3. Theses maximum top displacement demands on the structure were 869 mm and 1260 mm, respectively.

The flexural response of the four walls was modeled using the trilinear bending moment-curvature model presented in Chapter 2. The two interaction diagrams P - M_l and P - M_n developed for each wall type and used for input to program *2Frame-NL* are shown in Figure 5.9. In determining the interaction diagrams of Figure 5.9, the upper-bound response of the individual walls was adopted (i.e., full tension stiffening was accounted for).

Response of the headers was modeled as a bilinear relation with an effective stiffness of 0.4 $\kappa E_c I_g$, where κ is a factor to account for shear deformations. The κ factor is a function of the coupling beams dimensions and was determined from $1/(1+3*h_b/l_n)$ where h_b is the coupling beam depth and l_n is the clear span (CPCA 1995).

Pushover Analysis:

Program *2Frame-NL* was used to output the sequence of yielding of the coupling beams and the wall members, the effective stiffness of each member (particularly wall members) at any load increment, and the relation between top displacement and the total base shear.

Figure 5-10 shows the results from the pushover analysis that was done for the first mode distribution of forces. The first coupling beam yielded at a base shear of about 5300 kN. When the base shear was about 11,000 kN, many of the coupling beams had yielded and the structure became noticeably softer. After all the coupling beams yielded, the remaining structure became very flexible and the structure consisted of the four elastic walls. The walls did not yield at the base until the structure had deflected to about 1650 mm, which is a considerably larger displacement than is expected to occur during the 2500 year earthquake (See Figure 5.11). Prior to yielding of the walls, the effective stiffness of the walls in the lower portion of the structure had reduced to about 0.3 $E_c I_g$ as shown in the table inset in Figure 5.11. The effective stiffness

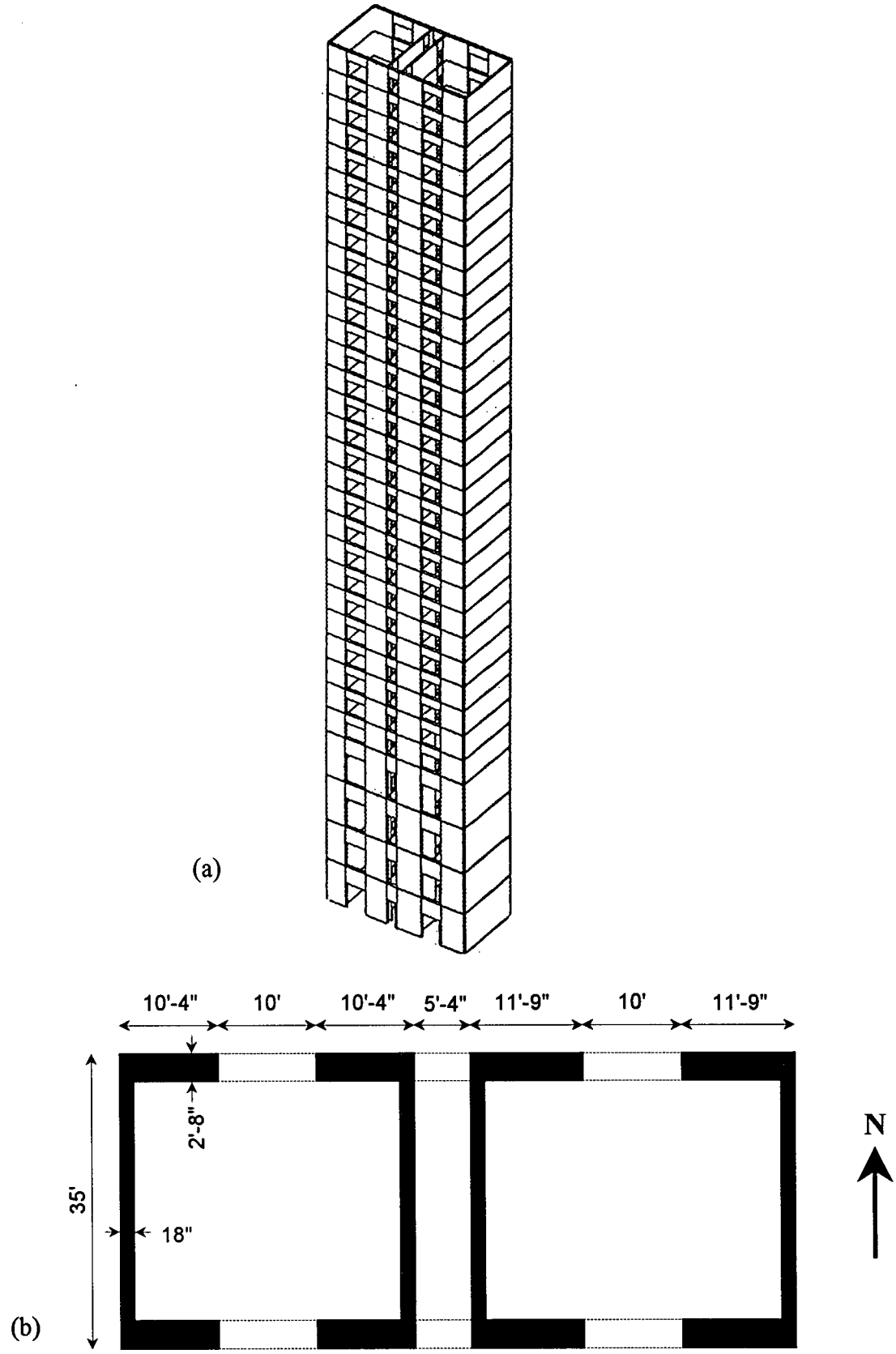

Figure 5.7 (a) Isometric view of the core wall example, (b) cross section dimensions (3.28 ft = 1 m).

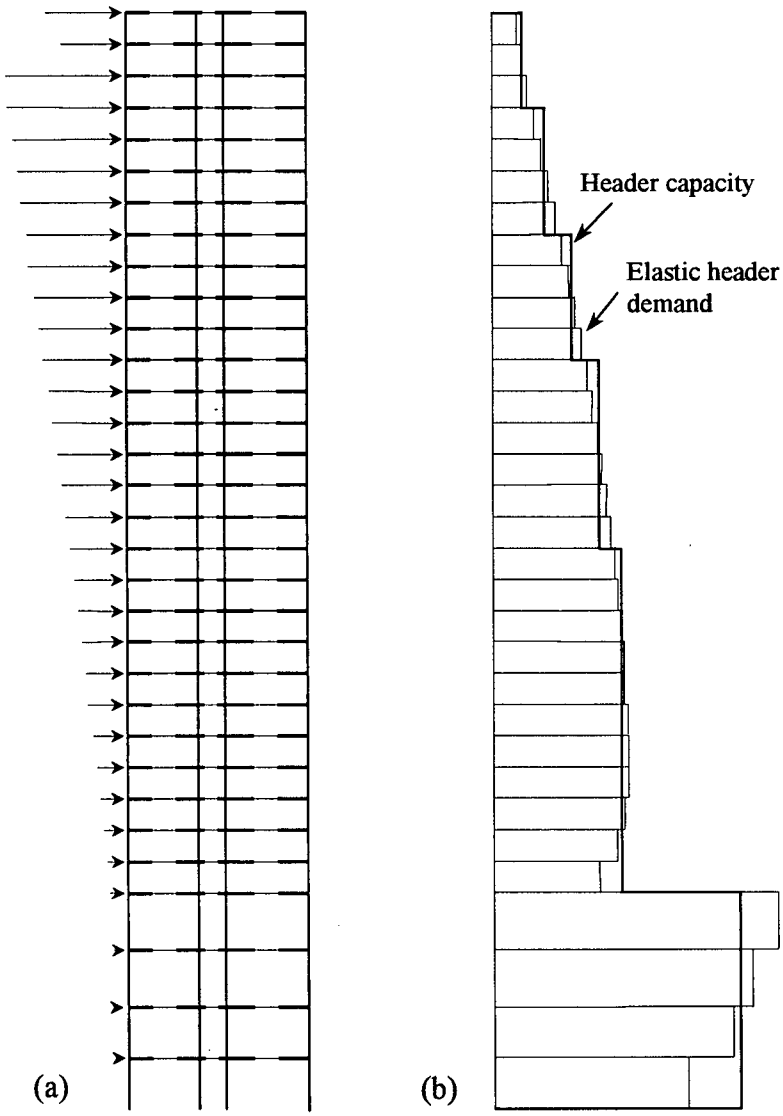

Figure 5.8 (a) two-dimensional plane frame model subjected to first mode loading, (b) coupling beam shear capacity and demand.

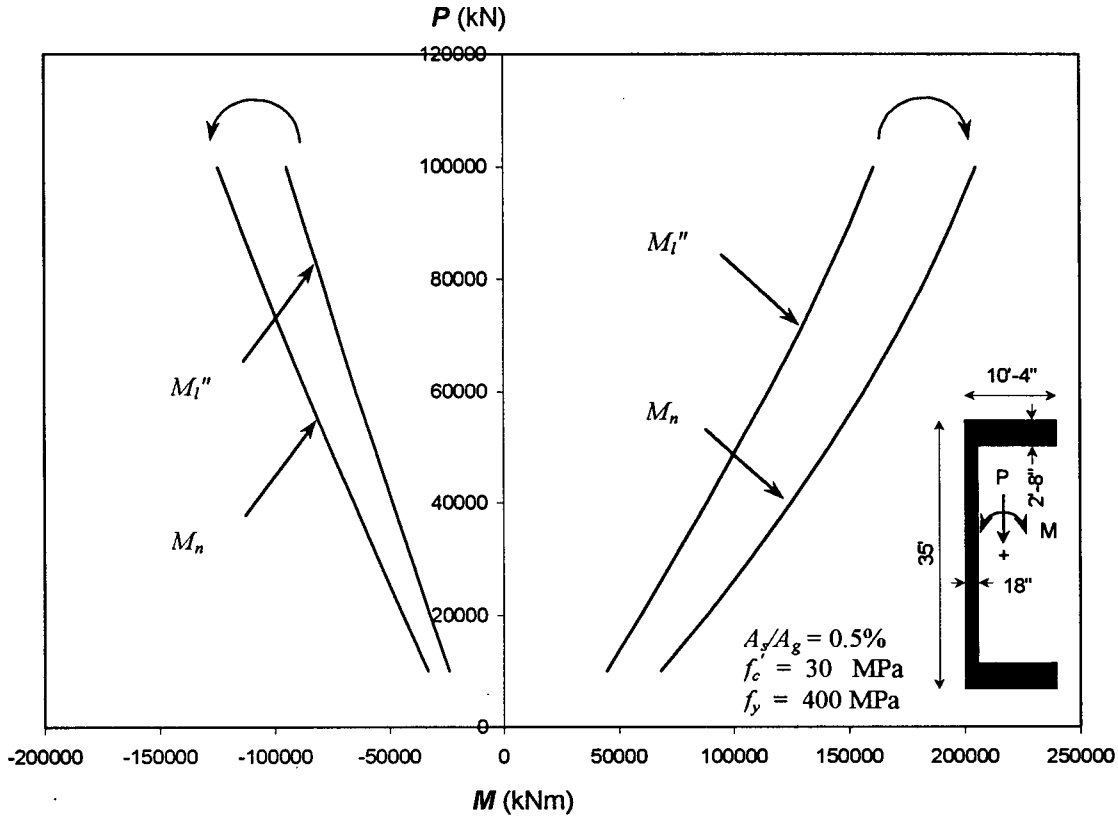

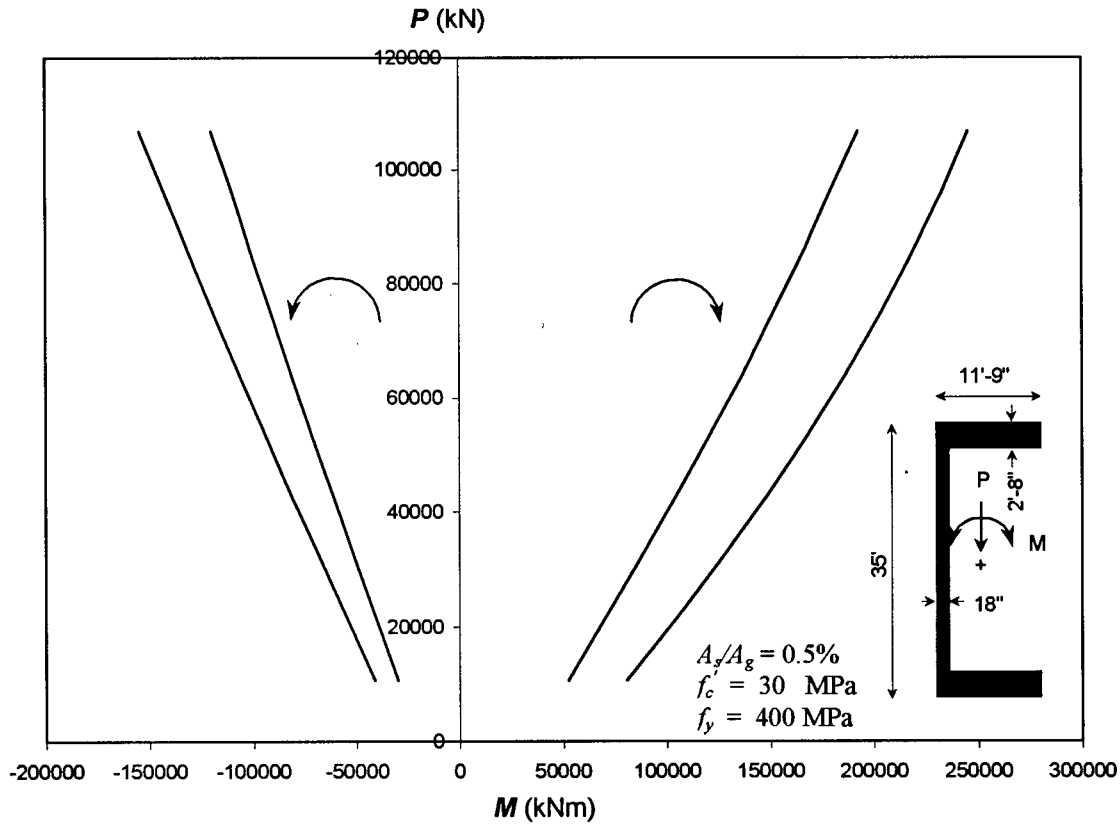

Figure 5.9 Interaction diagrams for the four core walls and used for input to the pushover analysis.

results shown in this table pertains to the wall with the least compression in the core configuration (the first wall from the left side). Note that this degradation of stiffness in the lower portion of the wall is not detected if using a simple bilinear model with one constant effective stiffness prior to yielding.

As seen from the results in Figure 5-11, the highly coupled wall system dissipated the energy of the applied loading by yielding of the coupling beams and the walls remained elastic for a considerable displacement afterwards. Thus, it is of great importance to accurately model the flexural deformations of the wall members within the elastic range.

In addition to illustrating the importance of modeling the elastic deformations of the wall structure, the results of the example also provide useful insight into the behavior of the highly coupled core wall system. It is usually conservative to assume a lower than actual stiffness, as the displacement demand is correspondingly increased. However, assuming lower than actual (or alternatively, the lower-bound rather than the upper-bound) flexural stiffness of the individual walls in this case does not significantly influence the initial stiffness of the highly coupled wall system but rather results in unconservative larger elastic deflections prior to yielding of the walls and smaller inelastic demands on the walls.

The analysis indicated that the wall elements yielded approximately at the same time step. As soon as any particular wall began to yield, a mechanism started and the shear force demand increased significantly on the other wall elements leading eventually to their yielding.

The highly coupled core wall system is a highly desirable system for resisting earthquake loading in high-rise buildings. In the example shown, walls with minimum reinforcement amount remained elastic during a 2500 yr. earthquake. It is very desirable to have a system in which the gravity load resisting elements remain elastic.

The pushover results shown in this example did not consider the contribution of higher modes to the deflection of this tall core wall structure. Since the interest is to assess the ductility of such systems and as the maximum displacement demand on the structure will be first mode dominated, this analysis seems appropriate.

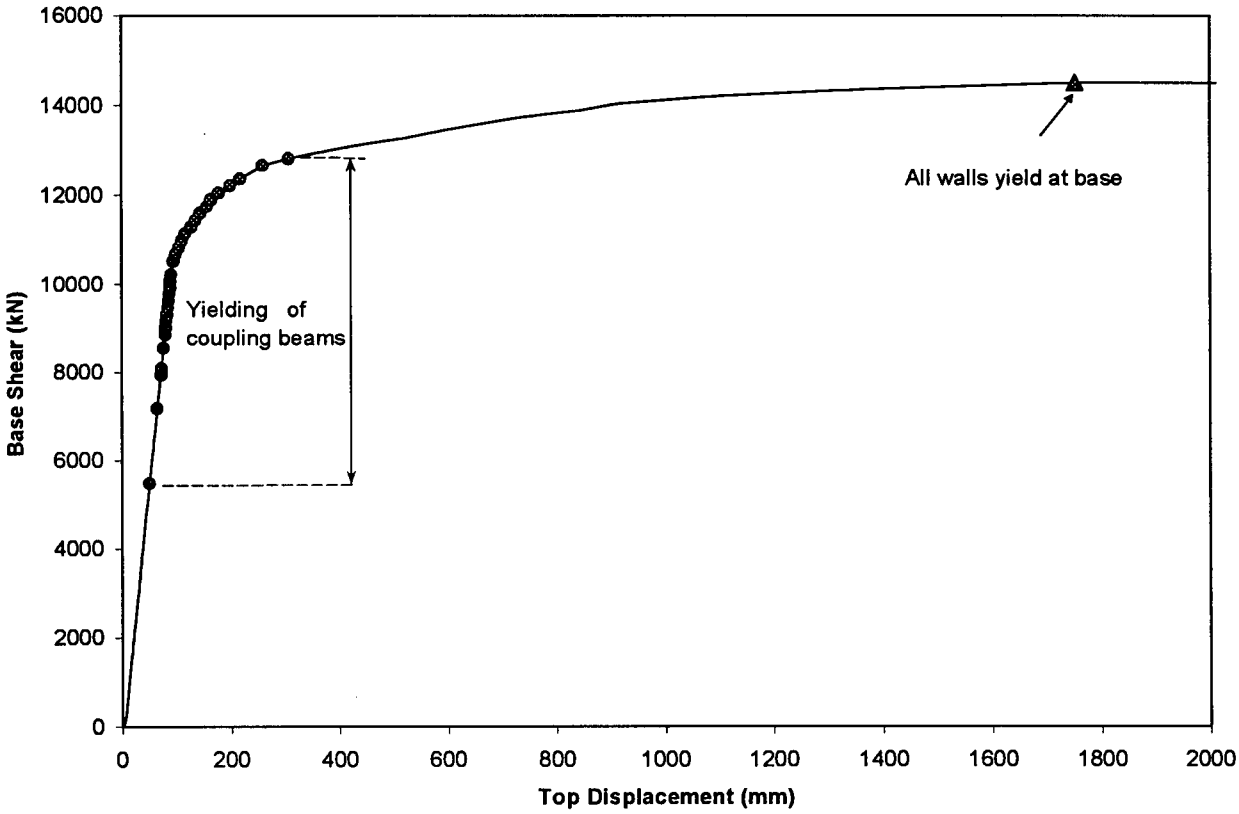

Figure 5.10 Sequence of yielding of the different members in the two-dimensional frame model.

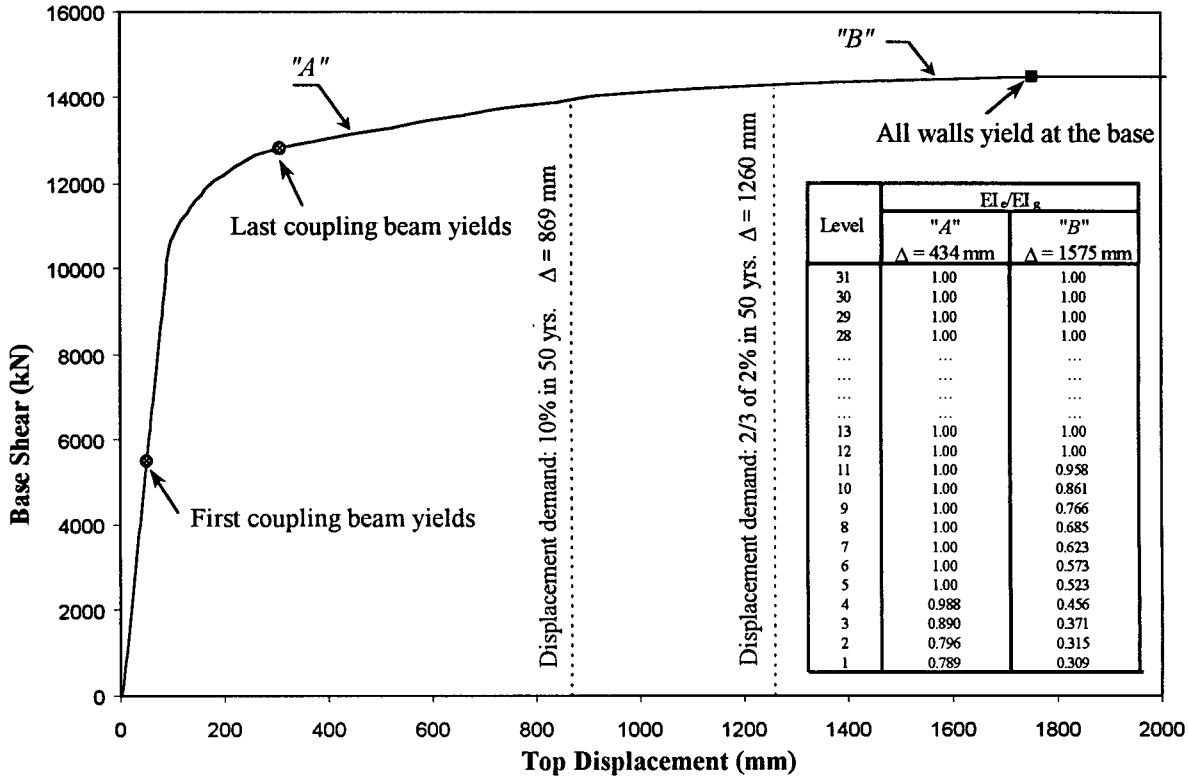

Level	EI_e/EI_g "A" Δ = 434 mm	EI_e/EI_g "B" Δ = 1575 mm
31	1.00	1.00
30	1.00	1.00
29	1.00	1.00
28	1.00	1.00
...	...	...
...	...	...
...	...	...
...	...	...
13	1.00	1.00
12	1.00	1.00
11	1.00	0.958
10	1.00	0.861
9	1.00	0.766
8	1.00	0.685
7	1.00	0.623
6	1.00	0.573
5	1.00	0.523
4	0.988	0.456
3	0.890	0.371
2	0.796	0.315
1	0.789	0.309

Figure 5.11 Predicted nonlinear static response of 450 ft high coupled walls.

Chapter 6

Conclusions and Recommendations

6.1 Summary and Conclusions

In the seismic design of high-rise wall buildings, the fundamental period of the building (which influences the design base shear) and the building drift are usually determined using linear dynamic analysis. To carry out the analysis, designers need to use an effective flexural stiffness of the wall sections that accounts for the effects of cracking. The effective stiffness recommendations from different design guidelines vary by about a factor of three and it is not clear which stiffness value should be used for any particular wall.

The nonlinear static analysis method can be used to assess the inelastic deformations that are expected to occur in walls and coupled wall systems, but requires an appropriate material model in order to yield useful results. While plane sections computer models that can predict the full nonlinear response of wall sections commonly exist, using such a complex material model would add an unnecessary degree of complexity to the analysis. One of the main advantages of the nonlinear static method is the transparency of the procedure. Most nonlinear static analysis is currently done using a simple bilinear (elastic-plastic) model for concrete walls. Thus what is needed is a simple piece-wise linear model that properly accounts for the effect of cracking.

The inconsistency in the recommended stiffness for linear seismic analysis and the need for a simple nonlinear model for nonlinear seismic analysis of concrete walls prompted the following contributions made in this thesis.

A study of the bending moment - curvature response of concrete walls with significant axial compression and low amounts of vertical reinforcement (typical in high-rise walls) indicated that the elastic deformations are not appropriately represented by a simple bilinear idealization. In particular, a bilinear relationship with the linear stiffness defined as the capacity divided by the yield curvature greatly underestimates the effective stiffness. The bending moment - curvature relationship for concrete walls can be better approximated using a trilinear model.

In Chapter 2 of this thesis, a trilinear bending moment curvature model for the flexural response of concrete walls was introduced. In order to capture the effect of cracking on the flexural stiffness of concrete walls in a simple transparent way, the elastic portion of the bending moment - curvature relationship was modeled as bilinear. The model accounts for the influence of cyclic loading on tension stiffening of the cracked concrete by introducing the concept of upper-bound response for a previously uncracked wall and lower-bound response for a severely cracked wall. The trilinear model is defined by four parameters: the slope of the initial linear response $E_c I_g$, the slope of the second linear segment $E_c I_{cr}$, the bending moment defining the intersection of the first and second linear segments, M_l, and the flexural capacity M_n. Two of these parameters $E_c I_g$ and M_n are well known to designers and can easily be determined by hand calculation. The third parameter $E_c I_{cr}$ is also well known, but is very difficult to determine by hand calculation for typical wall sections with distributed vertical reinforcement. Thus design charts were developed as part of this thesis. Finally, an equation was developed to permit the easy calculation of the fourth parameter M_l. It is this parameter that accounts for the difference between the upper-bound and lower-bound response that captures the effect of cyclic loading. The proposed trilinear bending moment – curvature model can easily be incorporated into a nonlinear static analysis program for concrete walls (as was done in Chapter 5), or can be used as the foundation of a general rational model for determining the effective linear stiffness of concrete walls (as was done in Chapter 4).

A large-scale test was conducted on an approximately quarter-scale model of a slender wall. Based on the results of a literature search, it appears that this is the most slender wall ever tested. The specimen was 40 ft "high" and 5.3 ft long, which corresponds to a height-to-length ratio of 7.5. The purpose of the test was to observe the response of a slender wall with a low percentage of vertical reinforcement and subjected to significant axial compression, and to obtain the information needed to validate the proposed trilinear bending moment - curvature model.

The observed initial stiffness of the concrete wall corresponded reasonably well to the predicted uncracked gross section stiffness $E_c I_g$. When the wall was reloaded after having been significantly cracked, the initial stiffness was again approximately equal to the uncracked section stiffness $E_c I_g$ due to the axial compression closing the cracks when the bending moment was removed. As predicted by the proposed model, the extent of the initial linear range, i.e., M_l,

reduced after the wall was cracked. The predicted lower-bound response corresponded reasonably well to the response of the wall after it had been subjected to global drift levels of about 1.5%. The experimentally measured relationship between curvature and the corresponding applied bending moment were found to agree well with the predicted relationship.

The trilinear bending moment - curvature model, having been calibrated to the results of the large-scale wall test, was used to develop a general, consistent method to predict the effective (linear) flexural stiffness of concrete walls. To account for the degradation of stiffness during the cyclic motion of an earthquake, the effective stiffness of concrete walls was considered to range from an upper-bound effective stiffness to a lower-bound effective stiffness. The general method uses the two non-dimensional parameters that describe the bending moment - curvature relationship of the cross section at the base of the wall: the ratio of the cracked section moment of inertia to the uncracked section (gross) moment of inertia I_{cr} / I_g, and the ratio of the linear bending moment to the capacity of the wall section at the base M_l / M_n.

The general method was used to study the influence of a variety of parameters on the effective stiffness of concrete walls. The results of the study indicate that the effective flexural stiffness of concrete walls can vary from as little as 0.1 I_g to as high as 1.0 I_g depending on: state of cracking, magnitude of axial compression, geometry of the wall cross section, amount of vertical reinforcement, yield strength of the vertical reinforcement and concrete compressive strength. Thus, the very large variation in effective stiffness that is seen in various design guidelines does actually exist, and each guideline is correct for certain types of walls under certain conditions. The general method presented in this thesis is the only method that accounts for all the parameters and gives the appropriate stiffness for a particular wall.

Based on the general method for determining the effective flexural stiffness of concrete walls, a set of simplified expressions for the upper-bound and lower-bound effective stiffness was proposed. The simplified expressions capture the influence of several parameters that affect the stiffness in an approximate way and are particularly useful in the initial stages of design when the concrete geometry has not been finalized and the amount of reinforcement is not known.

The upper-bound effective flexural stiffness can be used in a force-based design where engineers start the design process by estimating the fundamental period of the building and the

corresponding design accelerations and forces. The upper-bound stiffness is used to get a lower-bound estimate of the period and thus a higher estimate of the design forces and seismic actions. In a displacement-based design, where the displacement is the major concern, designers should estimate the period and the corresponding displacements using the lower-bound effective stiffness.

The proposed trilinear bending moment – curvature model was implemented into a nonlinear static analysis program. Numerical techniques used to implement the trilinear model were presented in Chapter 5. The nonlinear static analysis program was used to demonstrate the use and advantages of the proposed model over other suggested models through two example applications. Further validation of the proposed trilinear model was illustrated in the first example where the predicted load-deformation relationship for the slender wall test compared well with the measured response of the wall. The nonlinear static response of a high-rise coupled wall system was presented in the second example. The nonlinear static analysis was used to assess the ductility of a coupled wall core system that is currently being constructed near the city of Seattle, Washington. Results from the example showed the importance of accurately modeling the elastic deformations of concrete walls using the proposed trilinear model and provided useful insight into the behavior of such highly coupled wall systems.

6.2 Recommendations for Further Work

The proposed trilinear bending moment - curvature model assumes no increase in the capacity of the wall after all the vertical reinforcement has yielded. As seen from the slender wall test, a significant increase in the bending moment capacity is possible at very large drift ratios. For simplicity, strain hardening of the reinforcement was ignored in the proposed trilinear relationship. The third linear segment in the bending moment - curvature relationship could be inclined at a certain slope to account for strain hardening. However, as the strain hardening characteristics vary significantly for different types of reinforcing steel, it is difficult to define such a slope in the same generic way as has been done for the other elements of the proposed trilinear model.

While the majority of concrete walls and coupled walls in high-rise buildings are subjected to significant axial compression, there are cases where the wall segment of a coupled wall system

may be subjected to axial tension, particularly in medium to low rise buildings. As the lateral earthquake displacements are increased, the coupling beams yield sequentially creating a gradually increasing compression force in one wall and tension force in the other wall. The tension force due to the coupling beam shears can offset the initial axial compression due to gravity loads and result in a net tension force being applied to the wall segment. The proposed trilinear bending moment – curvature relationship is not appropriate when the axial tension applied to a wall section causes the entire wall section to be subjected to vertical tension strains. Additional work needs to be done to develop an appropriate model for this condition.

The proposed trilinear model represents the loading portion of the full cyclic bending moment - curvature response (hysteresis loop) of a concrete wall. The loading portion of the response is precisely what is needed for a nonlinear static analysis. To perform a nonlinear dynamic analysis, however, a full hysteresis model is needed. It is proposed that the trilinear bending moment - curvature relationship be used as the basis of a hysteretic model for concrete walls in high-rise buildings, and that the experimental results from the slender wall test be used to calibrate such a model.

References

Abrams, D. P. (1991), "Laboratory definitions of behavior for structural components and building system," ACI SP-127, Vol. 127,no. 4,pp. 91-152, April1991.

Adebar, P., and Ibrahim, A.M.M. (2000), "Simple non-linear flexural stiffness model for concrete shear walls," Earthquake Spectra, EERI, In press.

Adebar, P., Ibrahim, A.M.M., and Bryson, M. (2000), "Large-scale test of a slender concrete shear wall," Report, Department of Civil Engineering, University of British Columbia, 210 pp.

Adebar, P., Mutrie, J.G., and Ibrahim, A.M.M. (1999), "Inelastic static analysis to evaluate the ductility of coupled walls in a tall building," 8th Canadian Conference on Earthquake Engineering, Vancouver, BC, pp. 421-426.

Applied Technology Council (1996), "Seismic evaluation and retrofit of concrete buildings," Report ATC 40, Applied Technology Council, Paio Alto, California.

Bracci, J.M., Kunnath, S.K., and Reinhorn, A. M. (1997), "Seismic performance and retrofit evaluation of reinforced concrete structures," Journal of Structural Engineering, ASCE, 123, 3-10.

Bryson, M. (2000), "Testing of the lateral stiffness of a lender concrete shear wall," CIVL 598 Directed Studies Report, Department of Civil Engineering, The University of British Columbia, pp. 162.

Charney, F.A. (1991), "Correlation of the analytical and experimental inelastic response of a 1/5 scale seven-story reinforced concrete frame-wall structure," ACI SP-127, pp. 261-361.

Chopra, A.K. (1995), "Dynamics of structures: Theory and applications to earthquake engineering," Prentice Hall, New Jersey.

Collins, M.P., and Mitchell, D. (1991), "Prestressed concrete structures," Prentice Hall, 766 pp.

Council on Tall Buildings and Urban Habitat (1992), "Cast-in-place concrete in tall building design and construction," McGraw-Hill.

CPCA (1995) Explanatory notes on CSA standard A23.3-94, Concrete design handbook, 2nd ed., Ontario, Canada.

CSA (1994), "Design of concrete structures," CSA Standard A23.3-94, Canadian Standards Associations, Rexdale, Ontario, 199 pp.

FEMA 273 (1997), "NEHRP Guidelines for the seismic rehabilitation of buildings," Federal Emergency Management Agency, Washington, D. C.

FEMA 274 (1997), "NEHRP Commentary on the guidelines for the seismic rehabilitation of buildings," Federal Emergency Management Agency, Washington, D. C.

Fintel M. (1991), " Shearwalls – an answer for seismic resistance?", Concrete International, Vol. 13, No. 7, pp. 48-53.

Freeman, S. A., Nicoletti, J.P., and Tyrell, J.V. (1975), "Evaluations of existing buildings for seismic risk – A case study of Puget sound naval shipyard," Bremerton, Washington, Proceedings of 1st U.S. National Conference on Earthquake Engineering, EERI, Berkeley, 113-122.

French, C.W., and Schultz, A.E. (1991), "Minimum available deformation capacity of reinforced concrete beams," ACI SP-127, pp. 363-419.

Fronteddu, L. (1993), "Response of reinforced concrete to reverse cyclic loading," M.A.Sc. Thesis, Department of Civil Engineering, The University of British Columbia.

Fronteddu, L., and Adebar, P. (1992), "Response of structural concrete to axial tension," Proceedings of the Annual CSCE Conference, Vol. IV, Quebec City, pp. 89-98.

Ibrahim, A.M.M., and Adebar, P. (2000), "Effective flexural stiffness of concrete shear walls," Journal of Structural Engineering, ASCE, In press.

Meigs, B. E., Eberhard, M. O., and Garcia, L. E. (1993), "Earthquake-resistant systems for reinforced concrete buildings: a survey of current practice," Report no. sgem 93-3, Department of Civil Engineering, University of Washington, Seattle.

Mutrie, J.G., Adebar, P., and Leung, K. (2000), "Design of high-rise concrete shear wall buildings: Canadian vs. U.S. practice," Proceedings of SEAOC Convention, Vancouver, B.C., Aug. pp. 169-179.

Mutrie, J.G. (1998), " Program 2Frame, In-House program for plane frame analysis of buildings," Jones Kowng Kishi, North Vancouver, Private communication.

Naeim, F., and Lobo, R.F. (1998), "The ten commandments of push-over analysis," Proceedings of the 1998 annual meeting, Los Angeles Tall Buildings Structural Design Council, Los Angeles, CA.

NZS 3101 (1995) Commentary on the design of concrete structures, Standard New Zealand, New Zealand.

Owen, D.R.G., and Hinton, E. (1980), "Finite elements in plasticity: theory and practice," Pineridge Press, Swansea, U.K.

Paret, T. F., Sasaki, K. K., Eilbekc, D.H., and Freeman, S.A. (1996), "Approximate inelastic procedures to identify failure mechanisms from higher mode effects," Paper no. 966, 11th World Conference on Earthquake Engineering, Acapulco, Mexico.

Park, R., and Paulay, T. (1975), "Reinforced concert structures," John Wiley and sons, New York.

Paulay, T. (1997), "Seismic torsional effects on ductile structural wall systems," Journal of Earthquake Engineering, Vol. 1, No. 4, pp. 721-745.

Paulay, T., and Priestley, M. J. N. (1992), "Seismic design of reinforced concrete and masonry buildings," John Wiley and sons, New York, 744 pp.

Priestley, M. J. N. (2000), "Performance Based Seismic Design," Paper no. 2831, 12th World Conference on Earthquake Engineering, Auckland, New Zealand.

Priestley, M. J. N., and Hart, G. C. (1989), "Design recommendations for the period of vibration of masonry wall buildings," Research Report SSRP 89/05, University of California, San Diego and Los Angeles, 46 pp.

Priestley, M.J.N., and Kowalsky, M.J. (1998), "Aspects of drift and ductility capacity of rectangular cantilever structural walls," Bulletin of the New Zealand National Society for Earthquake Engineering , Vol. 31, No. 2, pp. 73-85.

Saatcioglu, M. (1991) "modeling hyestertic force deformation relationship for reinforced concrete elements," ACI Sp-127, pp. 153-198.

Saatcioglu M., and Bruneau M. (1993), "Performance of structures during the 1992 Erzincan earthquake," Canadian Journal of Civil Engineering, 20, pp. 305-325.

SEAOC 1996. Seismology committee, Structural Engineers Associations of California (SEAOC), "Recommended lateral force requirements and commentary".

Thomsen IV, J.H., and Wallace, J. W. (1995), "Displacement-based design of RC structural walls: an experimental investigation of walls with rectangular and T-shaped cross sections," Report No. CU/CEE-95/06, Department of Civil and Environmental Engineering, Clarkson University, Potsdam, New York.

Veechio, F.J. (1999), "Towards cyclic load modeling of reinforced concrete," ACI Structural Journal, Vol. 96, pp. 193-202.

Vecchio F. and Collins M.P. (1986), "The modified-field compression theory for reinforced concrete elements subjected to shear", ACI Journal, Vol. 83, No. 2, pp. 219-231.

Wallace, J. W., and Moehle, J. P. (1992), "Ductility and detailing requirements of bearing wall buildings," Journal of Structural Engineering, ASCE, Vol. 118, No. 6, pp. 1625-1644.

UBC 1997. Uniform Building Code, International conference of building officials, Whittier, California.

Appendix A

Plane Sections Analysis Procedure

Determination of the actual nonlinear bending moment-curvature relationship is done using plane sections analysis that satisfies the equilibrium of forces, strain compatibility and the stress-strain relationships. The analysis procedure assumes linear strain distribution along the wall cross section; and that the stress-strain relationship for concrete and steel are known.

The stress-strain relationship for concrete in compression and for steel in tension and compression used in this work are shown in Figure A.1. The stress-strain relationship for concrete in tension was illustrated in Chapter 2 (Figure 2.5).

Linear strain distribution along the cross section is defined by two variables, for instance, strain at centroid and strain gradient (curvature). If the strain distribution is known or assumed, then the stress-strain relationships for concrete and steel can be used to find the distribution of stresses along the section. Knowing the stresses, bending moment and axial capacities of the cross section can be determined from the following equilibrium equations.

$$P = \int_{A_c} f_c \, dA_c + \int_{A_s} f_s \, dA_s$$

$$-M = \int_{A_c} f_c \, y \, dA_c + \int_{A_s} f_s \, y \, dA_s$$

These equilibrium equations involve performing the integration over the area of cross section. Since the strain distribution is non uniform across the depth of the wall, evaluation of these integrals is not a straightforward task. One convenient procedure to evaluate these integrals is to idealize the wall cross section as a series of rectangular layers and to assume uniform strain in each layer. If the strain is uniform within a layer, then the stress within the layer is also uniform. The equilibrium integrals then become a matter of multiplication of area of each layer times the corresponding uniform stress. Figure A.2 summarizes the layered approach to solve the equilibrium equations.

To determine the bending moment at a given curvature, the strain distribution across the wall section must be determined so as to satisfy the equilibrium equations. Commonly, axial load is known providing one condition of equilibrium. For a given/assumed curvature, a trial value of strain at a given reference is assumed (strain at centroid for example) and an iterative technique is performed to satisfy the known axial load. Once this condition is satisfied, strain distribution across the wall section is thus known and the corresponding bending moment is determined from the second equilibrium equation.

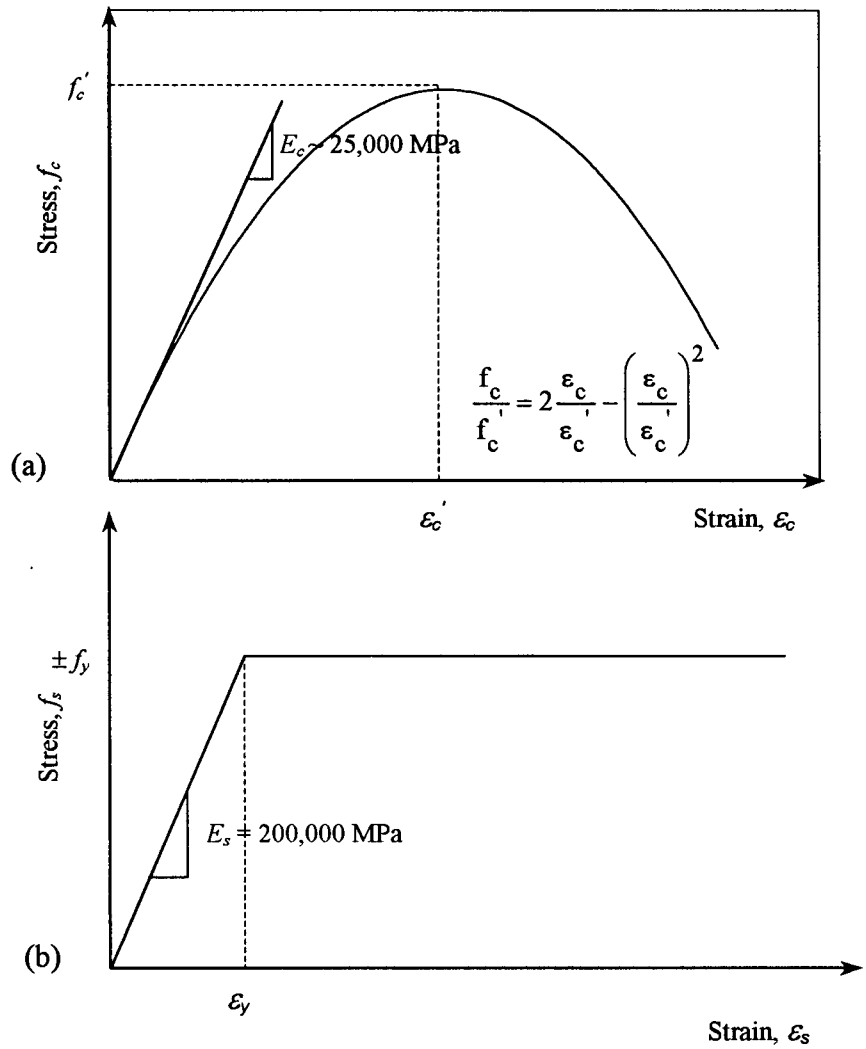

Figure A.1 Stress-strain relationship for a) concrete in compression, b) steel in compression and tension.

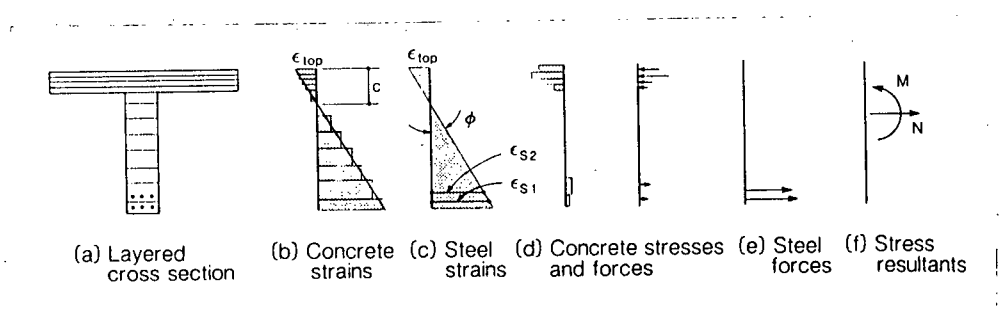

Figure A.2 Evaluating equilibrium equations using layer by layer procedure (from Collins and Mitchell, 1991)

Appendix B

Bending Moment-Curvature Relationship Considering Residual Strains due to Cyclic Loading

The bending moment-curvature relationships shown previously in Figure 2.7, were predicted ignoring the effect of residual strains due to cyclic loading as the influence of these were assumed to be small. In the following, the bending moment-curvature relationships for the same wall configuration are repeated considering the effect of residual compressive strains in concrete and residual tension and compression strains in reinforcement.

Figure B.1-a shows the bending moment-curvature relationships considering the cyclic response of concrete in tension (as explained previously in section 2.5) and residual strains in concrete and reinforcement. The stress-strain relationship for concrete in compression was assumed to unload and reload to the envelope of the monotonic relationship parallel to the initial gross stiffness resulting in residual compressive strains at zero stress (Fig. B.1-b). The stress-strain relationship for the reinforcement was assumed bilinear. Unloading and reloading to an increased deformation follow the same initial linear slope resulting in residual strains at zero stress (Fig. B.1-c). Note that the lower-bound bending moment-curvature relationship shown in the figure was assumed to reach the strain at peak stress ($\varepsilon_c' = 0.0033$ for $f_c' = 50$ MPa).

As shown in the figure, the resulting loading curves are only slightly offset from the origin particularly during the early cycles. This small offset is attributed to the concrete compressive stresses being predominately linear prior to yielding of the reinforcement. The offset, however, can be of significance when the concrete reaches high values of compressive strains particularly for cycles with large drift ratios and when the reinforcement yields to large strain values. The experimental results, shown in Figure 3.11, indicate that the offset is relatively small in the range of expected drift/ductility.

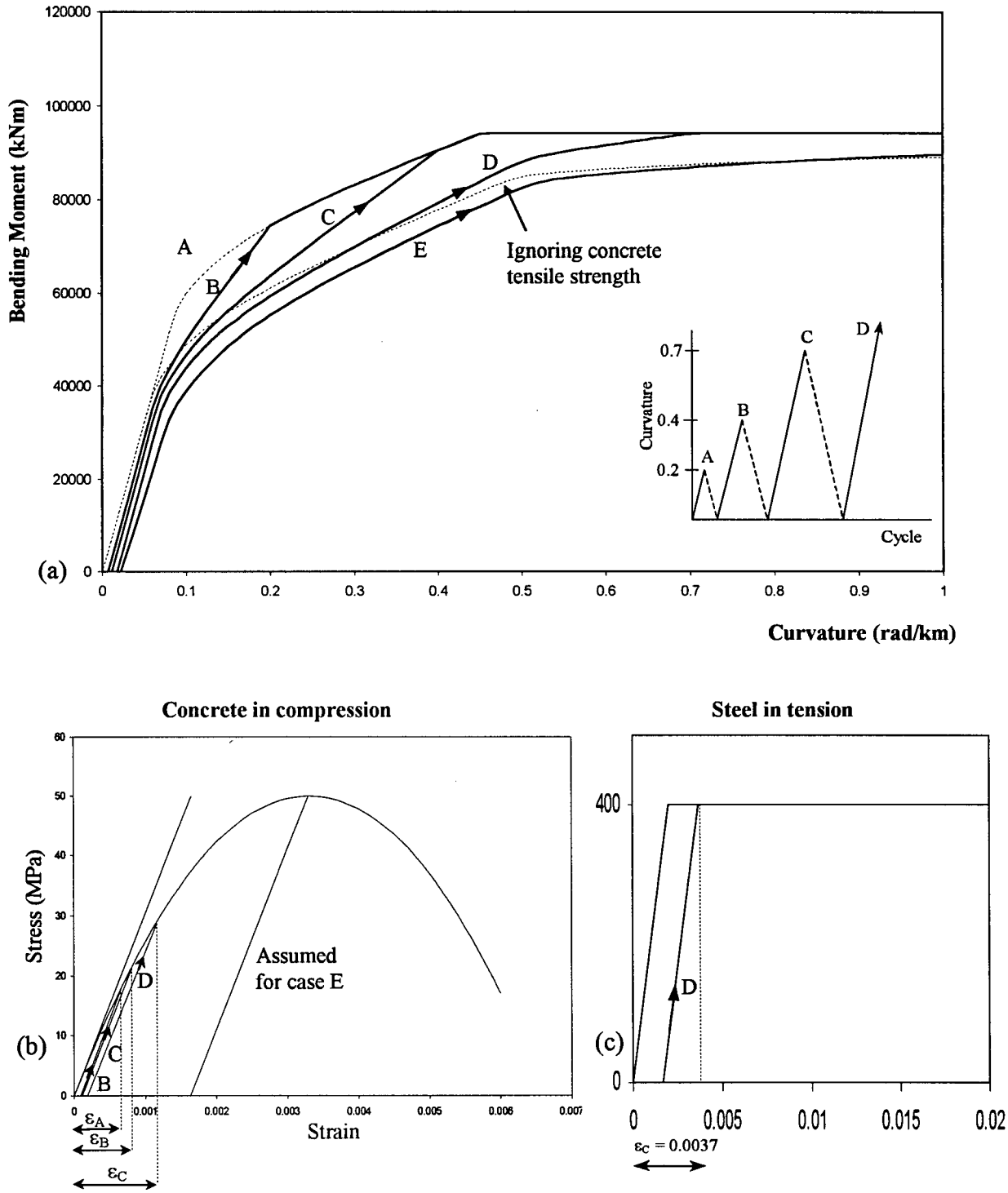

Curvature (rad/km)	Max. compressive strain previously reached:
$\phi_A = 0.2$	$\varepsilon_A = -0.00061$
$\phi_B = 0.4$	$\varepsilon_B = -0.0008$
$\phi_C = 0.7$	$\varepsilon_C = -0.0011$

Figure B.1 Bending moment-curvature relationships considering residual strains due to cyclic loading.

Appendix C

Determination of Cracked Section Moment of Inertia, I_{cr}, for a General Flanged Wall Section

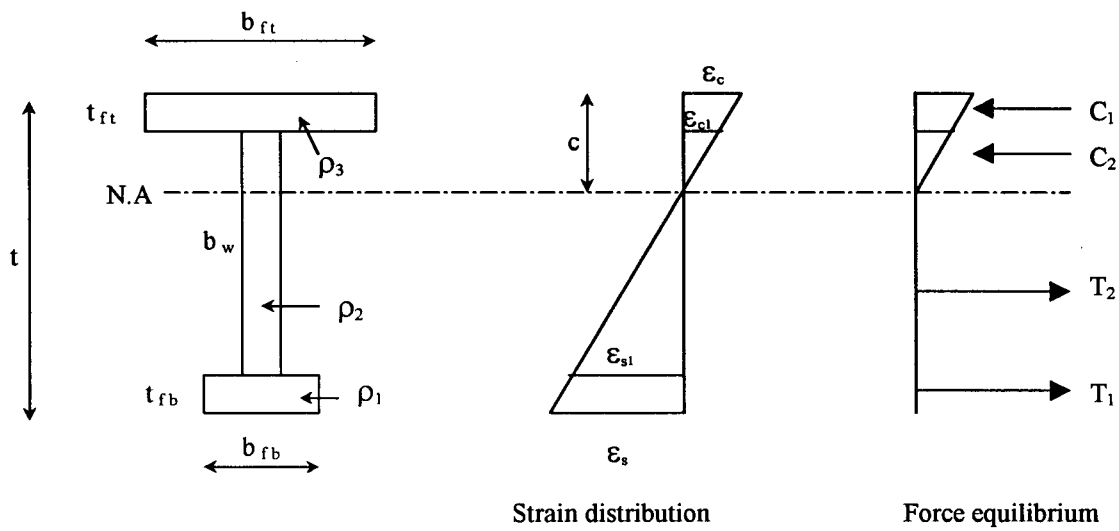

Assume:

Elastic stresses: $f_s = E_s \cdot \varepsilon_s$ $\quad f_c = E_c \cdot \varepsilon_c$ & $n = E_s / E_c$

Where: f_s = maximum steel stress; f_c = maximum concrete stress;

ε_s = maximum steel strain; ε_c = maximum concrete strain

I: Determine the depth of Netural Axis, c:

If N.A is in the web:

$$\frac{\varepsilon_c}{c} = \frac{\varepsilon_s}{(t-c)}$$

$$\varepsilon_{cl} = \left(\frac{c - t_{f_t}}{c}\right) \cdot \varepsilon_c$$

$$\varepsilon_s = \varepsilon_c \cdot \left(\frac{t}{c} - 1\right)$$

$$\varepsilon_{sl} = \left(\frac{t - c - t_{f_b}}{t - c}\right) \cdot \varepsilon_s$$

Equilibrium $\quad T = C$

- $T_1 = E_s \cdot \left(\frac{\varepsilon_s + \varepsilon_{sl}}{2}\right) \cdot t_{fb} \cdot b_{fb} \cdot \rho_1$

where $\left(\frac{\varepsilon_s + \varepsilon_{sl}}{2}\right) = E_c \cdot \left[\frac{t - c - (t_{fb}/2)}{c} - 1\right]$

- $T_2 = E_s \cdot \left(\frac{\varepsilon_{sl}}{2}\right) \cdot (t - c - t_{fb}) \cdot b_w \cdot \rho_2$

- $C_1 = E_c \cdot \left(\frac{\varepsilon_c + \varepsilon_{cl}}{2}\right) \cdot b_{ft} \cdot t_{ft}$

- $C_2 = E_c \cdot \left(\frac{\varepsilon_{cl}}{2}\right) \cdot (c - t_{ft}) \cdot b_w$

$$C_1 + C_2 = T_1 + T_2$$

$$E_s \cdot E_c \cdot \left[\frac{t - c - (t_{fb}/2)}{c}\right] \cdot t_{fb} \cdot b_{fb} \cdot \rho_1 + E_s \cdot \frac{\varepsilon_c}{2} \cdot \left[\frac{t - c - t_{fb}}{c}\right] \cdot (t - c - t_{fb}) \cdot b_w \cdot \rho_2 =$$
$$E_c \cdot \varepsilon_c \cdot \left[\frac{c - (t_{ft}/2)}{c}\right] \cdot b_{ft} \cdot t_{ft} + E_c \cdot \frac{\varepsilon_c}{2} \cdot \left[\frac{c - t_{ft}}{c}\right] \cdot (c - t_{f_t}) \cdot b_w$$

$$n \cdot \left[\frac{t - c - (t_{fb}/2)}{c}\right] \cdot t_{fb} \cdot b_{fb} \cdot \rho_1 + \frac{n}{2} \cdot \left[\frac{t - c - t_{fb}}{c}\right] \cdot (t - c - t_{fb}) \cdot b_w \cdot \rho_2 =$$
$$\left[\frac{c - (t_{ft}/2)}{c}\right] \cdot b_{ft} \cdot t_{ft} + E_c \cdot \frac{1}{2} \cdot \left[\frac{c - t_{ft}}{c}\right] \cdot (c - t_{f_t}) \cdot b_w$$

$$2n \cdot \left[t - \left(\frac{t_{fb}}{2}\right) - c\right] \cdot t_{fb} \cdot b_{fb} \cdot \rho_1 + n \cdot [t - t_{fb} - c] \cdot (t - t_{fb} - c) \cdot b_w \cdot \rho_2 =$$
$$2 \cdot [c - (t_{ft}/2)] \cdot b_{ft} \cdot t_{ft} + [c - t_{ft}] \cdot (c - t_{f_t}) \cdot b_w$$

$$n \cdot [t - t_{fb} - c]^2 \cdot b_w \cdot \rho_2 + [c - t_{f_t}]^2 \cdot b_w + 2n \cdot \left(t - \frac{t_{fb}}{2} - c\right) \cdot t_{fb} \cdot b_{fb} \cdot \rho_1$$
$$- 2 \cdot [c - (t_{fb}/2)] \cdot b_{ft} \cdot t_{ft} = 0.0$$

$$n \cdot \rho_2 \cdot b_w \cdot \left[(t - t_{fb})^2 - 2 \cdot (t - t_{fb}) \cdot c + c^2\right] - b_w \cdot \left[c^2 - 2 \cdot c \cdot t_{ft} + t_{ft}^{\,2}\right] +$$
$$2 \cdot n \cdot \rho_1 \cdot t_{fb} \cdot b_{fb} \cdot [t - (t_{fb}/2) - c] - 2 \cdot t_{ft} \cdot b_{ft} \cdot [c - t_{fb}/2] = 0.0$$

Quadratic Equation in c: $X \cdot c^2 + Y \cdot c + Z = 0$

Where:

$$X.\ c^2 = \quad n \cdot \rho_2 \cdot b_w \cdot c^2 - b_w \cdot c^2$$

$$Y.\ c = \quad -2 \cdot n \cdot \rho_2 \cdot b_w \cdot (t - t_{fb}) \cdot c + 2 \cdot b_w \cdot t_{ft} \cdot c - 2 \cdot n \cdot \rho_1 \cdot t_{fb} \cdot b_{fb} \cdot c - 2 \cdot t_{ft} \cdot b_{ft} \cdot c$$

$$Z = \quad n \cdot \rho_2 \cdot b_w \cdot (t - t_{fb})^2 - b_w \cdot t_{ft}^{\ 2} + 2 \cdot n \cdot \rho_1 \cdot t_{fb} \cdot b_{fb} \cdot (t - t_{fb}/2) + 2 \cdot t_{ft} \cdot b_{ft}/2$$

Then,

$$X: \quad (n \cdot \rho_2 - 1) \cdot b_w$$

$$Y: \quad -2 \cdot n \cdot \rho_2 \cdot b_w \cdot (t - t_{fb}) + 2 \cdot b_w \cdot t_{ft} - 2 \cdot n \cdot \rho_1 \cdot A_{fb} - 2 \cdot A_{ft}$$

$$Z: \quad n \cdot \rho_2 \cdot b_w \cdot (t - t_{fb})^2 - b_w \cdot t_{ft}^{\ 2} + 2 \cdot n \cdot \rho_1 \cdot A_{fb} \cdot (t - t_{fb}/2) + A_{ft} \cdot t_{fb}$$

Solution of the quadratic equation : $\frac{-Y \pm \sqrt{Y^2 - 4 \cdot X \cdot Z}}{2 \cdot X}$ gives the neutral axis depth, c.

II: Determine the moment of inertia, I_{cr}, from the parallel axis theorem:

$$I_{cr} = \frac{b_w . c^3}{3} + b_{ft} . t_{ft} . \left[c - \frac{t_{ft}}{2} \right]^2 + n . \rho_1 . t_{fb} . b_{fb} . \left[t - t_{fb}/2 - c \right]^2 + n . \rho_2 . \frac{b_w}{2} . \left[t - c - t_{fb} \right]^2$$

Note that if the N.A depth, c, lies in the flanges, the equilibrium equation need to be resolved for the new conditions.

Appendix D

Determination of Linear Bending Moment, M_l

- The three parameters: E_cI_g, E_cI_{cr}, M_n should be pre-calculated in order to determine the linear bending moment, M_l.

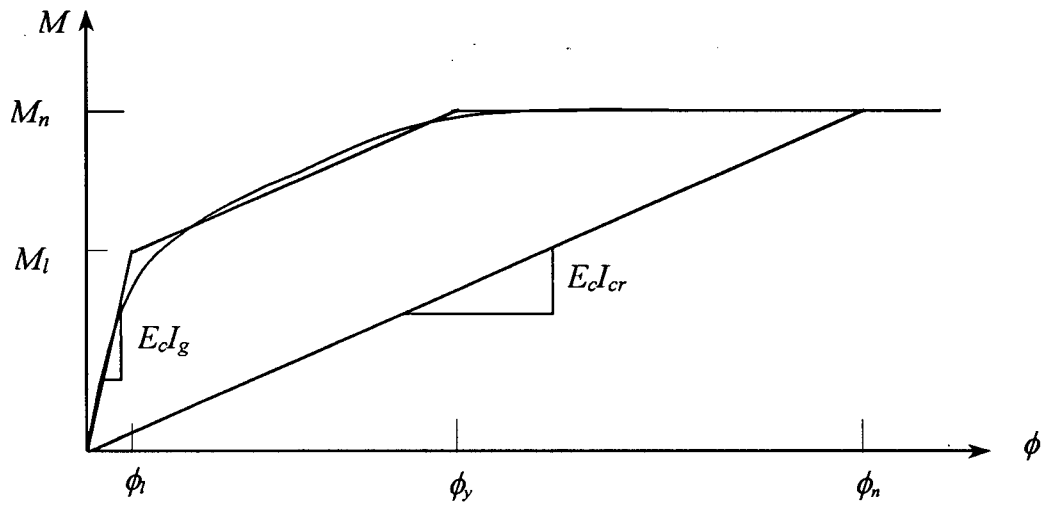

$$\phi_n = \frac{M_n}{E_c I_{cr}} \qquad \phi_y = \phi_l + \frac{M_n - M_l}{E_c I_{cr}} \qquad \phi_l = \frac{M_l}{E_c I_g}$$

$$\text{Area} = \int_0^{\phi_n} M \, d\phi$$ Area of actual nonlinear curve up to ϕ_n

$$\text{Area} = 0.5\,\phi_l . M_n + \left(\phi_y - \phi_l\right) . \left(\frac{M_l + M_n}{2}\right) + (\phi_n - \phi_y) . M_n$$

$$\text{Area} = 0.5\,(M_l^2 / E_c I_g) + \{(M_n - M_l)/E_cI_{cr}\}\{(M_n + M_l)/2\} + \{ M_n / E_cI_{cr} - (M_n - M_l)/ E_cI_{cr} - M_l / E_c I_g \} . M_n$$

$$= 0.5\,(M_l^2 / E_c I_g) + \{(M_n^2 - M_l^2)/2\,E_cI_{cr}\} + \{ M_l / E_cI_{cr} - M_l / E_c I_g \} . M_n$$

$$2 . \text{Area} = M_l^2 / E_c I_g + M_n^2 / E_c I_{cr} - M_l^2 / E_c I_{cr} + 2\,M_l M_n / E_c I_{cr} - 2\,M_l M_n / E_c I_g$$

$$= M_l^2 (1/ E_c I_g - 1/ E_c I_{cr}) - 2 M_l M_n (1/ E_c I_g - 1/ E_c I_{cr}) + M_n^2 (1 / E_c I_{cr})$$

Consider $C = (1/ E_c I_g - 1/ E_c I_{cr})$

$$C . M_l^2 - 2 . C . M_n . M_l + (M_n^2 / E_c I_{cr} - 2 . \text{Area}) = 0.0$$

$$M_l = \frac{2 C M_n - \sqrt{4 C^2 M_n^2 - 4 C \left(\frac{M_n^2}{E_c I_{cr}} - 2 . \text{Area} \right)}}{2 . C}$$

Appendix E

Additional Analyses to Justify Proposed Simplified Method

Additional analyses were carried out to determine the effective flexural stiffness (upper and lower- bound) for different walls of geometrical form and dimensions as shown in Figure E.1. Geometrical variables include: ratio of web thickness to wall length (b_w / l_w); ratio of flange thickness (if any) to wall length (l_f/ l_w); ratio of flange width to wall length (b_f / l_w). The amount of vertical reinforcement was varied between a practical minimum and maximum amount for each of the different wall cross sections. The length of the boundary zones with concentrated reinforcement was also varied for the appropriate shapes as shown in Figure E.1. Concrete compressive strength ranging from 30 to 60 MPa and the corresponding E_c and f_{cr} were used for the various wall sections. For each wall section, the effective flexural stiffness was determined for an applied axial compression ranging from 2% to 20% of $f_c' A_g$. The yield strength of the vertical reinforcement was not considered in this study since the majority (about 90%) of the reinforced concrete structures in North America are constructed with 400 MPa grade steel (Grade 60).

Each curve shown in the following figures was determined by connecting 10 calculated points (i.e., stiffness values) across the curve representing an interval of 0.02 $f_c' A_g$. Each calculated point was determined using the procedure described in Sections 4.2 and 4.3 and were done using program *Wall-Tools*.

When the variation of a geometrical variable did not result in any change in the effective stiffness value, this variable was omitted. For example, when changing the ratio of the thickness to the length of a rectangular wall (b_w/l_w) from 0.05 to 0.15, the effective stiffnesses were the same and therefore, only one set of results for this variable is considered.

Figure E-2 shows the upper and lower-bound effective flexural stiffness determined for the various geometrical dimensions, reinforcement amounts and material properties of a rectangular wall shape. As expected, large variations in the effective stiffness values were obtained depending on the various parameters considered in the analysis.

Figure E.3 shows the upper and lower-bound effective flexural stiffness determined for the various geometrical dimensions, reinforcement amounts and material properties of a flanged wall shape. Large scatter in the effective stiffness results were found. Upper-bound effective stiffnesses ranged from 0.4 I_g to about 1.0 I_g. The lower-bound effective stiffnesses were less scattered. The high values of the upper-bound effective stiffness resulted from the cases with very small amounts of vertical reinforcement (i.e., minimum vertical reinforcement) in the flanges combined with high tensile strength of concrete for $f_c' = 60$ MPa. Low values of upper-bound effective stiffness, on the other hand, resulted from large amounts of vertical reinforcement in the flanges and lower tensile strength of concrete (associated with $f_c' = 30$ MPa).

Figures E.4 and E.5 show the upper and lower-bound effective flexural stiffness determined for the various geometrical dimensions, reinforcement amounts and material properties of a "C" or "T" shaped wall. Similar conclusions were found. Note that the lower-bound effective stiffness for C or T shaped wall sections subjected to small axial compression, can be as low as 0.1 I_g.

As seen in the figures, the two simple expressions (Equation [4.3] a and b) provide a reasonable approximate stiffness value for most wall shapes with various reinforcement arrangements and material properties.

Shape "A"

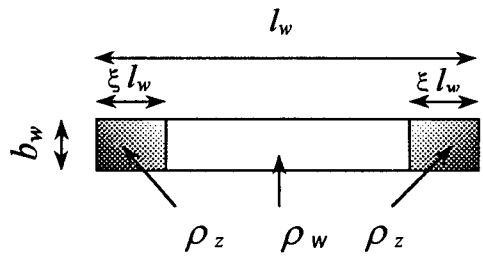

Shape A:		
b_w/l_w	=	0.05 - 0.15
ξ	=	0.05 - 0.2
ρ_z	=	1.0 - 4.0%
f_c'	=	30 - 60 MPa

Shape "B"

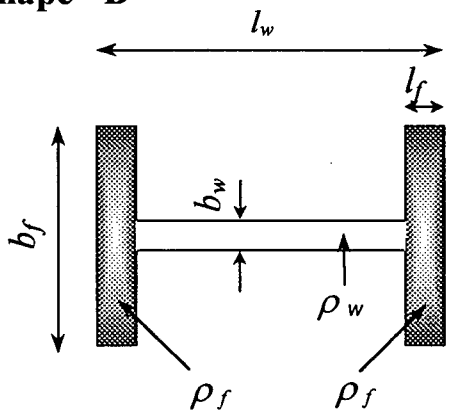

Shape B:		
b_w/l_w	=	0.05 - 0.15
l_f/l_w	=	0.05 - 0.15
b_f/l_w	=	0.25 - 2.0
ρ_f	=	0.5 - 3.0%
f_c'	=	30 - 60 MPa

Shape "C"

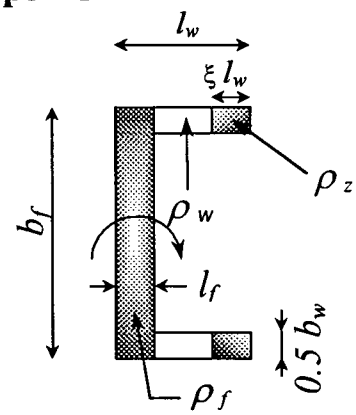

Shape "D"

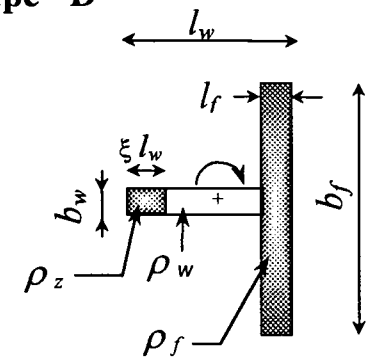

Shape C and D:		
b_w/b_f	=	0.05 - 0.20
b_f/l_w	=	3.0 - 1.0
l_f/l_w	=	0.05 - 0.20
ξ	=	0.05 - 0.20
ρ_f	=	0.5 - 3.0%
ρ_z	=	1.0 - 4.0%
f_c'	=	30 - 60 MPa

Figure E.1 Different wall shapes and dimensions examined in the study.

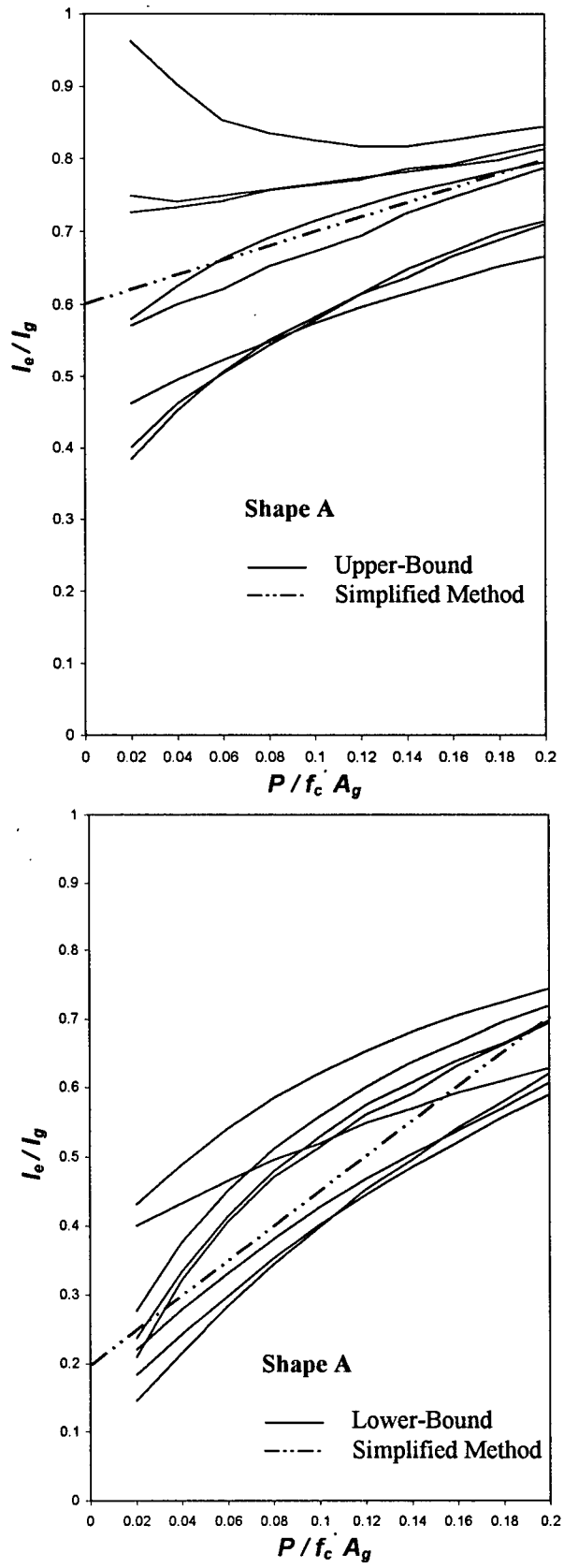

Figure E.2 Effective flexural stiffnesses for various configurations of rectangular wall.

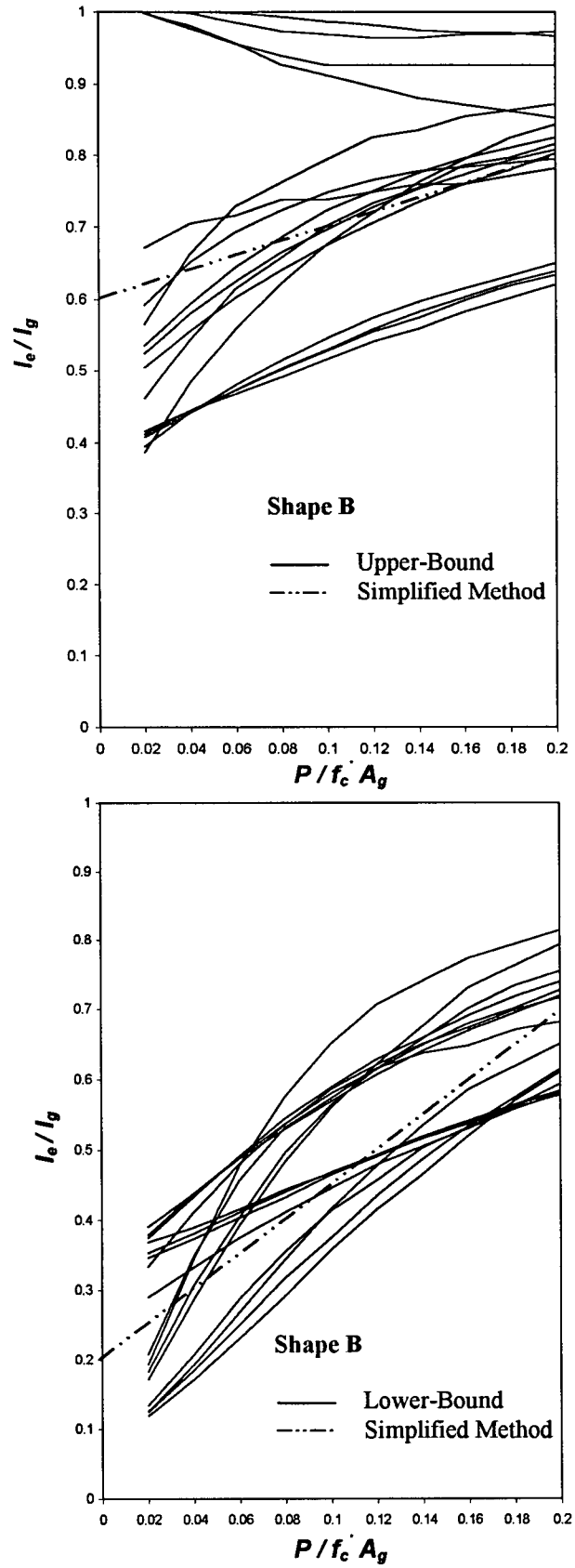

Figure E.3 Effective flexural stiffnesses for various configurations of flanged wall.

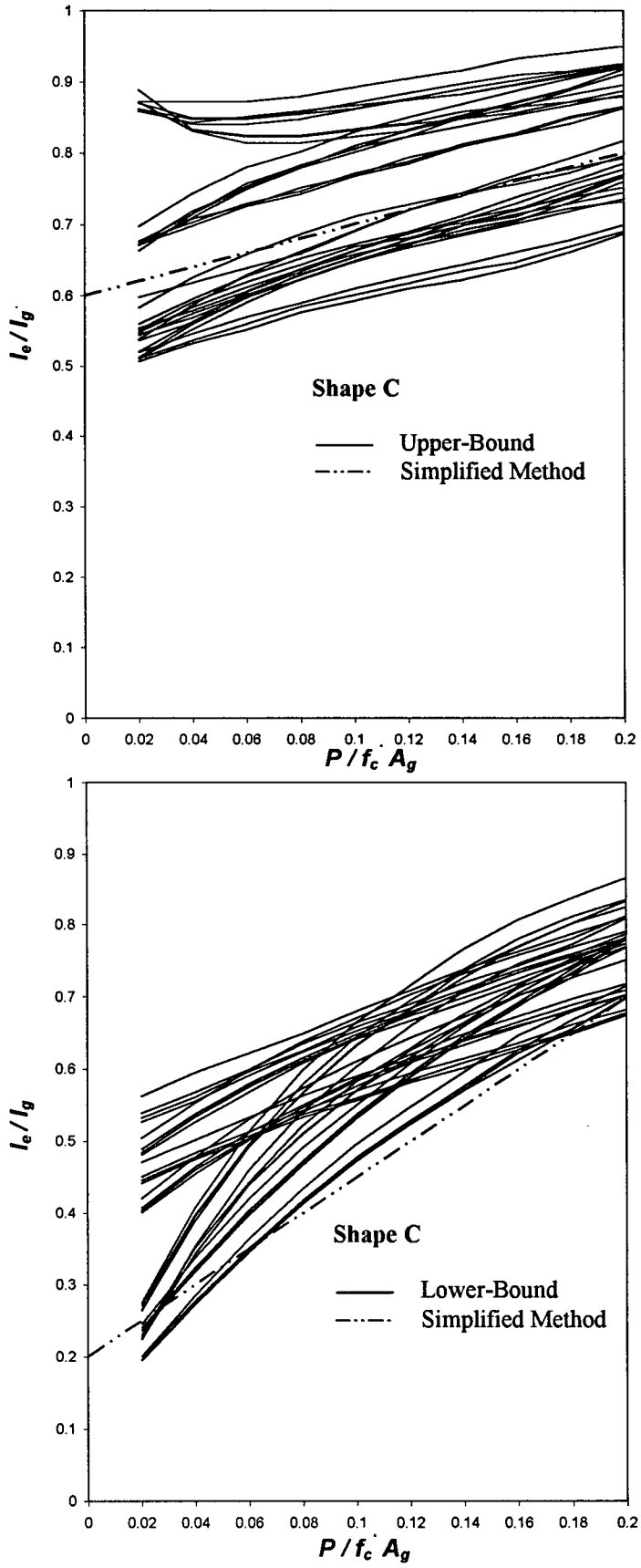

Figure E.4 Effective flexural stiffnesses for various configurations of C shape wall.

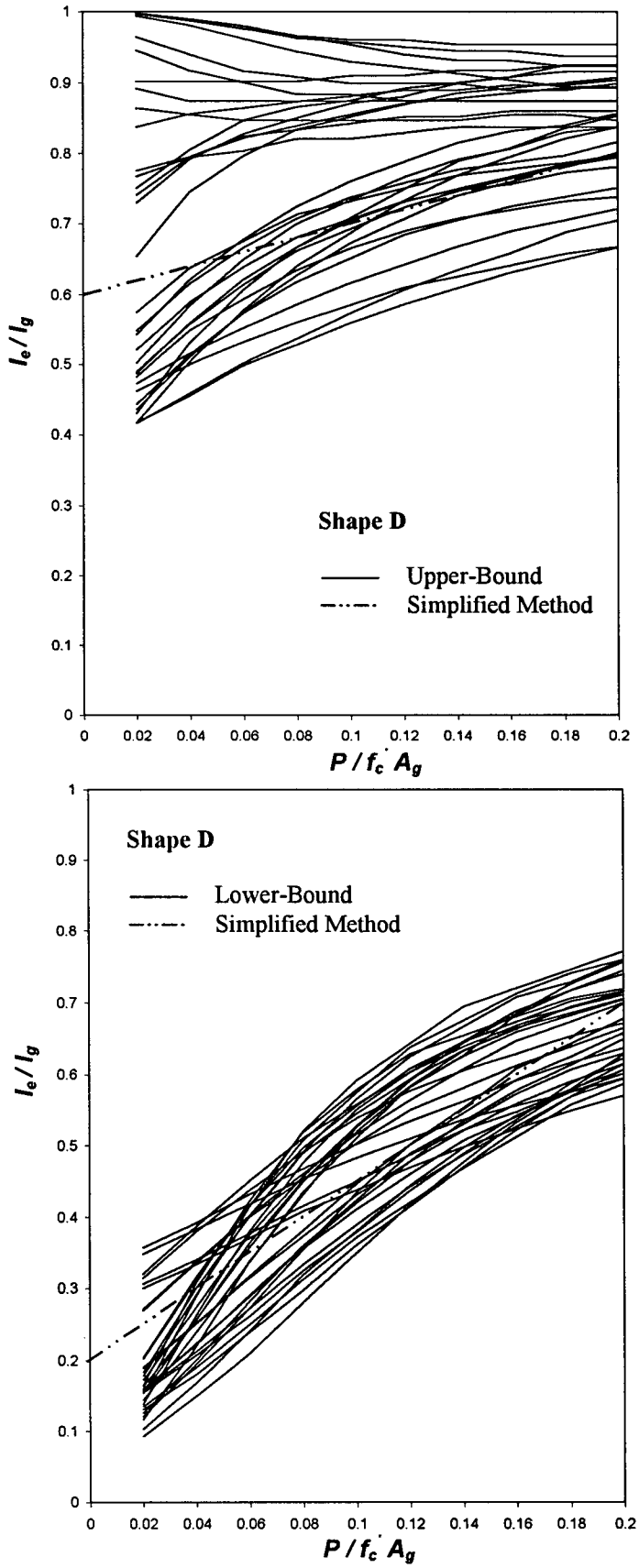

Figure E.5 Effective flexural stiffnesses for various configurations of T shape wall.

Appendix F

Computational Procedure for Determining Effective Member Stiffness

Computational procedure to determine the effective member stiffness, E_cI_e, using the equal rotation criteria (i.e., equivalent rotation between the two ends of the member).

- Illustrative example:

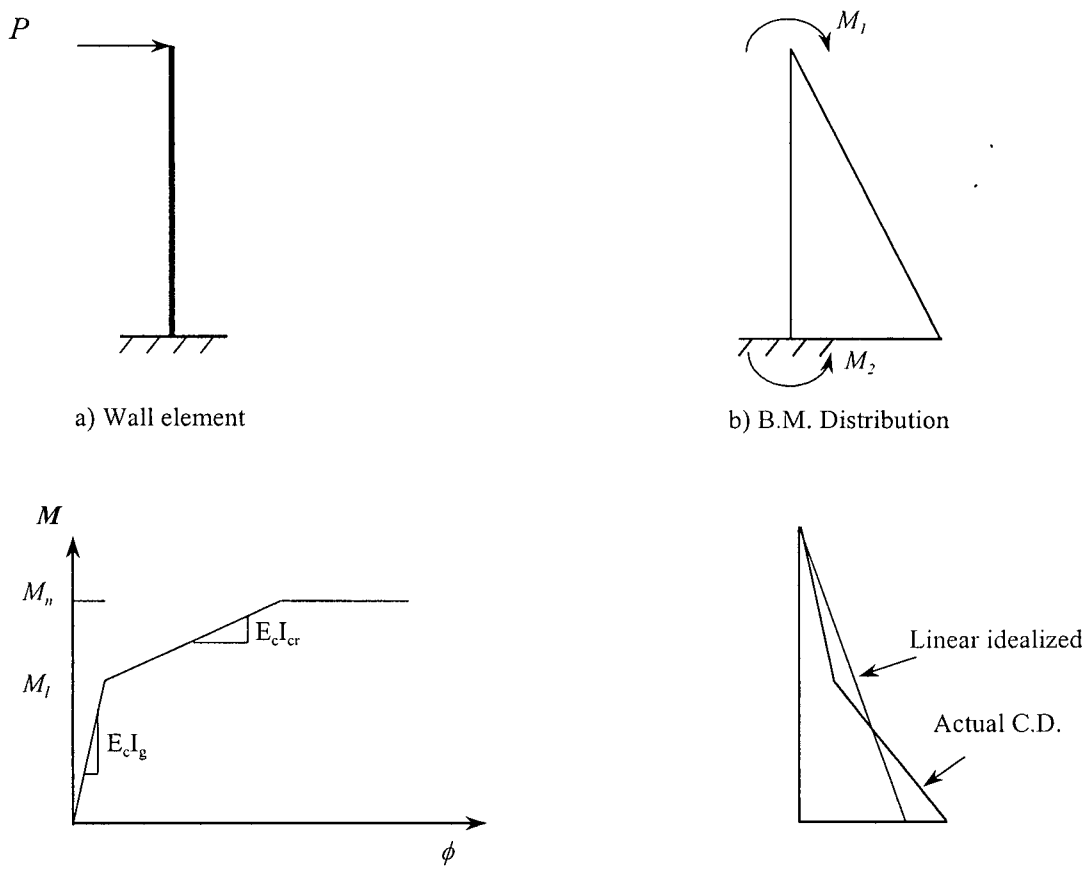

a) Wall element

b) B.M. Distribution

c) Material modeling

d) Curvature distribution

$$\theta = \int \phi(x)\, dx$$

For similar rotation between the two ends of the member whether computed by actual or idealized curvature distributions:

$$\int \phi(x)\, dx_{\text{Idealized}} = \int \phi(x)\, dx_{\text{Actual}}$$

$$\int \frac{M(x)}{E_c I_e} dx = \int \frac{M(x)}{E_c I(x)} dx$$

$$E_c I_e = \int \frac{M(x)\,dx}{\frac{M(x)}{E_c I(x)} dx} = \frac{Area\ under\ B.M.D}{Area\ under\ actual\ \phi\ dist.}$$

$$E_c I_e = \frac{\sum M(x)\,\Delta x}{\sum \frac{M(x)}{E_c I(x)} \Delta x}$$

If Δx is constant:

$$E_c I_e = \frac{\sum M(x)}{\sum \frac{M(x)}{E_c I(x)}} \qquad [F.1]$$

To implement this procedure in "*2Frame-NL*", any wall member is discritized into 99 layers.

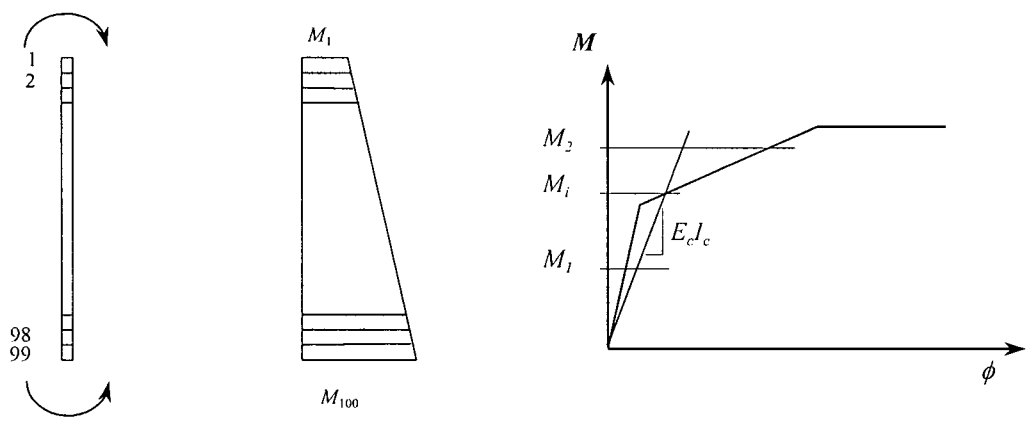

a) Wall member b) Discritized B.M.D c) Definition of $E_c I_c$

$$E_c I_e = \psi E_c I_g = \frac{\sum_{i=1}^{100} M_i}{\sum_{i=1}^{100} \frac{M_i}{E_c I_i}} \qquad [F.2]$$

Depending on the moment distribution along the length of the member (single curvature or double curvature moment diagram), different cases to compute the effective member stiffness are identified and described:

Single Curvature Distributions: $M_1 . M_2 > 0.0$

(I) $$\|M_1\| \le M_l \ and \ \|M_2\| \le M_l$$

$$E_c I_e = E_c I_g \qquad \text{i.e., } \psi = 1.0$$

Note that equation [F-2] is not needed in this case.

(II) $$M_1 > M_l \ or \ M_2 > M_l$$

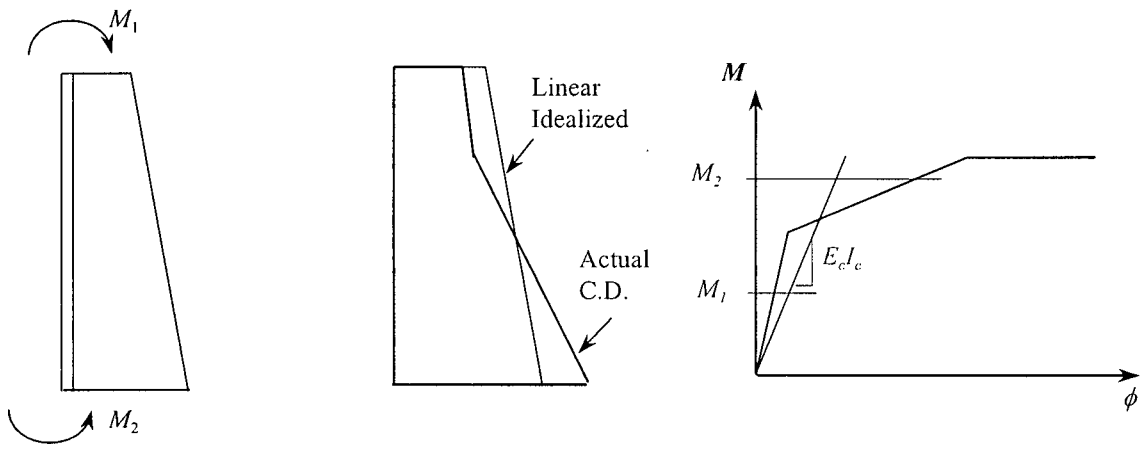

a) B.M.D b) C.D. c) Effective member stiffness

$E_c I_e$ is obtained using Equation [F.2]

Double Curvature Distributions: $M_1 . M_2 < 0.0$

(III) $$\|M_1\| \le M_l \ and \ \|M_2\| \le M_l$$

$$E_c I_e = E_c I_g \qquad \text{i.e., } \psi = 1.0$$

Note that equation [F-2] is not needed in this case.

(IV)

$$\|M_1\| > \|M_l\| \ or \ \|M_2\| > \|M_l\|$$

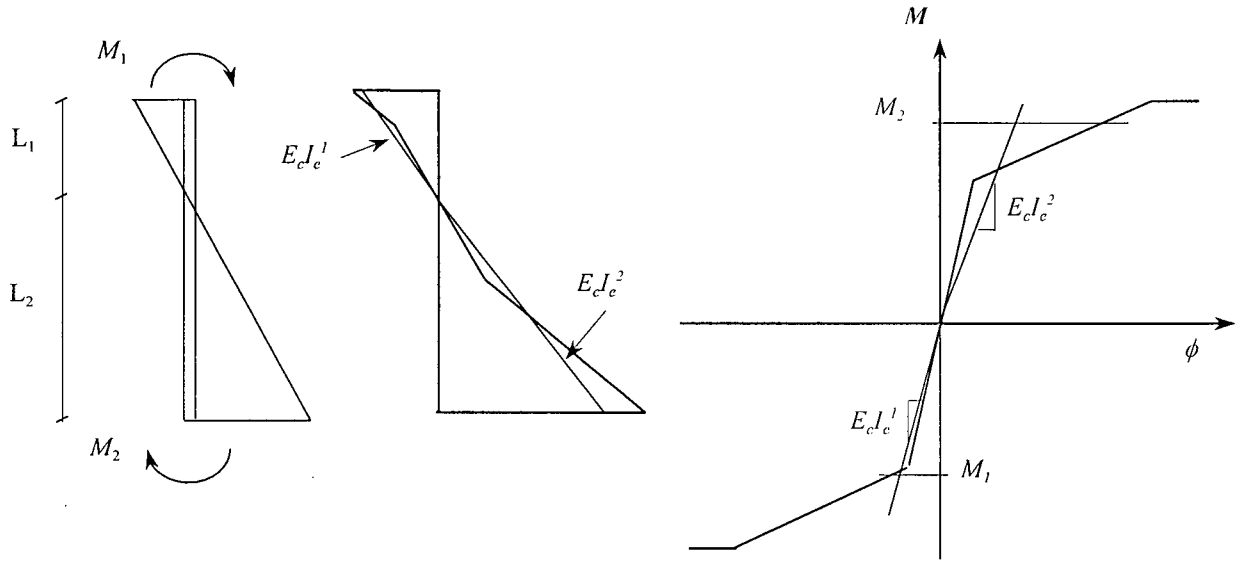

a) B.M.D b) C.D. c) Effective member stiffness

In this particular case, point of contraflexure is determined along the length of the member. Equation [F.2] is applied twice, one for each side resulting in $E_cI_e^1$ and $E_cI_e^2$. Note that number of layers are adjusted according to the length of each side.

Effective member stiffness, E_cI_e, is considered as the equivalent sum of the two springs (stiffnesses) connected in series. Each stiffness is weighted by its appropriate length of the member.

$$\frac{1}{E_cI_e} = \frac{1}{E_cI_e^{\,1}} * (\frac{L_1}{L}) + \frac{1}{E_cI_e^{\,2}} * (\frac{L_2}{L})$$

$$\frac{1}{E_cI_e} = \frac{E_cI_e^{\,2} * (\frac{L_1}{L}) + E_cI_e^{\,1} * (\frac{L_2}{L})}{E_cI_e^{\,1} * E_cI_e^{\,2}}$$

$$E_cI_e = \psi E_cI_g = \frac{E_cI_e^{\,1} * E_cI_e^{\,2}}{E_cI_e^{\,1} * (\frac{L_2}{L}) + E_cI_e^{\,2} * (\frac{L_1}{L})} \qquad \text{[F.3]}$$

Appendix G

Program *"Wall-Tools"*

Program "*Wall-Tools*" is designed for structural engineers performing seismic analysis and design of reinforced concrete walls. The program provides three basic analysis tools essential in the flexural design of concrete sections:

1- Moment Curvature Analysis: the bending moment-curvature characteristics of a reinforced concrete section is determined for given axial load until default, or user defined strain limits are reached. The analysis is performed for a single axial load level or for a range of axial loads expected on the described reinforced concrete section. Idealized tri-linear approximations to the theoretical moment-curvature relation are also calculated. Strain profile across the section is given at any moment state.

2- Axial Load - Bending Moment Interaction: nominal moment capacity of the reinforced concrete section is calculated for the entire range of axial load. The capacity is controlled either by reaching maximum strain limits or by checking the ultimate resistance at a cracked section location. Factored, Nominal, and Probable resistance factors are allowed.

3- Effective Flexural Stiffness: flexural stiffness of reinforced concrete shear wall is determined based on the characteristics of the cross section at the base. Trilinear approximation of the moment curvature relation of the cross section at the base along with the assumption of axial gravity being linear with height are used to construct the curvature distribution over the wall height. The force-displacement curve is obtained by integrating the curvature distribution over the wall height repeatedly for different load steps. The program uses the equal energy (area) principle of the force-displacement curve to determine the equivalent bilinear idealization.

Program features include:

- Dual SI and Imperial units.
- User friendly input format.
- Full tabular output and graphical representation.

Program Wall-Tools

Moment-Curvature Analysis

Axial Load-Bending Moment Interaction

Effective Flexural Stiffness

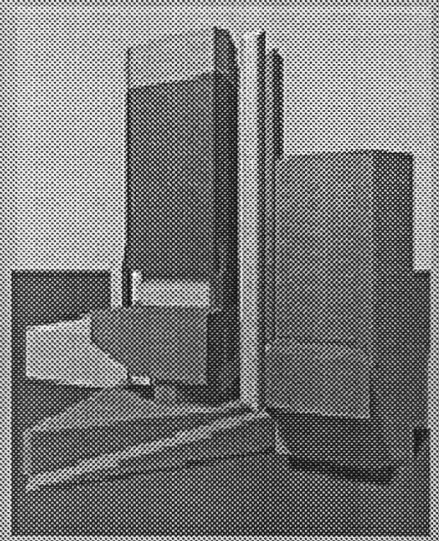

The University of British Columbia
Civil Engineering Department

Ahmed M. M. Ibrahim
Perry Adebar